BIOLOGICALLY REINFORCED GEOPOLYMER COMPOSITES

BY

DANIEL S. ROPER

THESIS

Submitted in partial fulfillment of the requirements
for the degree of Master of Science in Materials Science and Engineering
in the Graduate College of the
University of Illinois at Urbana-Champaign, 2017

Urbana, Illinois

Adviser:

Professor Waltraud M. Kriven

ABSTRACT

A series of studies detailing the characteristics of biologically reinforced geopolymers is presented. Cork particle reinforced sodium geopolymer composites were shown to have a maximum flexural strength of 2.5 MPa, and an average strain-to-failure of 0.75%. Abaca fiber reinforced sodium geopolymer composites had flexural strengths exceeding 25 MPa. The main focus of this study was abaca fiber reinforced potassium geopolymer composites, which had flexural strengths exceeding 50 MPa at 8 wt% abaca fibers. This new composite was shown to have good water and saltwater durability, decent sodium hydroxide and freeze cycle durability, and poor sulfuric acid durability. The composite was also tested for heat sensitivity, and showed a steady decrease in flexural strength as it was exposed to higher temperatures. The composite was unable to carry any load after being treated to 300°C. Weibull statistical analysis was used to better understand the range of flexural strengths within different sample groups. Finally, SEM analysis was employed to characterize fracture surfaces and mode of failure in the different sample sets.

ACKNOWLEDGEMENTS

I would first like to thank my adviser, Professor Waltraud M. Kriven, for giving me the opportunity to conduct research within her group. Without her guidance and support, this project would never have come to fruition. Within the Kriven group, I would like to thank Gregory Kutyla and Kaushik Sankar for teaching me the art of geopolymer processing.

I would also like to thank my mother and father who always encouraged and supported me. My scientific curiosity, which extends into this work, is due in no small part to them. Finally, I'd like to thank Craig, Brian and Emily.

TABLE OF CONTENTS

CHAPTER 1

INTRODUCTION

1.1 Geopolymers

Geopolymers are a class of inorganic, amorphous, repeating-unit materials comprised of alumina, silica, and an alkali metal oxide. They are formed by mixing amorphous silica dissolved in an alkaline solution with an aluminosilicate source, most often metakaolin or fly-ash [1-11]. Geopolymers have no defined stoichiometric chemical formula, although typically molar ratios of the form $M_2O•Al_2O_3•\ xSiO_2•yH_2O$ are employed where M is an alkali metal cation, x is between 2 and 6 and y is between 7.5 and 13 [6, 11, 12]. The details of geopolymer formation within these stoichiometric ranges are important when trying to understand various properties of geopolymers:

"The essence of the geopolymerization reaction is due to the highly strained AlO_5^{-2} coordination polyhedra in the amorphous metakaolin which forms a double bond with one Al atom and which is then susceptible to dissolution by the highly caustic, alkali metasilicate solution ("water glass") of standard composition e.g. $Na_2O•2SiO_2•11H_2O$ [12]. The amorphous aluminosilicate source is susceptible to dissolution in the highly alkaline solution where the Al^{3+} then forms AlO^{4-} tetrahedra. These attract charge-balancing Group I cations and react with SiO_4 tetrahedra to form an amorphous 3D network. The dissolution is the rate-determining step" [12].

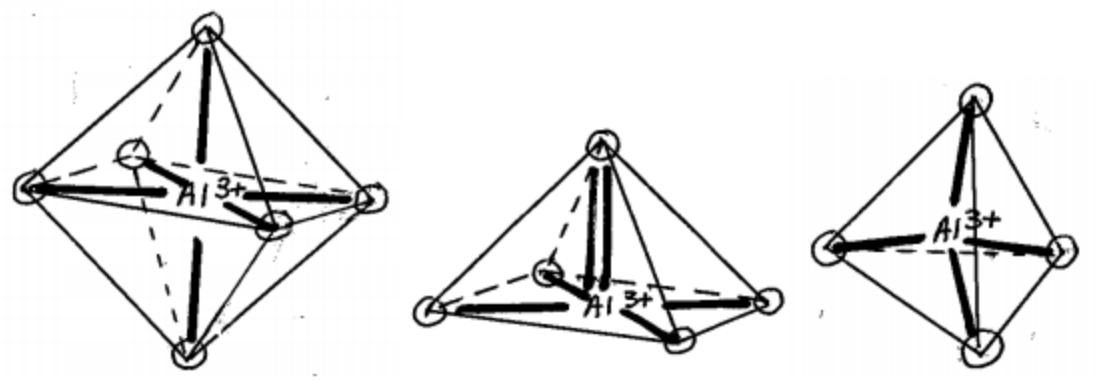

Fig. 1. Evolution of aluminum ion from dissolution to just before polymerization with silicate.

Once formed, geopolymers consist of tetrahedral units of SiO_2 and AlO_4^-. The amorphous structure, shown below, surrounds the alkali metal cation and water as added to a predetermined stoichiometric ratio.

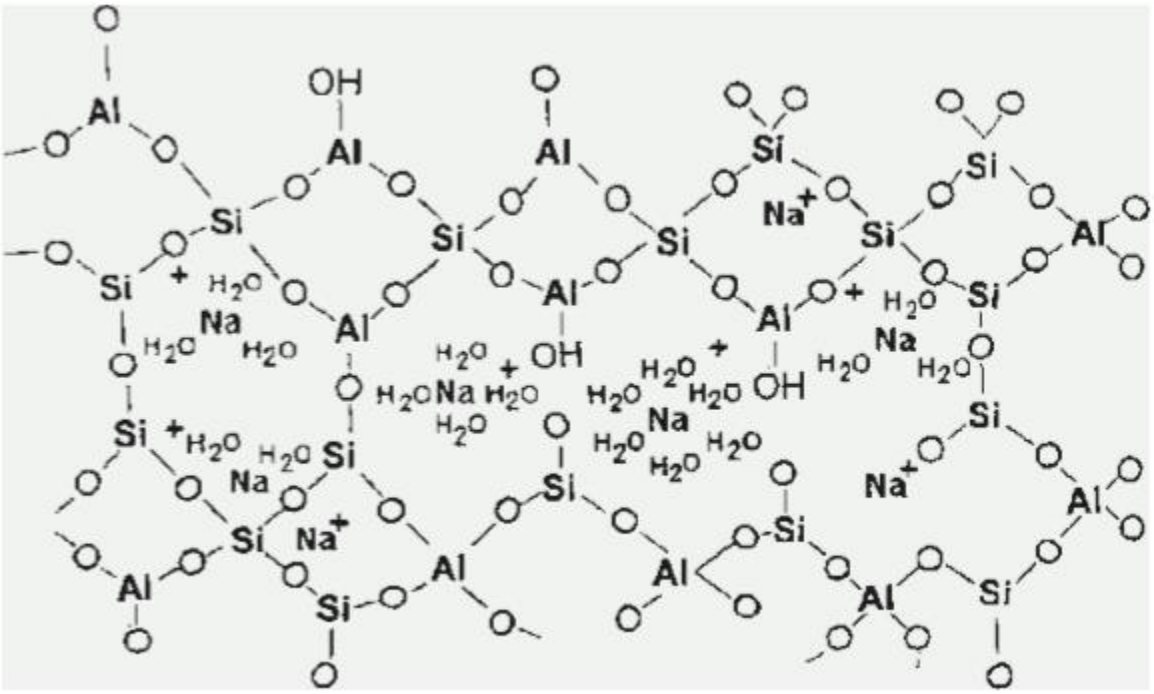

Fig. 2. Atomic model of sodium geopolymer formed at room temperature [11, 13].

An appealing aspect of geopolymers is its use of various waste materials as both aluminosilicate sources and as reinforcement. Additionally, its viability as an environmental structural material is strengthened by virtue of the fact that its manufacture liberates about 25% of the CO_2 into the atmosphere when compared to Ordinary Portland Cements (OPCs) [1, 4, 7]. As geopolymers continue to garner attention in the materials science field, applications in refractory materials, coatings and composites are being researched and developed [1-12].

1.2 Reinforcements in Geopolymers

A number of reinforcements have been tested in geopolymer matrices over the decades [12]. These reinforcements, both inorganic and biological, have succeeded in improving upon the material properties of pure geopolymers, such as toughness, strength and durability. Some inorganic reinforcements and the strengths they yielded in geopolymers can be seen below.

Table 1. Properties of inorganically-reinforced geopolymers [12].

Reinforcement	Wt % Additions	Flexure strength (MPa)
Chamotte (25 μm)	50	15.33
Dolomite (45 μm)	20	15.92
Mica phlogopite platelets (50-100 μm)	20	11.4
Granite powder (≤ 90 μm)	55	10.3
Dicalcium phosphate ($2CaO•P_2O_5$)	15	10.4
Hydroxyapatite bone ash	15	10.0
Bangladeshi Mymensingh clay containing 40 wt % quartz reinforced with dicalcium phosphate ($2CaO•P_2O_5$) and glass frit	7.5 7.5	14.28
Alumina platelet grinding media (50 μm)	70	20 (RT) to 40 (at 1200°C)
Alumina chopped Saffil® fibers (ϕ = 3 μm)	20	20
Carbon chopped fibers (60 μm x 7 μm ϕ)	20	22.2
Carbon chopped fibers (100 μm x 7 μm ϕ)	20	29.9
Basalt chopped fibers (1/4")	10	19.5
Basalt chopped fibers (1/2")	10	27
Graphene nanoplatelets	3	12
Basalt felt	10	22.2
Fiberglass felt	10	5.6
Basalt 4" chopped strand mat	20	31
Basalt fiber weave	30	41
E-glass Leno weave	25	25.6
Carbon unidirectional fiber	20	269
Nextel 610 alumina (8 satin weave)	50	45.8
Nextel 720 (mullite +15 vol % alumina)	50	46
Xtegra® auxetic fibers from Advanced Fiber Technologies, Inc.	50	12.9 25 % strain to failure

This table shows the great promise that geopolymers have as a structural material. Whereas OPCs have flexural strength on the order of 5-6 MPa, many of these composites have strengths in the 10-30 MPa range, greatly improving upon pure geopolymer strength which is about 2-7 MPa. Additionally, inorganic reinforcements such as granite powder have the added environmental appeal as granite powder is often treated as a waste material at stone processing

quarries [14]. Since this study is focused upon a biological reinforcement in geopolymer, more detail will be presented on biologicals as a viable reinforcement option.

1.3 Biological Reinforcements

A number of biological reinforcements have been used with varying success to strengthen and improve upon existing geopolymer properties. While 'biological' does encompass animal matter, this study is dedicated to reinforcement from plants.

Natural fibers have long been used by humans for ropes and bags due to their abundance, strength and durability. By improving processing techniques, chemical treatments, and orientation of fibers, one can create geopolymer composites with truly remarkable properties. Below is a table of several plant fiber and orientations that have been used to create geopolymer composites.

Table 2. Properties of biologically-reinforced geopolymers [12].

Reinforcement	Wt % Additions	Flexural strength (MPa)
Polypropylene chopped fibers (1/2")	2.5	14.5
Polypropylene chopped fibers (1")	2.5	15
Polypropylene chopped fibers (2")	2.5	18.3
Cork particles[82]	60	2.5 (0.75 % strain to failure)
Abaca (banana leaf fibers or "Manila hemp")	8	52
Corn husk fibers	13	7.6 (7 % strain)
Rice husk stems in rice husk silica-based GP	7	12.4
Jute weave	30	20.5
Colombian *fique*/*sisal* (unidirectional)	50	11.4
Amazonian *malva* (unidirectional)	5.5	31.55
Amazonian *curaua* (unidirectional)	8.3	18.86
Amazonian *Guadua Angustifolia chopped bamboo* dispersed in Amazonian clay-based geopolymer	20	7
Bangladeshi *coconut coir*	10	7.50
Bangladeshi *palm tree coir*	10	7.61

Here, improvements upon the strengths of pure geopolymer and OPCs are again apparent. Many of the shown composites have flexural strengths above the 10 MPa mark.

An important aspect of using plant fibers as reinforcement in geopolymers are the lignin and cellulose contents. Cellulose forms the backbone of plant fibers, while lignin provides little structural support to the fiber itself. By soaking plant fibers in a caustic, basic solution, lignin can be dissolved away, leaving the cellulose backbone intact. This cellulose backbone can then bond to geopolymer in a composite, increasing the composite's overall strength.

The first biological processed in this study was particulate cork. Cork is harvested bark from the Cork Oak, a tree native to southwest Europe and northwest Africa. The material is known for its Poisson ratio of zero and extremely low density. While cork was a very small part of this study, it is mentioned as its shortcomings as a reinforcement for geopolymers led to successes in the abaca geopolymer studies.

The fiber primarily used in this study, abaca, is obtained from the leaf-steam of Manila hemp, a species of banana tree native to the Philippines. It is used in high-grade papers, and can be obtained in the form of stiff, cardboard-like sheets. Upon processing, fibers can be extracted from these sheets and made suitable for introduction into a geopolymer composite.

1.4 Mechanical Testing

To get a general idea of a sample's strength, four-point flexural testing was used. Flexural testing allows samples to be subjected to both tensile and compressive forces simultaneously. Due to the nature of ceramic composites, the samples all fail on the tensile side first, giving a degree of continuity across all the tested samples.

Four-point flexure is suggested in the ASTM standard as a more precise alternative to three-point flexure, particularly when Weibull statistics are employed for characterization [15]. An extension of simple beam theory, the standard makes a few assumptions about the samples being tested. While these assumptions are not entirely true, the fact remains that four-point flexure tests allow for comparison across a number of different sample strengths. These assumptions include the material being isotropic, the moduli of elasticity in tension and compression are comparable, and the material is linearly elastic.

By employing the testing conditions set forth in the standard, the flexural strength of various samples could be calculated and compared using Equation (1)

$$\sigma = \frac{3\mathrm{FL}}{4bd^2} \tag{1}$$

where σ is flexural stress, F is load, L is the support span, b is the sample width and d is the sample height. This equation for four-point flexural strength assumes that the loading span is half of the supporting span [15].

1.5 Durability Testing

Durability has long been an important aspect to consider when structural materials are in question. A number of studies exist that explore problems of durability in both concretes and geopolymers, but one study in particular served as an inspiration to pursue the study of durability in abaca reinforced geopolymers. "Durability of Fly Ash Based Geopolymer Concrete Against Sulphuric Acid Attack" explored the decrease in compressive strengths of geopolymer concretes when exposed to sulfuric acid for varying times [16]. The study measured mass change and physical appearance as metrics as to whether or not a given material was 'durable' [16].

Since the samples used in the abaca study were much smaller, inspection of any swelling was too inaccurate to depend upon. Instead, various solutions (sulfuric acid, sodium hydroxide, salt water and deionized water) were mixed to be used with the geopolymer composites. Borrowing from the durability study, samples were placed in each solution and soaked for 14 days, followed by 14 days drying at ambient conditions. Flexural tests were carried out on each sample group, allowing for comparison in strength across all durability samples, as well as the untreated samples. These strengths then became metrics by which relative durability could be calculated and compared.

1.6 Statistical Analysis

For each set of mechanical testing data, Weibull analysis was used to characterize sample set strength and consistency. A distribution function, *F*, was created relating a sample's rank *i* (which ranged from 1 to *n*, the total number of samples in a set) [17]. This relation can be seen in Equation (2).

$$F = \frac{i-0.3}{n+0.4} \tag{2}$$

The distribution function can also be expressed in terms of *v*, the non-dimensional volume, σ, the stress, σ_o, the scale parameter and *m*, the Weibull modulus. This relation can be seen in Equation (3).

$$F = 1 - e^{[-v(\frac{\sigma}{\sigma_o})^m]} \tag{3}$$

It was assumed that the gage length would remain unchanged in the samples, so $v = 1$. This allowed for the Weibull parameters to be solved for by rearranging Equation (3) in Equation (4) [17].

$$\ln\left[\ln\left(\frac{1}{1-F}\right)\right] = m\ln(\sigma) - m\ln(\sigma_o) \quad (4)$$

As Equation (4) fits the standard slope-intercept form, plotting of $\ln\left[\ln\left(\frac{1}{1-F}\right)\right]$ against $\ln(\sigma)$ allows for the Weibull modulus to be ascertained from the plotted slope, and for the scale parameter to be solved from the y-intercept [17].

1.7 X-ray Diffraction

X-ray Diffraction (XRD) is a method of determining the microstructural ordering of crystalline materials. The method takes advantage of the fact that repeating structures will statistically reflect incident x-rays at specific angles. This method has been used since the late nineteenth century to identify micro-ordering in materials and to identify and characterize unknown materials.

Although metakaolin-based geopolymers have an amorphous structure, they still have a unique XRD profile [18]. A properly-reacted geopolymer will have an amorphous hump centered around a two theta value of 28.5 degrees. An XRD pattern of fully reacted metakaolin-based geopolymer can be seen below [18]. The four patterns represent geopolymers of varying silica, alumina and sodium ratios, demonstrating that the XRD hump is centered at the same point regardless of these ratios.

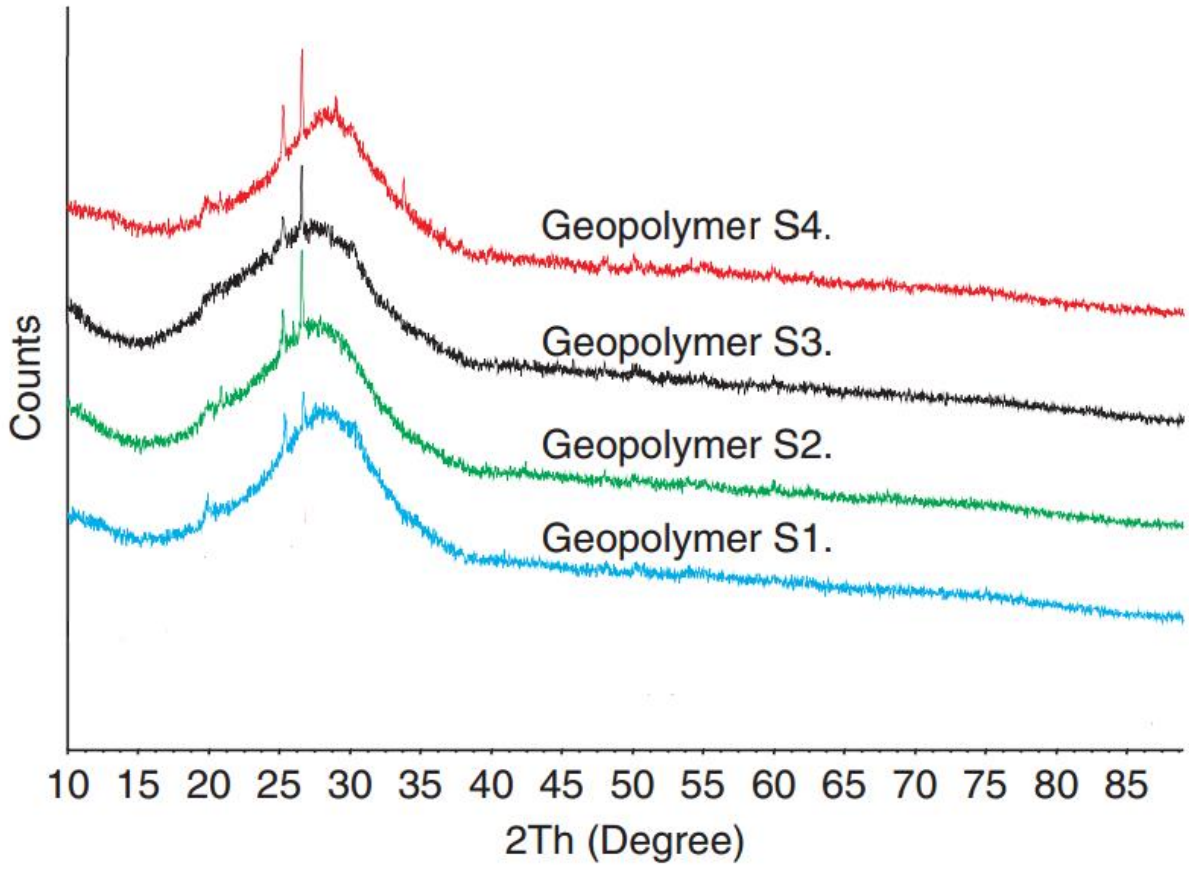

Fig. 3. XRD patterns of fully-reacted metakaolin-based geopolymers with patterns offset [18].

When an XRD pattern for metakaolin-based geopolymers features a hump shifted from the two theta = 28.5-degree mark, it is indicative of unreacted or only partially reacted metakaolin. This could be due to a number of reasons, from improper stoichiometry to lack of proper mixing in the preparatory steps. However, when XRD reveals a properly centered amorphous hump, it indicates that the metakaolin has fully reacted, ensuring strengths as high as possible from a chemical perspective.

CHAPTER 2

EXPERIMENTAL PROCEDURE

2.1 Cork Particle Reinforced Sodium Geopolymer

The first system analyzed in this study was cork particulate reinforced sodium geopolymer. To create sodium geopolymer, sodium waterglass ($Na_2O{\cdot}2SiO_2{\cdot}11H_2O$) was created by mixing sodium hydroxide and fumed silica (Cab-o-sil, Cabot Corp., Boston, MA) with deionized water. The sodium waterglass was allowed to mix for several hours on a plate with a magnetic stirrer. As both sodium hydroxide and silica give off heat when mixed with water, the entire mixture was massed once the waterglass had reached room temperature. Any missing mass was assumed to be from evaporated water, and was replaced with deionized water and mixed further. Once the waterglass was homogenously mixed, it was stored in a plastic container in a refrigerator set at 2°C.

To create sodium geopolymer, sodium waterglass was mixed with metakaolin (Metamax HRM, BASF Corp., Florham Park, NJ) in the ratio of 1.7123:1 in terms of sodium waterglass and metakaolin mass, respectively. Once the metakaolin was added to the sodium waterglass, it was first mixed with an IKA overhead stirrer with high shear blade for three minutes at 1500 rpm.

Once thoroughly mixed in the overhead stirrer, the sodium geopolymer was then placed on an FMC Syntron vibrating table (FMC Technologies, Houston, Texas) for one minute for degassing. After one minute, the geopolymer was placed into a Thinky ARE-250 planetary conditioning mixer (Intertronics, Kidlington, Oxfordshire, England). The geopolymer was then further mixed with the planetary mixer at 1200 rpm for three minutes, and at 1500 rpm for another three minutes. After mixing in the Thinky, the geopolymer was subjected to another

round of high shear stirring, vibration degassing, and planetary conditioning at the same conditions.

Particulate cork was then added to the sodium geopolymer, and mixed at 200 rpm using the IKA overhead stirrer until homogenous. Cork was added to the geopolymer until it was at its limit of workability, such that the mixture could still be pressed into molds. This limit was found to be about 60 wt% cork. In order for equal spacing in the data groups, sample sets were made at 0, 15, 30, 45 and 60 wt% cork. A total of six samples were made for each sample group, for a total of thirty samples.

Once the appropriate amount of cork had been mixed into the geopolymer, the mixture was once again vibrated in order to remove trapped air bubbles. The mixture was poured and pressed into 1”x1”x6” Delrin molds. Once all the molds were filled, the molds were clamped to the vibrating table and vibrated to remove any air bubbles that had manifested themselves during the molding process. The molds were then covered in plastic wrap and allowed to set in an oven at 50°C for 24 hours.

Upon removal from the oven, samples were immediately taken for mechanical testing. The samples were tested using an Instron Universal Testing Frame following ASTM C1161 for four-point flexure of ceramic materials. Lower supports were placed equidistant from the points of load application, with the outer span set at 2.4 in and the inner span set at 1.2 in. The displacement rate of the head was adjusted throughout testing in order to maintain an increase of less than 1 MPa/min [19]. Data was collected from each flexural test to compare the flexural stress and flexural strain of each sample, and plotted appropriately.

2.2 Abaca Fiber Reinforced Sodium Geopolymer

The second system focused on in this study was sodium geopolymer reinforced with abaca fibers. Sodium waterglass was created in the same stoichiometry as in the cork system. The mixing of fumed silica and sodium hydroxide, storage methods, overhead stirring and planetary conditioning settings were identical to those used in the cork system.

Unbleached abaca sheets were obtained (Arnold Grummer's Paper Making, Appleton, Wisconsin) to convert into abaca fibers. The sheets were first hand cut into approximately 1 cm^2 pieces before being placed into a DCG-20N coffee grinder (Cuisinart, East Windsor, New Jersey). Only 10-15 abaca sheet pieces could be placed into the grinder at any one time, both to avoid overheating and because the fiber's volume increased once violently agitated. Each batch of abaca sheet pieces was ground for 20 seconds before being inspected. If any tangible particles of abaca sheet remained, the batch was ground again until the abaca had a homogenous, 'cotton candy-like' texture, pictured below. All abaca fibers that had been ground were stored at 50°C to prevent water buildup.

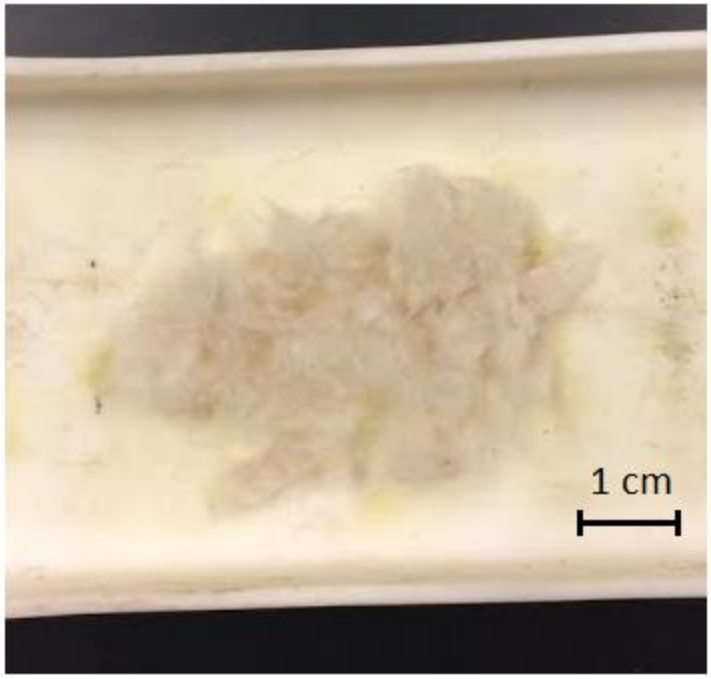

Fig. 4. Abaca fiber with appropriate 'cotton candy-like' texture in an alumina vessel.

Sodium geopolymer was prepared in the same manner as in the cork study. When the geopolymer was ready, the as-ground abaca fibers were added to the system and mixed in with the IKA overhead stirrer at 100 rpm. Again, abaca was added to the geopolymer until it was at its limit of workability, such that the mixture could still be pressed into molds. This limit was found to be about 5.2 wt% abaca fiber. In order for approximately equal spacing in the data groups, sample sets were made at 0, 1, 2, 3, 4 and 5.2 wt% abaca. At least ten samples were made for each sample group in order to attempt to decrease sample variance.

Once the appropriate amount of abaca fiber had been added to the geopolymer, the mixture was vibrated and prepared for molding. Due to the smaller reinforcement size (relative to the cork study), molds sized 1x1x10 cm were utilized. For lower solids loading (0, 1 and 2 wt% abaca), the mixture could easily be poured into the Delrin molds. However, the higher solids loading groups were not very flowable, and needed to be forced into the molds with a

spatula. As before, molded samples were covered in plastic wrap, and placed into an oven at 50°C for 24 hours to set.

Upon removal from the curing oven, samples were demolded and immediately mechanically tested. The same ASTM standard as noted in the cork study was used, with the primary difference being the sample size. Lower supports were once again placed equidistant from the points of load application. The outer span was set equal to 40 mm and the inner span was 20 mm, following the same ratios of spans as seen in the cork study. The displacement rate of the head continued to be adjusted throughout the experiment so as to keep the stress increase in samples less than 1 MPa/min. Data from each sample group was recorded and plotted to compare maximum flexural stress across each sample group. This data was also compared against the potassium geopolymer abaca composite data.

2.3 Abaca Fiber Reinforced Potassium Geopolymer

2.3.1 Sample Preparation

The final system analyzed in this study was abaca fiber reinforced potassium geopolymer. Potassium waterglass ($K_2O{\cdot}2SiO_2{\cdot}11H_2O$) was created by mixing potassium hydroxide and fumed silica with deionized water. The potassium waterglass was allowed to mix for several hours on a magnetic stir place. As both potassium hydroxide and silica give off heat when mixed with water, the entire mixture was massed once the waterglass had reached room temperature. Any missing mass was assumed to be from evaporated water, and was replaced with deionized water and mixed further. As with the sodium waterglass, the mixture was poured into a plastic container and stored at 2°C once homogenously mixed. To prepare potassium geopolymer, potassium waterglass was mixed with metakaolin in the ratio of 1.8574:1 mass

waterglass to metakaolin. The mixture was mixed and degassed as in the sodium geopolymer studies.

Abaca fibers were produced from unbleached abaca sheets in the same manner as the sodium geopolymer abaca study. Once more, abaca was added to the geopolymer until it was at its limit of workability, such that the mixture could still be pressed into molds. Due to potassium geopolymer's lower viscosity (relative to sodium geopolymer), more abaca fiber could be mixed into the geopolymer before the limit of workability was reached. This was hypothesized to lead to an increase in flexural strength when compared to abaca fibers in sodium geopolymer. The limit of workability was found to be 8 wt% abaca in potassium geopolymer. In order to generate equal spacing between sample group data, samples were created at 0, 2, 4, 6 and 8 wt% abaca fiber additions.

As in the abaca-sodium geopolymer system, once the appropriate amount of abaca fiber had been added to the geopolymer, the mixture was vibrated and prepared for molding. Again, molds sized 1x1x10 cm were utilized. For lower solids loading (0 and 2 wt% abaca), the mixture could easily be poured into the Delrin molds. However, the higher solids loading groups were not very flowable, and needed to be forced into the molds. This forcing was hypothesized to contribute to larger macroscopic flaws as air bubbles could not be vibrated out of the thick, high solids loaded samples. As before, molded samples were covered in plastic wrap, and placed into an oven at 50°C for 24 hours to set. During removal from Delrin molds after setting, thin flakes often chipped off the top of the sample, leading to surfaces with a rough appearance. These chips, despite having a relatively small effect on sample height (usually 0.1-0.2 mm) were nevertheless accounted for in the calculations of load carried in mechanical testing.

Mechanical testing was carried out in the same manner as in the abaca sodium geopolymer system. In the following durability and heat treatment sections, all mechanical testing was performed under the same conditions.

2.3.2 Durability Testing

In order to determine the durability of the samples, the highest solids loaded samples were exposed to a number of harsh environments. Since no single standard existed for the acid, base, water and freeze durability of biologically-reinforced geopolymers, experiments were developed based on methodology presented in existing geopolymer durability papers [20].

Five different durability test were carried out. Four were 'soaking' tests: water, salt water, sulfuric acid and sodium hydroxide durability. The fifth was a 'cycle' test: samples subjected to a cycle of frozen and thawed water.

Each of the 'soaking' tests were carried out over a four-week period. In each instance, twelve 8 wt% abaca samples were placed into the respective solutions for 14 days. After those 14 days, the samples were removed and allowed to dry at ambient room conditions for another 14 days. In the case of the 'cycle' test, twelve 8 wt% samples were placed into deionized water. For the next 14 days, the water alternated spending 24 hours in a freezer at -4°C and 24 hours at ambient room temperature. After those 14 days, the samples were removed and allowed to dry at ambient room conditions for another 14 days.

The solutions for the durability tests were prepared in the following ways. "Water durability" samples were merely added to deionized water. "Salt water durability" samples were subjected to a mixture of deionized water and sodium chloride. The solution contained 7.5 wt% sodium chloride. "Sodium hydroxide durability" samples were placed in a 1M NaOH solution

made by mixing NaOH pellets with deionized water. Finally, "sulfuric acid durability" samples were subjected to 1M H_2SO_4 prepared by diluting concentrated sulfuric acid with deionized water.

In each of the above experiments, samples were immediately mechanically tested at the end of their respective 28-day period. These mechanical tests were carried out in an identical fashion as the original abaca fiber reinforced potassium geopolymer samples. This new data was compared to those original samples, and across all the sample groups in the durability study, then plotted thusly.

2.3.3 Heat Treatment Testing

In order to determine the heat sensitivity of the highest solids loading samples, abaca reinforced potassium geopolymer samples were subjected to a number of different heating profiles. These heating profiles maxed out at 50°C, 100°C, 150°C, 200°C and 250°C. One sample was subjected to 300°C in order to confirm that the composite would become structurally compromised at that temperature.

In the case of each heating profile, the dozen samples were placed on an alumina vessel without touching each other. The samples were then placed in a Fisher Scientific Isotemp Programmable Muffle Furnace (Fisher Scientific, Pittsburgh, PA) and heated at 1°C per minute until the maximum temperature was reached. At that point, the oven held the maximum temperature for once hour. After the hold, the oven decreased the temperature by 1°C per minute until room temperature was reached.

As with the durability testing, samples were removed after reaching room temperature and mechanically tested in four-point flexure. The data gathered was plotted and compared to original and durability study data.

To better understand when abaca fiber thermally degrades (and how effectively potassium geopolymer thermally shielded its reinforcement), pure abaca fiber was treated to identical heat profiles. The abaca fiber showed little visible change until the 200°C samples, and was completely burnt by the 250°C heating profile. New abaca fiber was treated to a profile that went to 240°C in order to more accurately predict the burning point of pure abaca fiber.

2.3.4 SEM Analysis

From each sample group, a fracture surface from one sample was analyzed in a scanning electron microscope (SEM). Three main groups were studied: plain abaca samples (0, 2, 4, 6 and 8 wt%), heat treatment samples (50°C, 100°C, 150°C, 200°C, 250°C and 300°C) and durability tested samples (water, salt water, sulfuric acid, sodium hydroxide and freeze cycle). When a sample from each group was selected, the surface was removed from the bulk of the sample with a circular saw approximately 1 cm from the fracture surface. These fracture surfaces were then Au-sputter coated in a Denton Desktop Pro (Denton Vacuum, Moorestown, NJ).

Upon removal from the sputter coater, samples were loaded into a Neoscope 6000 Plus SEM (Jeol, Peabody, MA). Samples were individually analyzed. The samples were subjected to "high-vacuum" mode, and analyzed at 15 kV. For each of the sixteen samples analyzed, four different magnifications were used: x24, x100, x500 and x1000. Images were then inspected for abnormalities, fiber debonding, fiber pullout, and other composite phenomena.

2.3.5 XRD Analysis

X-ray Diffraction (XRD) was used in two separate instances in this study. The first was to determine if potassium geopolymer had truly been prepared by comparing its XRD profile to that of a known potassium geopolymer with fully reacted metakaolin. If the metakaolin in the sample was not fully reacted, the amorphous humps noted in the XRD patterns would have been offset.

To prepare potassium geopolymer for XRD analysis, a segment of approximately 1 cm^3 of pure potassium geopolymer was taken and placed in a mortar and pestle. The geopolymer was hand-ground to a very fine powder with the consistency of baking flour. The powder was then placed on a slide and leveled per standard XRD practices.

The sample and its holder were placed into a Siemens Bruker 5000 X-ray diffractometer (Siemens, Munich, Germany). Settings were as follows: scan from two theta values of 10° to 45°, step size 0.01°, time/step 0.5 seconds. Scans were then analyzed and compared to existing patterns.

The second instance XRD was used was to identify an unknown crystal that appeared on the potassium geopolymer-abaca composite during sulfuric acid durability testing. The crystals were removed from the composite with a gloved hand, and any excess geopolymer stuck to the crystals was carefully scraped off with a needle.

The crystals were ground in a mortar and pestle similarly to the potassium geopolymer, and placed into the same XRD with identical step-size and time/step settings. The only difference was the two theta range was a broader 0° to 60°. The pattern generated was compared in a database to determine the chemical composition of the crystals.

CHAPTER 3

RESULTS AND DISCUSSION

3.1 Cork Particle Reinforced Sodium Geopolymer

Results from the cork particle reinforced sodium geopolymer mechanical tests were obtained from the Instron testing frame. Noted below in Fig. 5, the introduction of more and more cork particles did indeed increase the flexural strength of the composite in four-point bending. This increase is called into question due to the large amount of variance noted in Fig. 5, due in no small part to the six samples in each sample group.

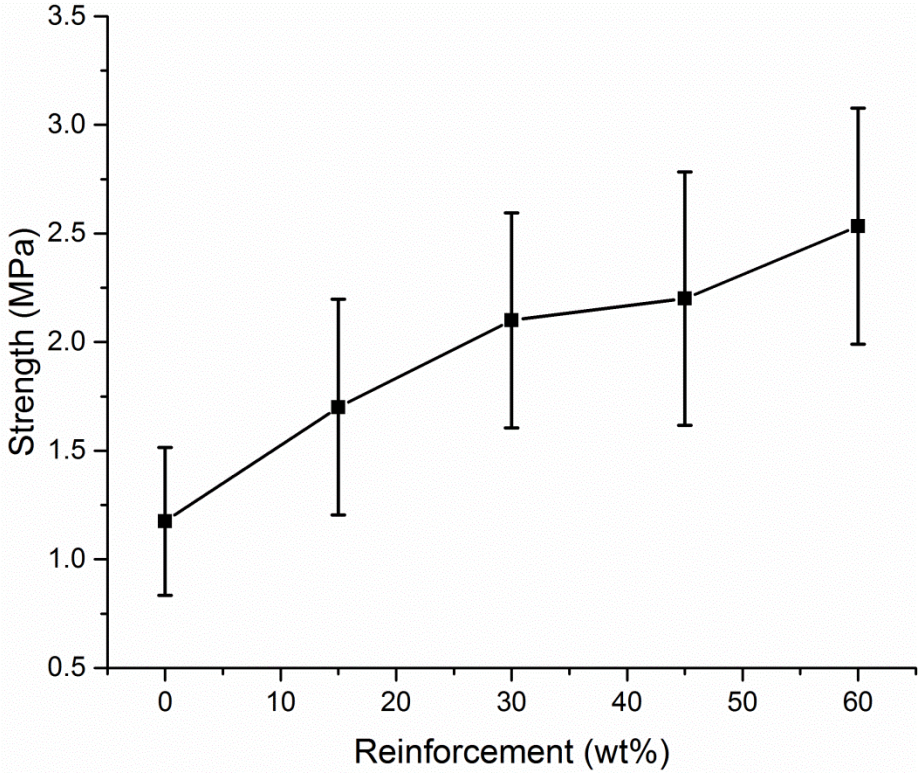

Fig. 5. Four-point flexural strength vs. wt% of cork particles in sodium geopolymer [19].

The highest solids loading flexural strength (~2.5 MPa), while unremarkable compared to other systems in this study, was still about double that of unreinforced sodium geopolymer. This

indicated good adhesion of the geopolymer to the reinforcement. A reason for the less-than-desirable increase in flexural strength might have been the size of the samples: these 1”x1”x6” samples were relatively large (compared to later studies), which statistically allowed for a greater chance of critical flaws to exist within the sample. The slight increase in flexural strength was also attributed to the fact that the nature of the cork particles allowed more than half of the composite weight to be reinforcement. Since the cork was in particle form (seen below in Fig. 6) on the millimeter scale, it was simple to pack a large quantity of reinforcement into the 1”x1”x6” molds. This was not the case for later studies involving fibrous reinforcement, which tended to self-interact, making the molding stages more difficult.

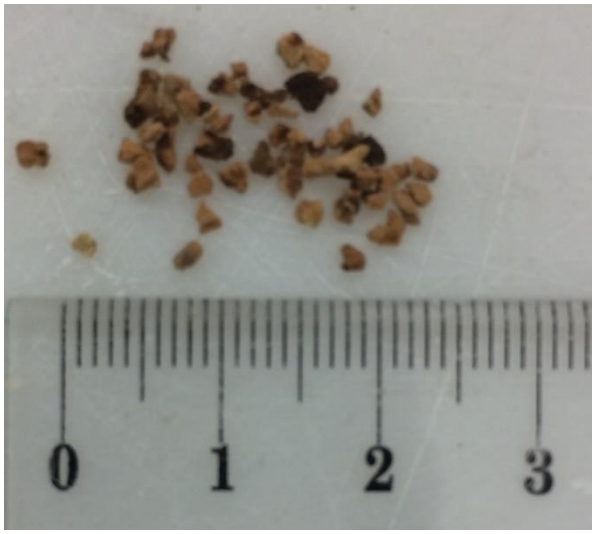

Fig. 6. Picture of cork particles used in sodium geopolymer composite (scale in picture is cm).

While the cork did not impress with its effect on the flexural strength of the composite, it did yield some interesting strain to failure properties. In normal structural ceramics, strain to failure is usually noted at about 0.1% strain. The cork reinforced composites with the highest solids loading managed an average flexural strain to failure of 0.9%. Once again, this unique

property was attributed to the fact that so much cork could be added into these composites, making it increasingly more cork-like and less brittle [19].

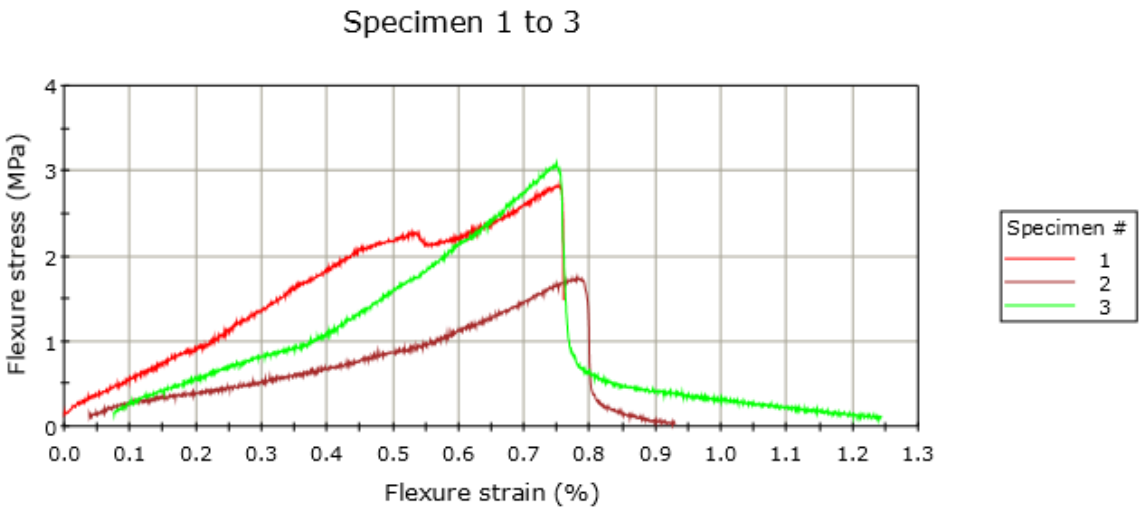

Fig. 7. Flexural stress vs. flexural strain plot for the first three samples of highest solids loading.

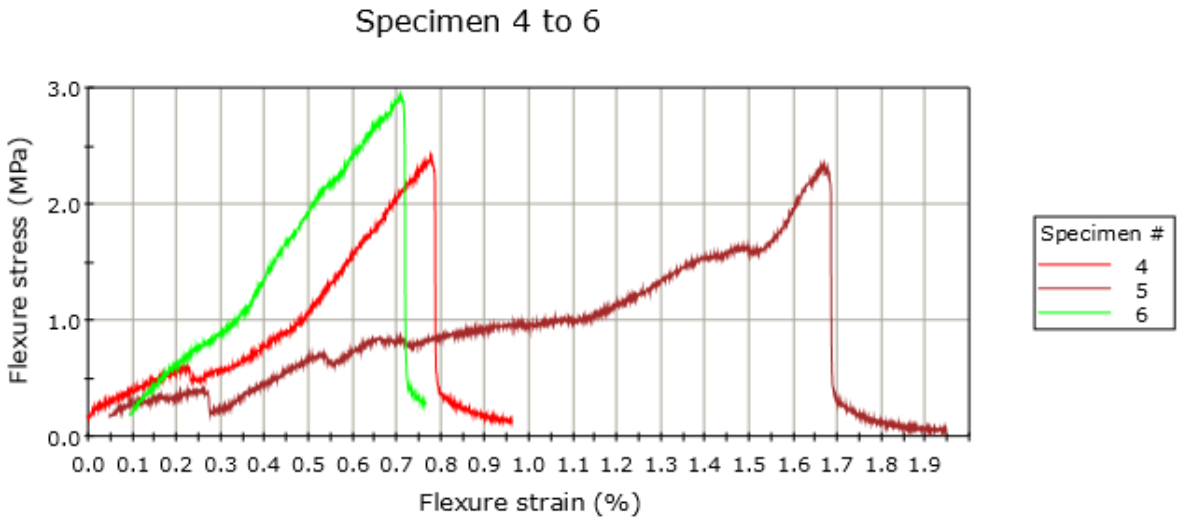

Fig. 8. Flexural stress vs. flexural strain plot for the final three samples of highest solids loading.

All in all, the cork particle reinforced sodium geopolymer did show an increase in flexural strength with the addition of the plant matter. More interestingly, it also vastly increased

the strain to failure that is normally seen in brittle ceramic materials. Ultimately, it was determined that a cork particle reinforced sodium geopolymer system, while interesting, was not a structurally feasible material for more ceramic-like applications. Thus, the study moved on to a new biological reinforcement of choice: abaca fibers.

3.2 Abaca Fiber Reinforced Sodium Geopolymer

After the cork study, an attempt was made to create a geopolymer composite with greater strengths than previously seen. It was hypothesized that a reinforcement with extremely high aspect ratio would provide the most load transfer per unit weight, allowing for composite strengths to increase. Abaca, as an extremely strong fiber, seemed liked the perfect biological reinforcement to choose.

As with the cork study, results from the mechanical testing of the abaca fiber reinforced sodium geopolymer were collected via the Instron testing frame. Seen in Fig. 9, it was again noted that an increase in biological reinforcement increased the flexural strength of the composite in question.

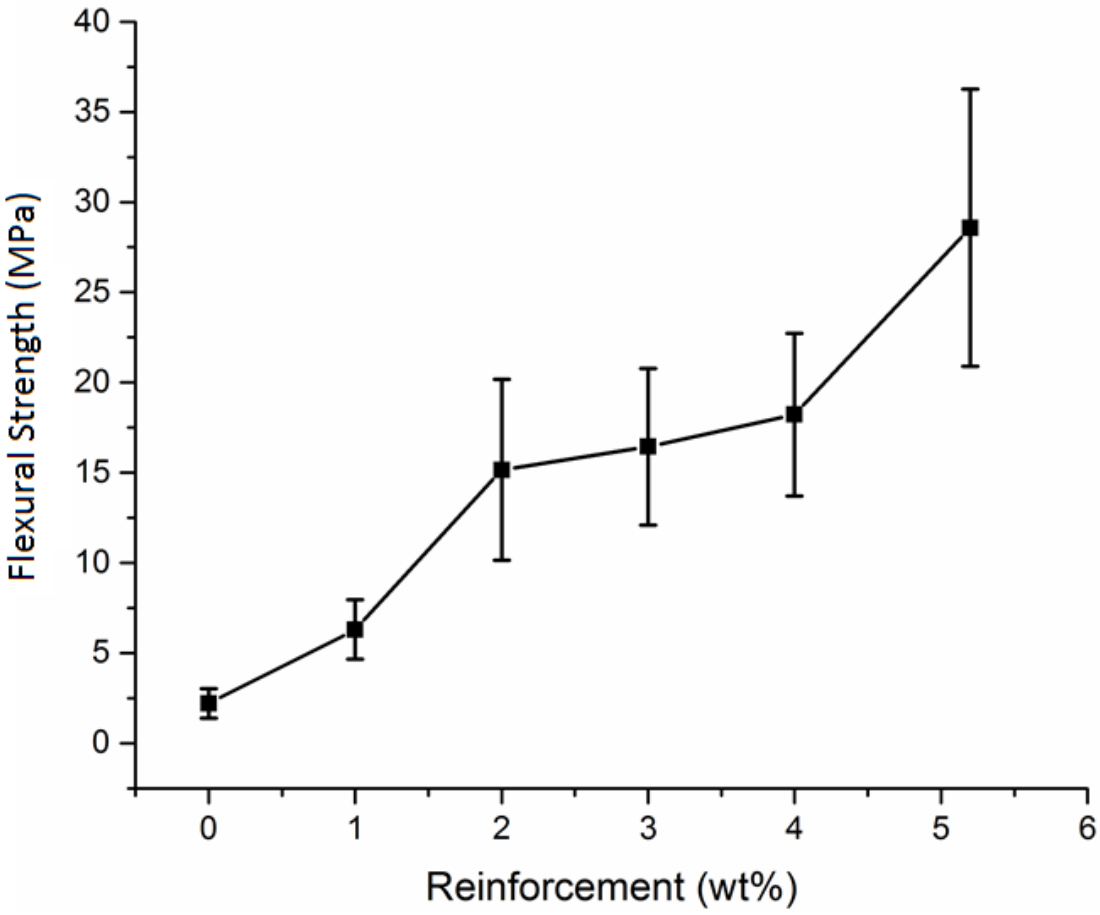

Fig. 9. Four-point flexural strength for different wt% of abaca fibers in sodium geopolymer.

Variance in sample groups increased as wt% reinforcement increased, but unlike in the cork study, a marked increase in strength was noted. Whereas unreinforced sodium geopolymer had an average flexural strength of ~2.5 MPa, the maximum fiber reinforced composite exhibited flexural strengths (~27 MPa) more than ten times greater than unreinforced composites.

These impressive increases in flexural strengths (when compared to the cork study) were attributed to two main features: the strength of the fibers themselves, and the aspect ratio of the fibers. Abaca fibers are one of the strongest natural fibers in the world, found to have tensile strengths exceeding 500 MPa [21]. This obviously was an important distinction when comparing

composites containing relatively delicate cork particles. Furthermore, generally spherical cork particles did not maximize the surface area of reinforcement in contact with geopolymer per unit weight. Abaca fibers, however, were perfectly suited for such contact.

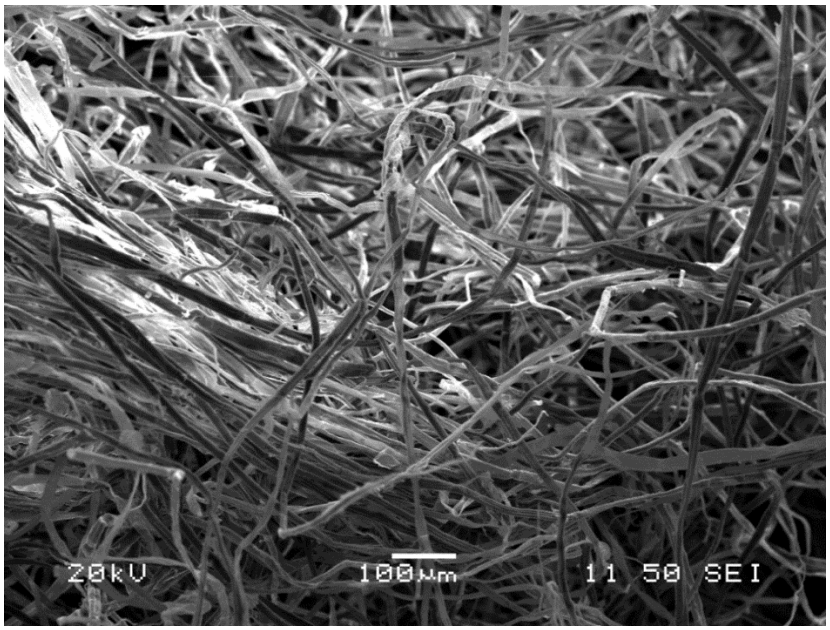

Fig. 10. SEM micrograph of abaca fibers used in geopolymer composites.

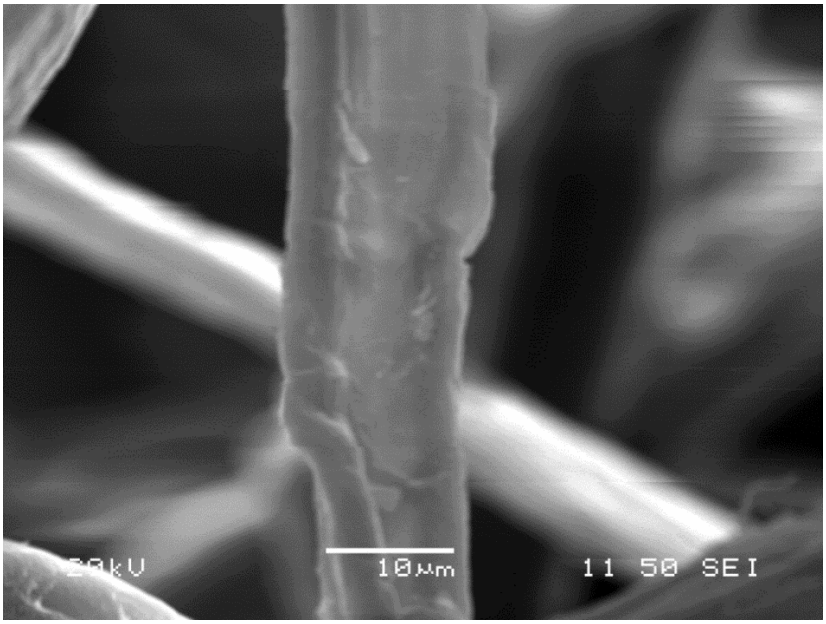

Fig. 11. SEM micrograph of a single abaca fiber.

Fig. 10 demonstrates the extreme aspect ratio inherent to the abaca fibers, while Fig. 11 shows the scale of abaca fiber diameters to be around 10 μm. Fig. 10 also demonstrates the degree of entanglement that the abaca fibers experience, discussed further in the abaca fiber reinforced potassium geopolymer system.

SEM micrographs were also taken of the fracture surfaces of various samples to better understand the modes of failure, and how well abaca fibers were dispersed within the geopolymer matrix.

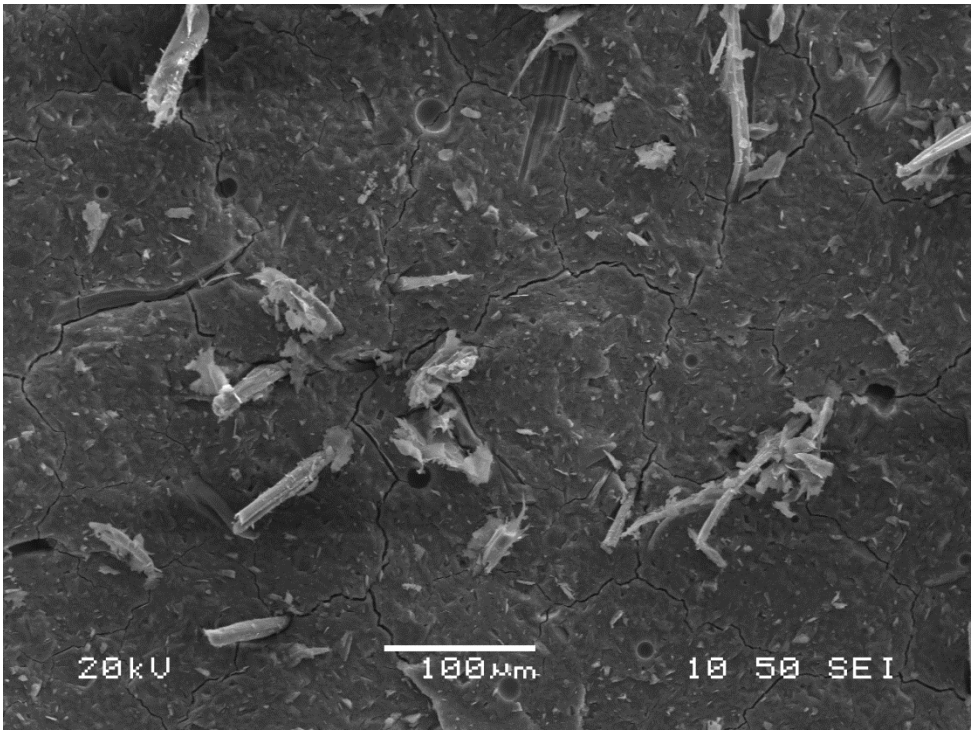

Fig. 12. Fracture surface of a 1 wt% abaca fiber reinforced sodium geopolymer composite.

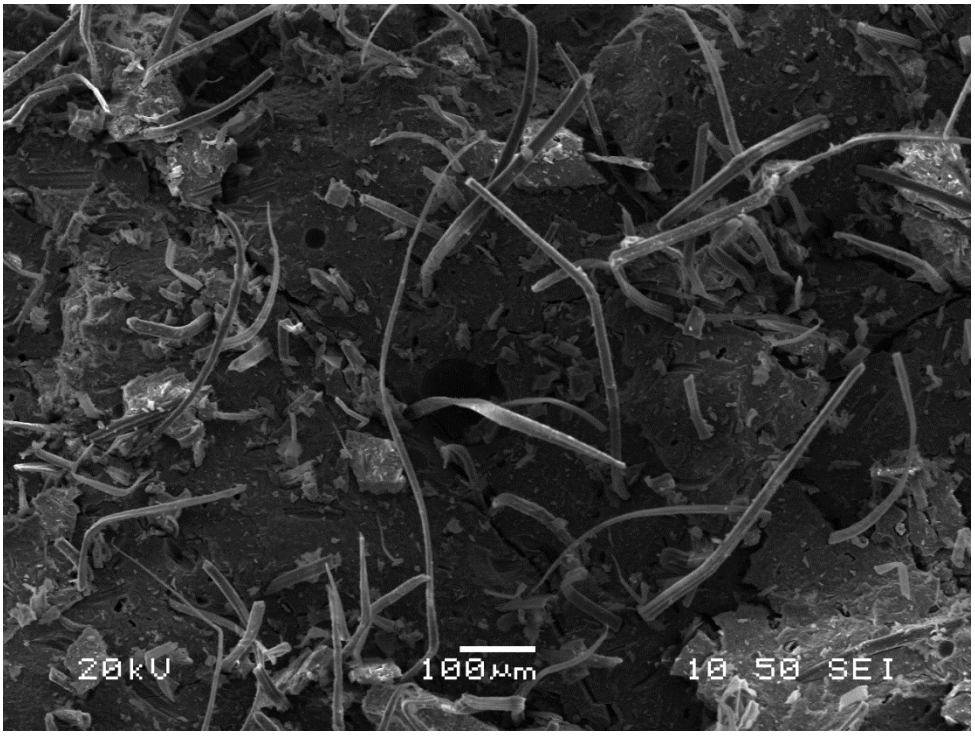

Fig. 13. Fracture surface of a 3 wt% abaca fiber reinforced sodium geopolymer composite.

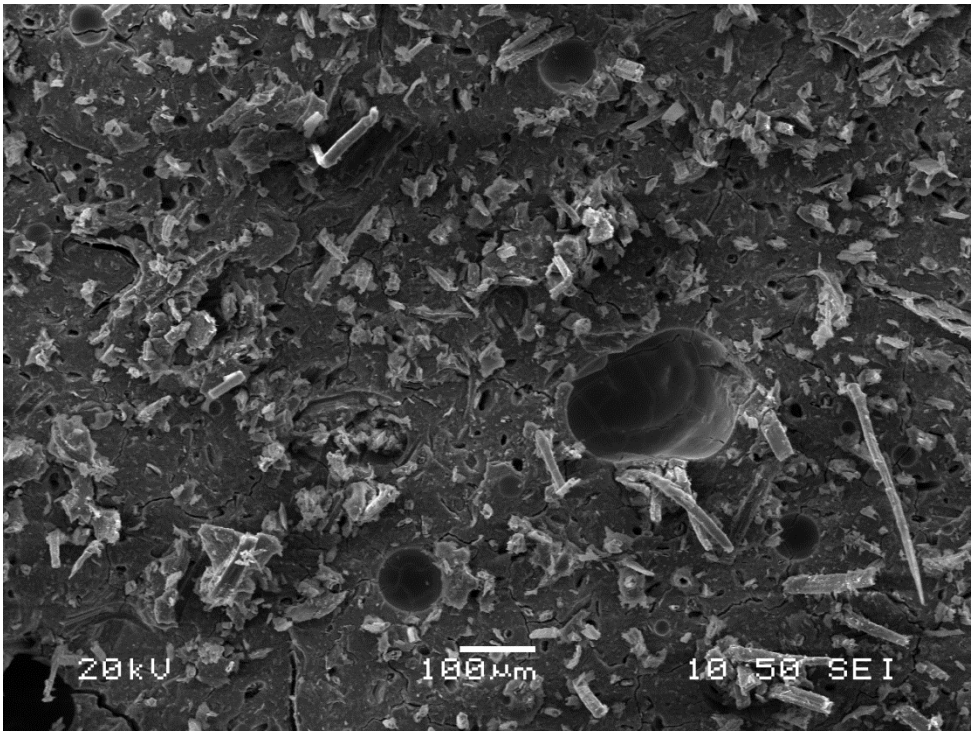

Fig. 14. Fracture surface of a 5 wt% abaca fiber reinforced sodium geopolymer composite.

As expected, images in the progression from 1 wt% abaca to 5 wt% abaca showed a proportional increase in abaca fibers. Abaca fibers seemed to distribute themselves throughout the composite in a relatively uniform fashion. This was important, as it was not known how the fibers would interact when placed within the sodium geopolymer matrix and forced into the molds.

Fiber pullout is visible in all three reinforcement groups, indicating some degree of composite toughening took place during the mechanical analysis. Microcracks can be seen traversing around fibers, another indication of toughening throughout the testing process. Finally, larger flaws can be seen (particularly in the 5 wt% image), likely a result of the difficult nature associated with forcing the composite into molds due to fiber entanglement.

All in all, the abaca reinforced sodium geopolymer study was extremely promising. Maximum fiber reinforcement yielded flexural strengths more than ten times greater than that of unreinforced sodium geopolymer. Clearly, the addition of abaca fibers steadily increased the strength of the composite. To reach even greater strengths, attempts were made to increase the amount of abaca fiber that could be incorporated into geopolymer composites. Those attempts constitute the remainder of this study.

3.3 Abaca Fiber Reinforced Potassium Geopolymer

3.3.1 Untreated Abaca Fiber Reinforced Potassium Geopolymer

It was hypothesized that potassium geopolymer, which is less viscous than sodium geopolymer, would allow more abaca fibers to be added to a geopolymer matrix. By increasing the weight percent of abaca fibers in the composite, it was further hypothesized that even greater flexural strengths could be attained.

It was indeed found that potassium geopolymer could handle more abaca fibers before reaching its limit of workability. That limit was found to be 8 wt% abaca fibers. In order to increase the confidence in results from this study, at least twelve samples were made in each sample group. Results from the flexural testing of the abaca reinforced potassium geopolymer can be seen in Fig. 15.

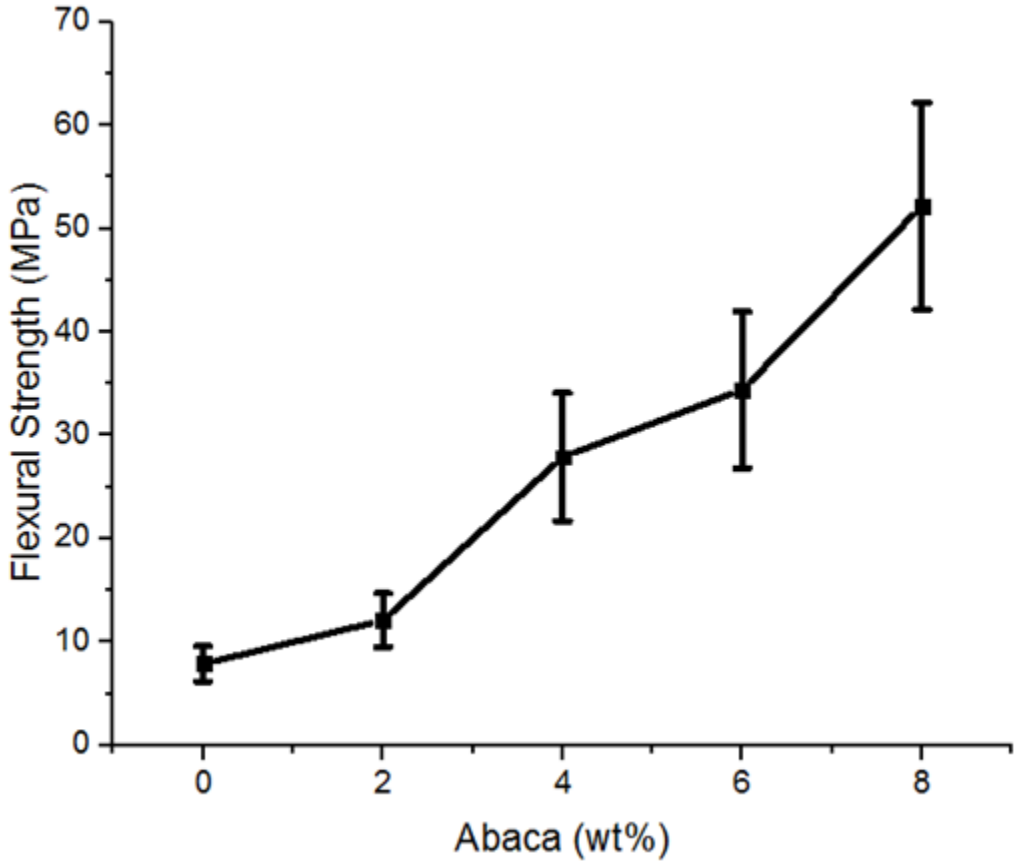

Fig 15. Flexural strength vs. abaca weight percent in potassium geopolymer composites.

Clearly, the addition of abaca fiber had a large impact on the flexural strengths of the composite samples. From unreinforced sample strengths around ~7 MPa, composite strength continued to increase with added abaca fiber to above 50 MPa at the 8 wt% abaca level. The increased number of samples in each group did help to reduce the variance in the less reinforced

samples, but large variance was still noted at the highest reinforcement. As with the other two studies, variance increased as fiber reinforcement increased.

Despite this variance, an average flexural strength of 50 MPa was regarded as a success. The flexural strength exceeded the average flexural strength of unreinforced geopolymers (2-7 MPa) by nearly an order of magnitude. With this new composite labeled a 'success', attempts were made to characterize its properties, with emphasis on its durability and sensitivity to heat treatments.

3.3.2 Durability of Abaca Fiber Reinforced Potassium Geopolymer

Two types of durability testing were conducted: tests where the samples were exposed to a constant environment (H_2SO_4, NaOH, water and salt water), and a test where the samples were exposed to a changing environment (freezing water cycle). As in the untreated abaca reinforced potassium geopolymer study, each group contained at least twelve samples. Samples used in durability testing were all fully reinforced with 8 wt% abaca fibers.

After 14 days of freezing and thawing, and another 14 days of drying, a picture was taken of a sample to determine if any macroscale physical changes had occurred to the sample, as seen below in Fig. 16.

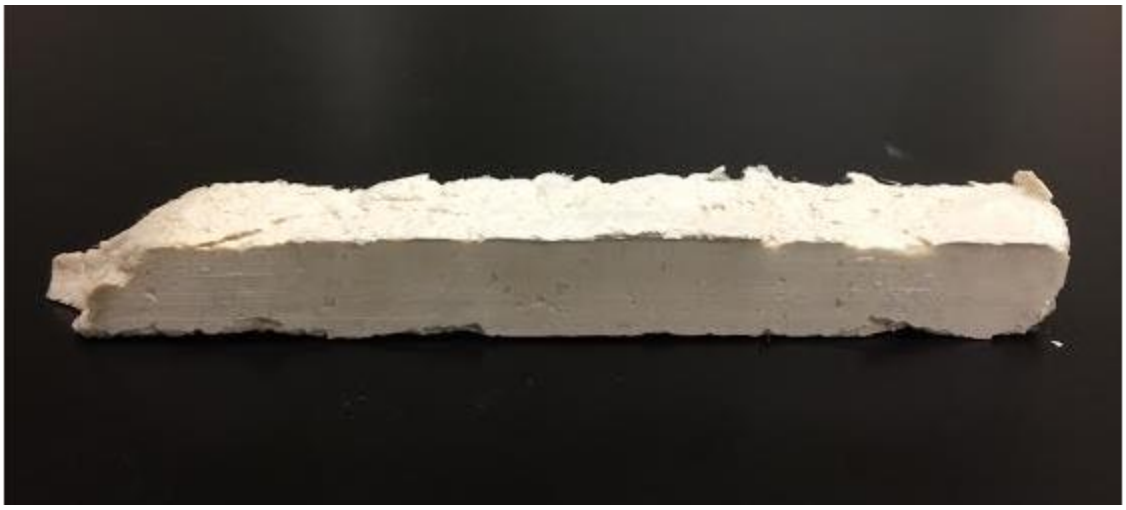

Fig. 16. 10 cm-long freeze cycle sample after 28-day durability testing period.

Fig. 16 shows that no major macroscale damage or discoloration was caused by the freeze cycle. Any imperfections noted on the edges existed previously as a result of the laborious molding process.

After the freeze cycle (and subsequent drying), the samples were subjected to mechanical testing as in previous studies. The result of that testing can be seen in Fig. 17.

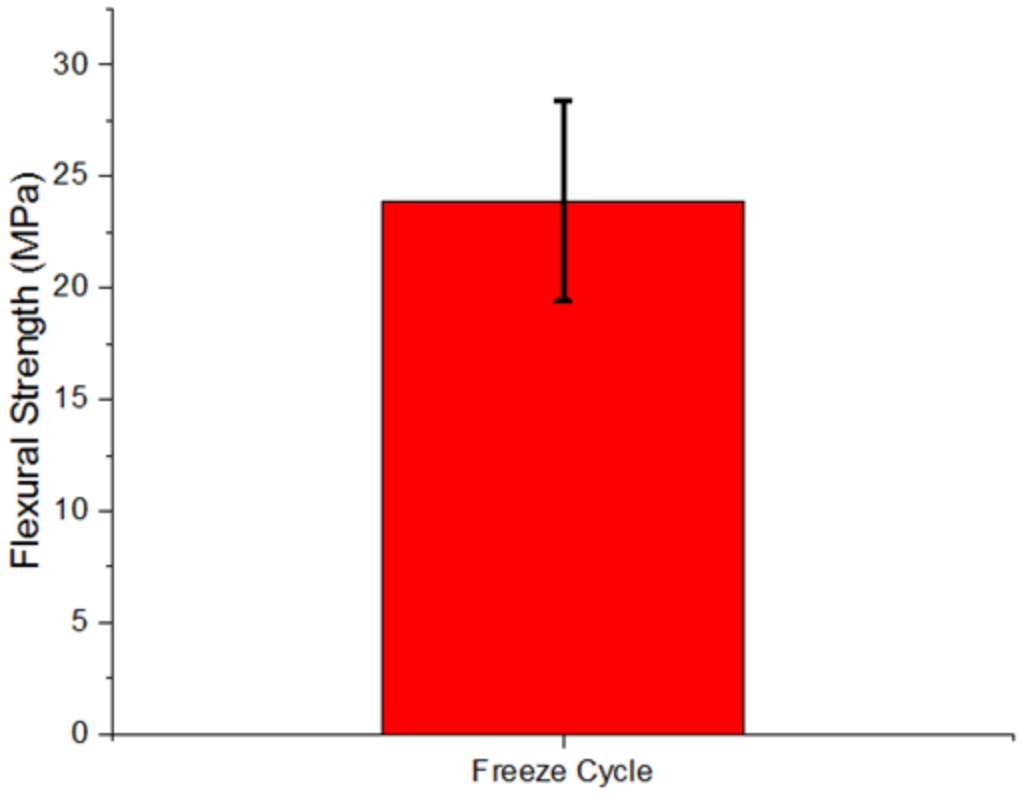

Fig. 17. Flexural strength of abaca fiber reinforced potassium geopolymer after freeze cycle.

Despite the lack of macroscale flaws as a result of the freeze cycle, the overall strength of the composite clearly suffered. As compared to the strength of untreated 8 wt% abaca fiber reinforced potassium geopolymer samples (~50 MPa), the strength of the freeze cycle samples was more than halved (~23 MPa). Microscale examination of the reasons attributed for this decrease in strength is carried out in the later SEM section.

Pictures were similarly taken of the samples in the unchanging environments after 14 days of soaking and 14 days of drying, pictured below.

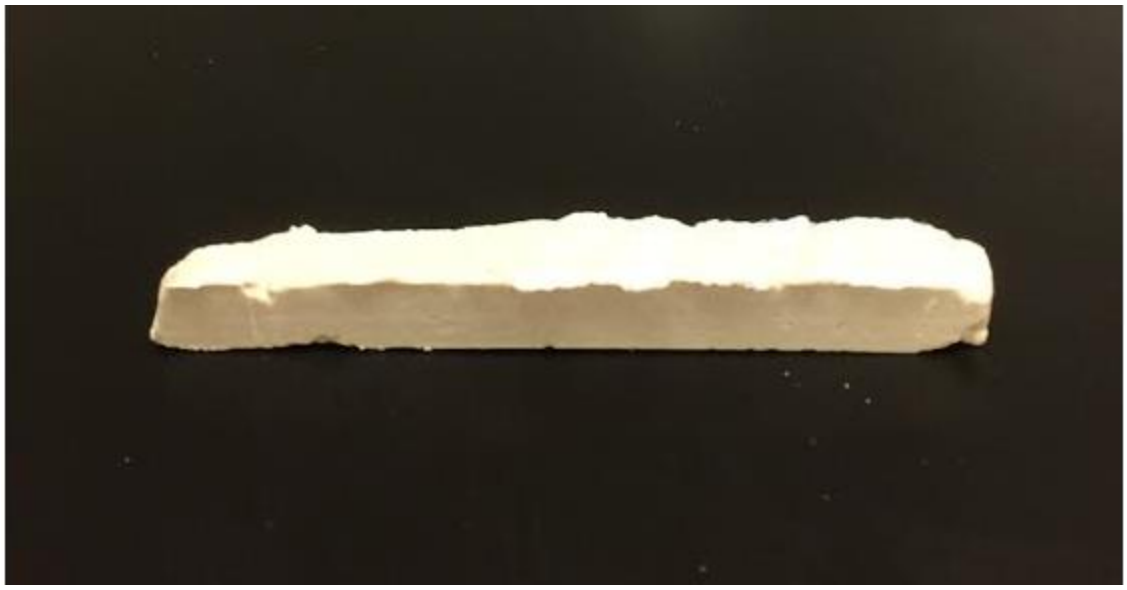

Fig. 18. 10 cm-long water durability sample after 28-day soaking period.

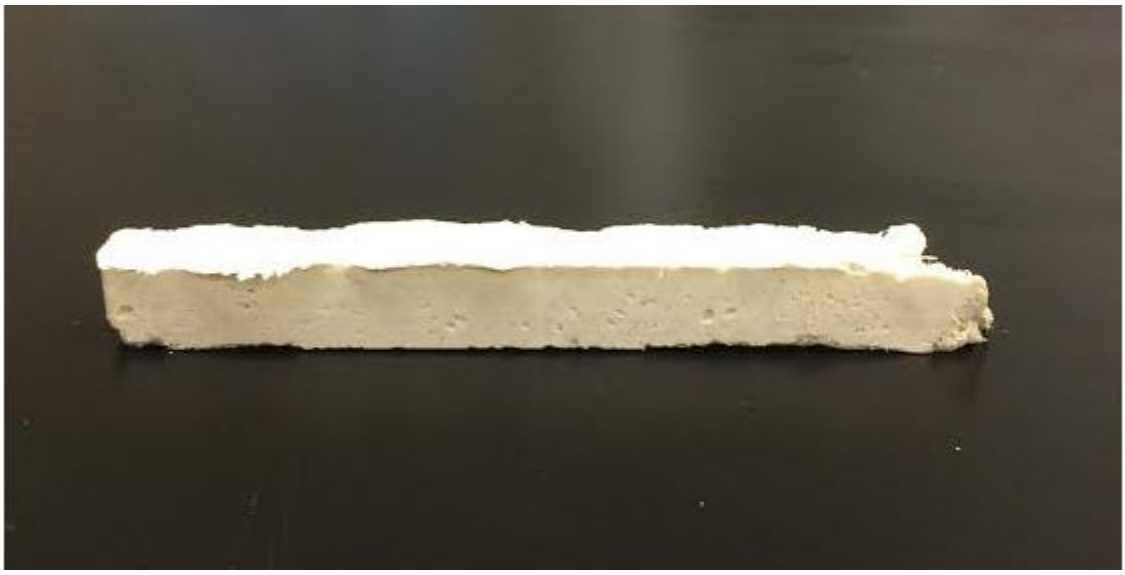

Fig. 19. 10 cm-long salt water durability sample after 28-day soaking period.

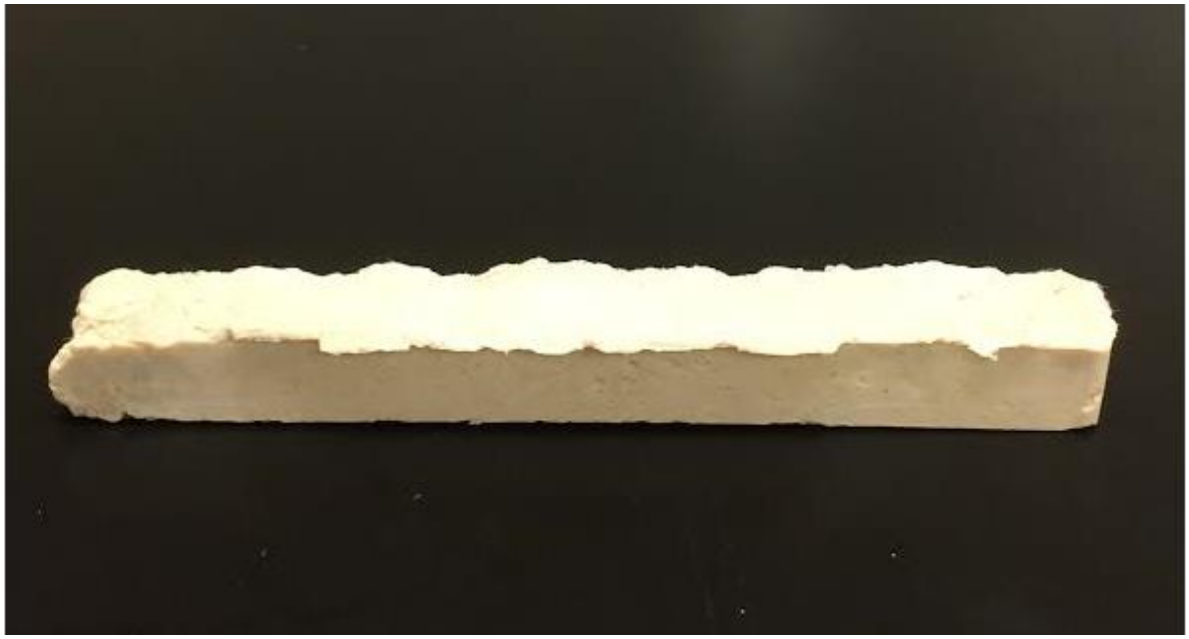

Fig. 20. 10 cm-long NaOH durability sample after 28-day soaking period.

Fig. 21. 10 cm-long H_2SO_4 durability sample after 28-day soaking period.

As with the freeze cycle samples, water, salt water and NaOH durability testing failed to yield any obvious macroscopic defects as a result of their environments. H_2SO_4 testing, however, caused samples to swell up, crack, and become extremely fragile. Because of this, H_2SO_4 durability samples were not mechanically tested. Mechanical data for the other groups is presented below.

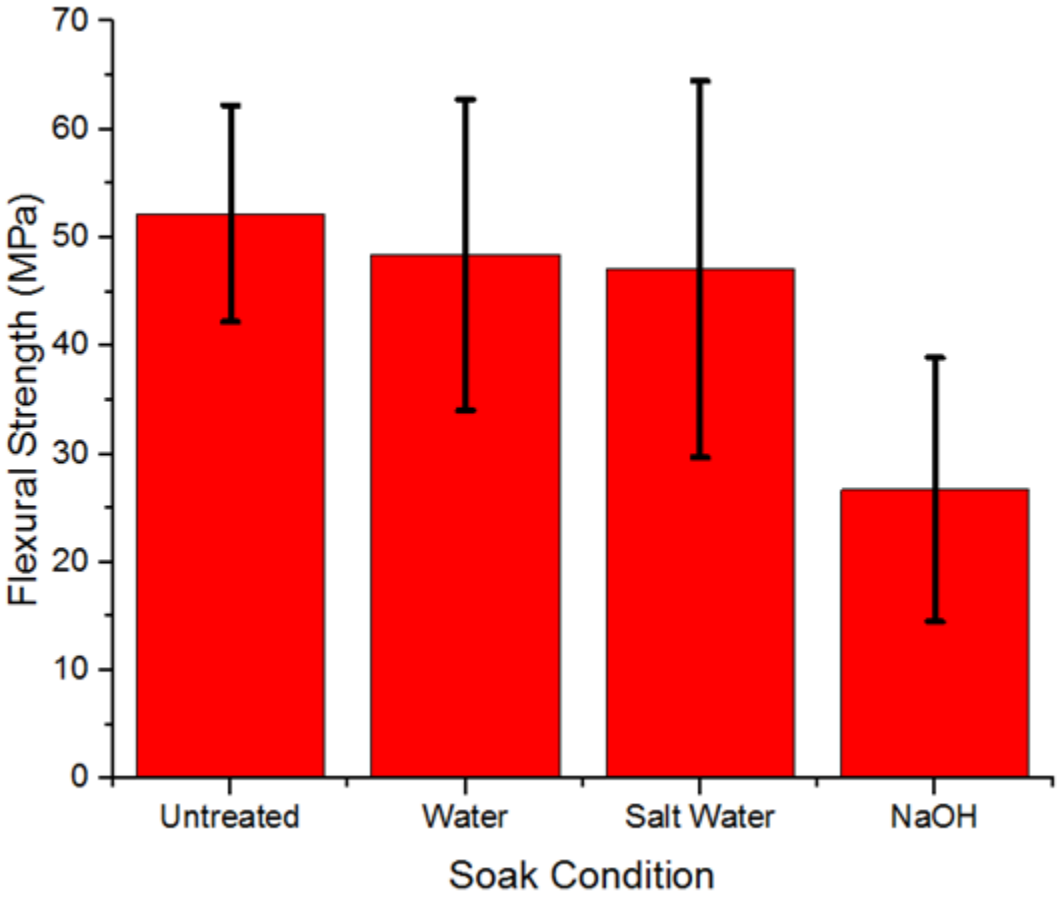

Fig. 22. Flexural strength of durability-tested abaca-potassium geopolymer composite.

Water and salt water durability testing did very little to decrease the flexural strength of the abaca fiber reinforced potassium geopolymer samples. This was viewed as

promising for structural or maritime applications of the composite, which might be frequently exposed to such environments. However, NaOH durability testing nearly halved the flexural strengths of the composite, similar to the results seen in the freeze cycle durability test.

As mentioned before, H_2SO_4 samples were not mechanically tested due to their negligible strength. Upon closer inspection, it was noted that the crevices within the H_2SO_4 sample contained a number of clear crystals, pictured below.

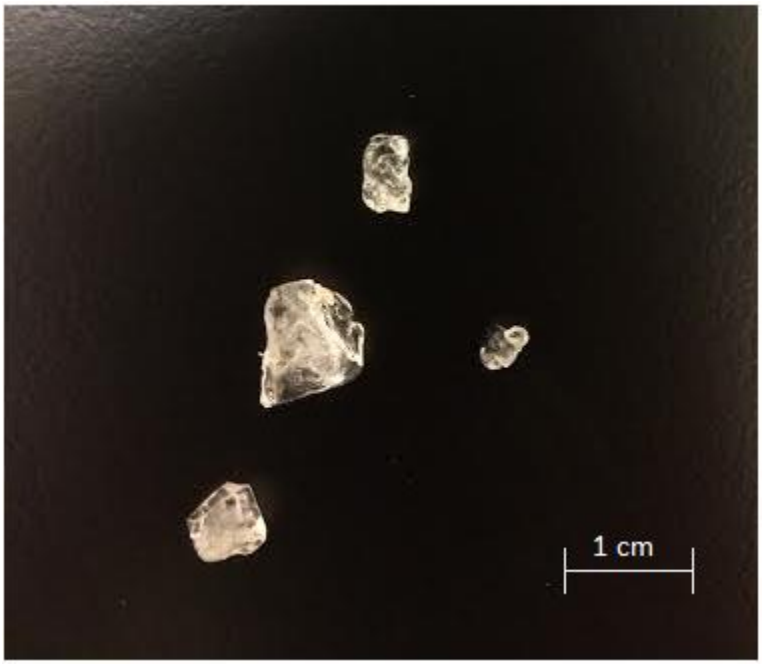

Fig 23. Crystals obtained from H_2SO_4 durability tested samples.

These crystals indicated that a chemical reaction had taken place during the durability testing, effectively ruining the samples. To identify the composition of these crystals, they were ground and subjected to XRD analysis. The results are shown below.

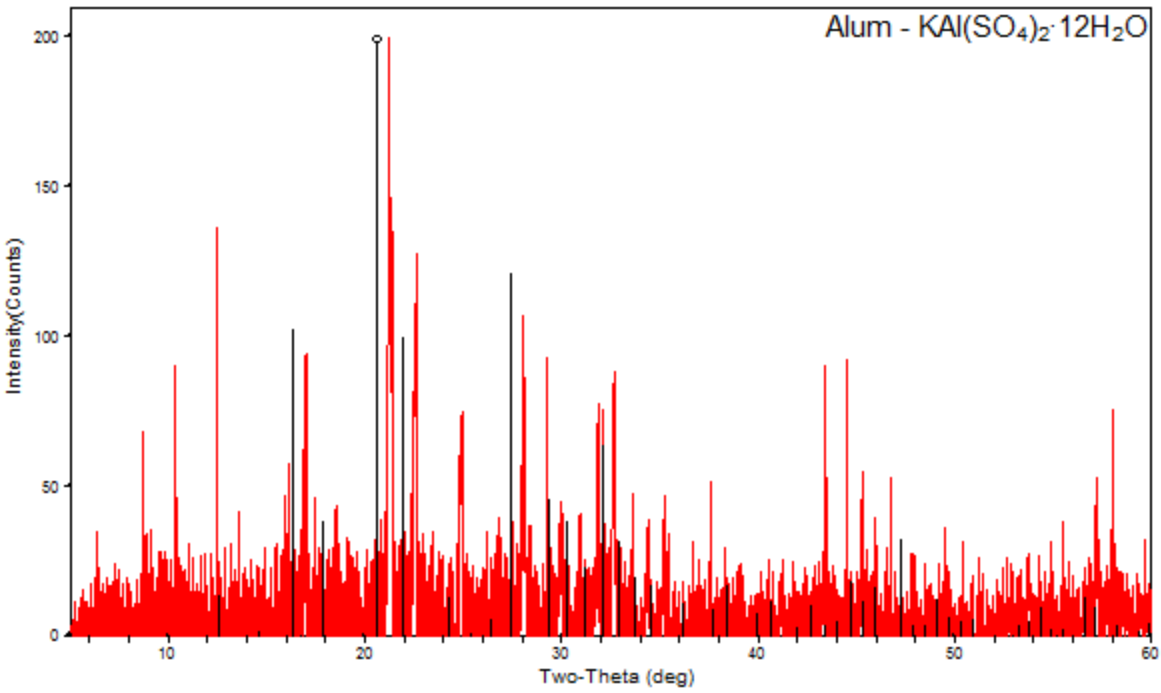

Fig. 24. XRD analysis of crystals determined to be $KAl(SO_4)_2 \cdot 12H_2O$.

XRD results best matched with alum, which has the chemical formula $KAl(SO_4)_2 \cdot 12H_2O$. The ~0.5 degree shift in Fig. 24 was likely due to tilt in the slide holder of the XRD. To confirm this result, a simple stoichiometric exercise was carried out: the ratio of the molar mass of anhydrous alum (258. 13 g/mol) and alum (462.24 g/mol) was determined to be 0.558. By weighing a large crystal before heating (0.0732 g) and after an hour of being subjected to 110°C (0.0424 g), the experimental ratio was found to be 0.579. This was within 4% of the theoretical value, thereby confirming the crystal as alum.

3.3.3 Heat Treatment of Abaca Fiber Reinforced Potassium Geopolymer

To test the heat resistance of the abaca fiber reinforced potassium geopolymer composite, samples were subjected to a variety of temperatures then mechanically tested as before. Once

more, each sample group contained a minimum of twelve samples, and pictures of samples were taken before mechanical testing for qualitative analysis, seen below.

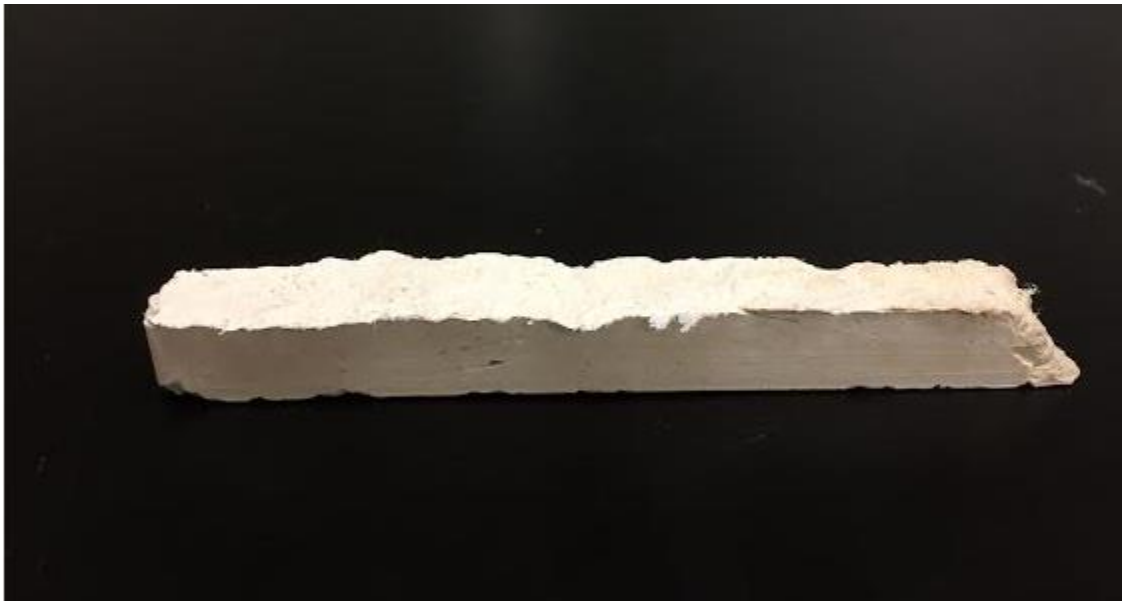

Fig. 25. 10 cm-long 100°C heat treated sample.

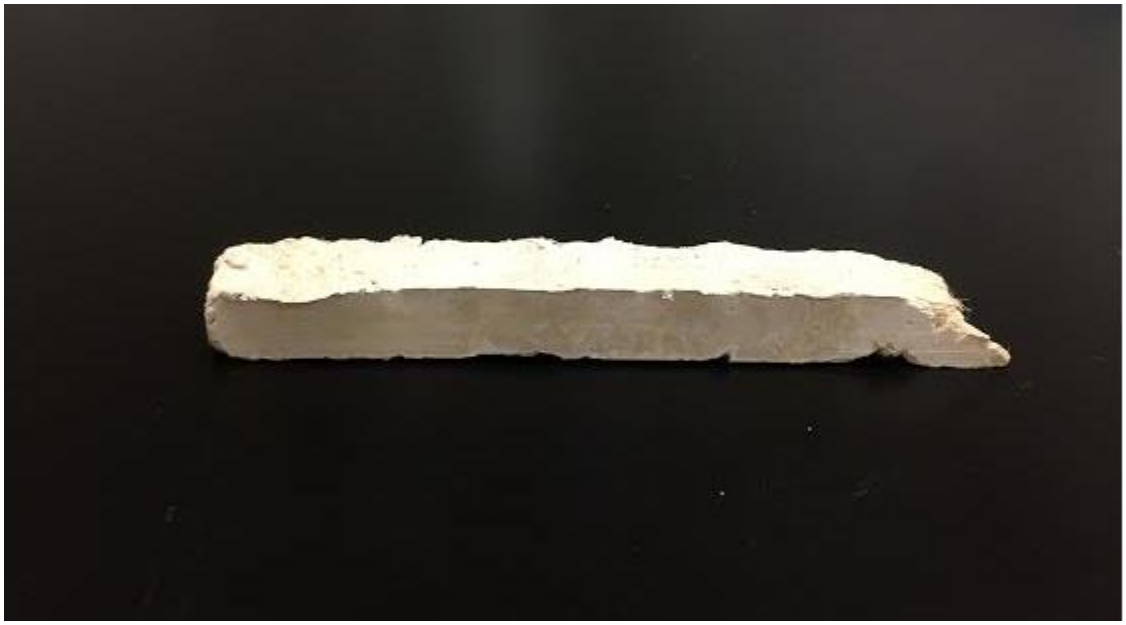

Fig. 26. 10 cm-long 150°C heat treated sample.

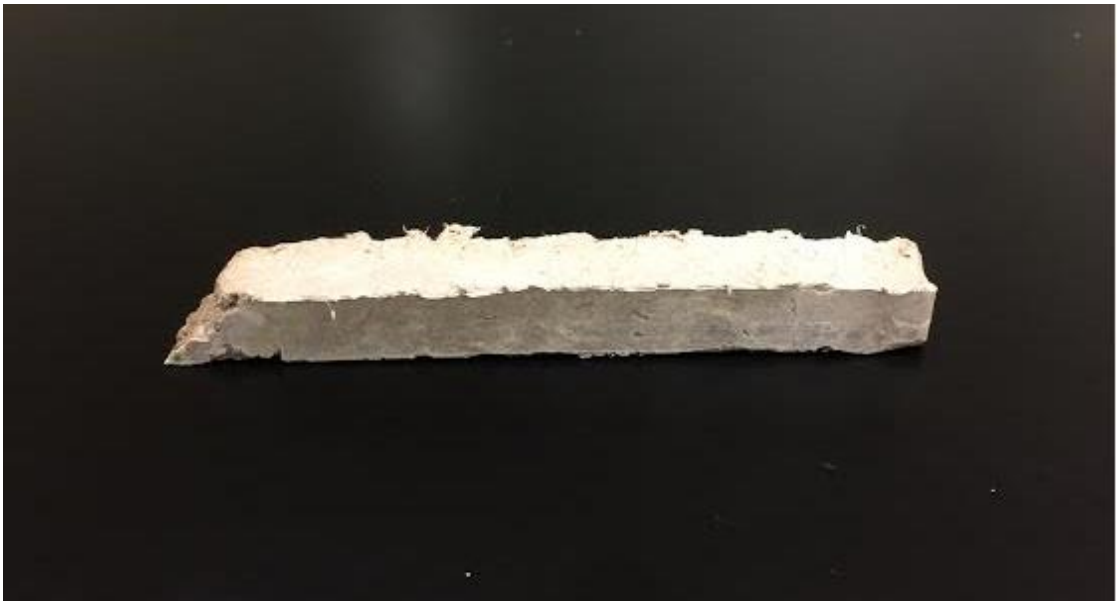

Fig. 27. 10 cm-long 200°C heat treated sample.

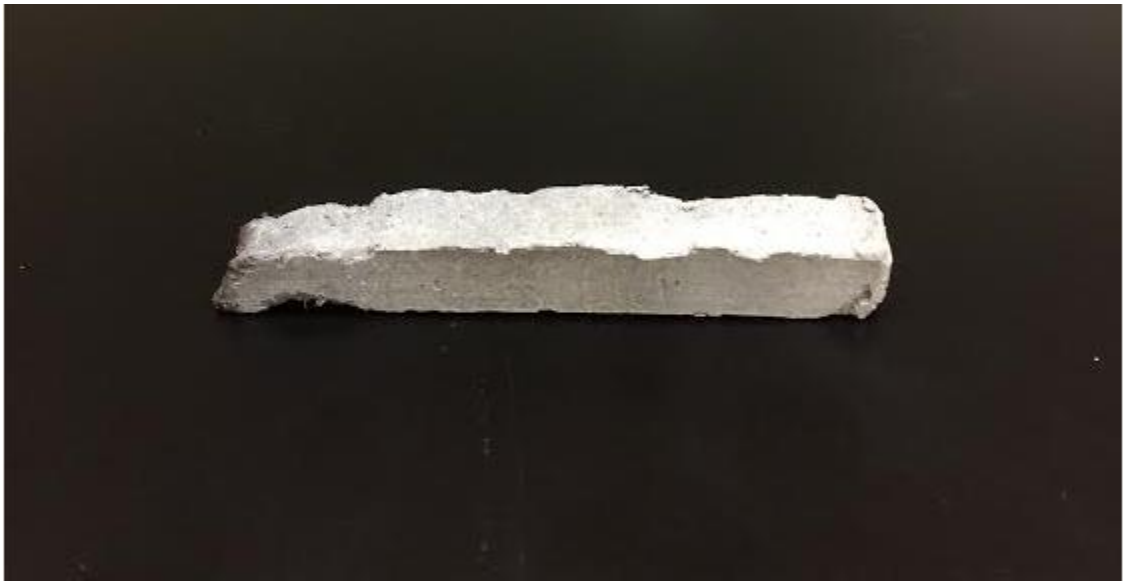

Fig. 28. 10 cm-long 250°C heat treated sample.

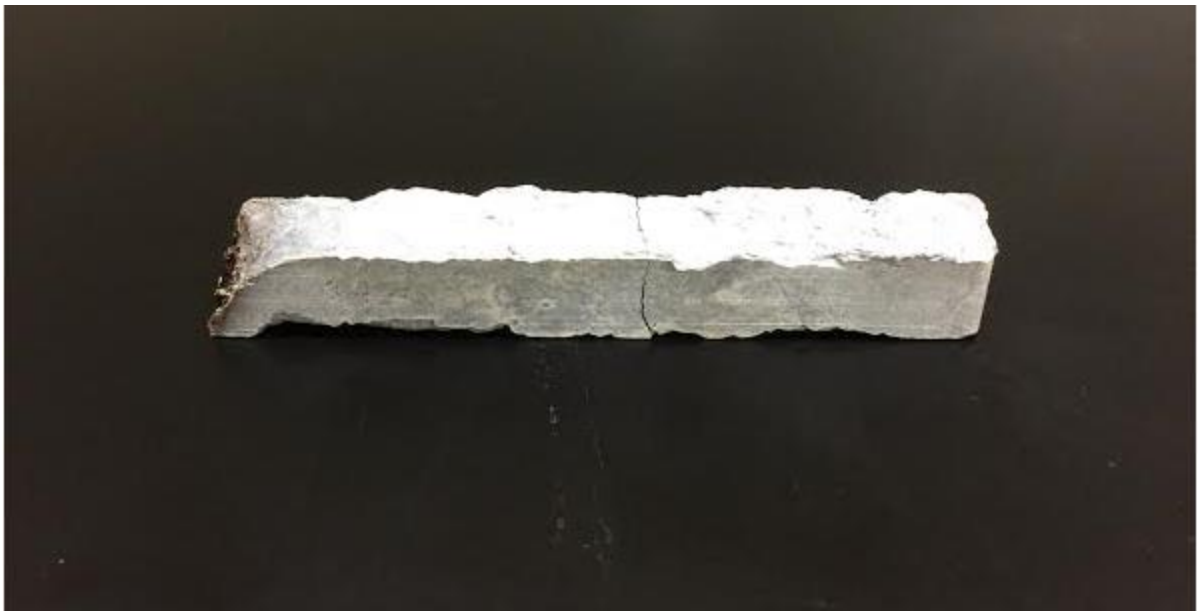

Fig. 29. 10 cm-long 300°C heat treated sample (broken during removal from oven).

Samples appeared physically unchanged through the 100°C and 150°C tests, maintaining their pale color with protruding fibers seemingly unaffected. At the 200°C test, samples began transitioning from pale to a chalky gray, indicating some sort of chemical change. This trend continued and became more extreme in the 250°C and 300°C samples, accompanied by the burning of exposed fibers at the ends of samples. The color change in the samples was likely due to a combination of dehydration of the geopolymer and burning of the fibrous biological reinforcement.

To better understand the heat sensitivity of abaca fiber, ground fiber was subjected to a series of heat treatments until it completely burned, seen below.

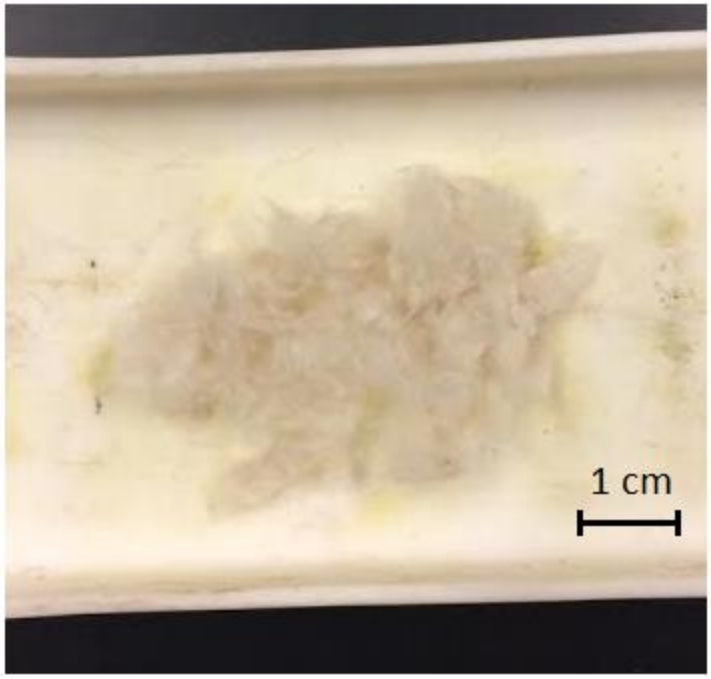

Fig. 30. Abaca fiber before exposure to any temperature testing.

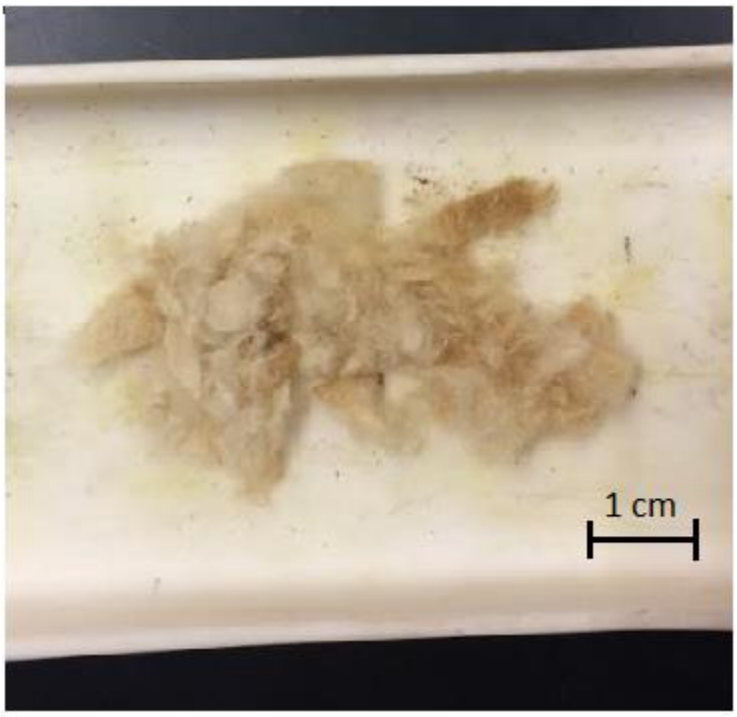

Fig 31. Abaca fiber after exposure to 225°C.

Fig 32. Abaca fiber after exposure to 250°C.

Very little discoloration was noted when the fiber was heated to 200°C. At 225°C, some browning occurred on the fringes of the fiber. By 250°C, the fiber was nearly completed burnt, and clearly past its burning point. In order to better determine the temperature at which abaca fiber began to burn, a final test was conducted at 240°C, pictured below.

Fig. 33. Abaca fiber after exposure to 240°C.

While the abaca fiber showed signs of burning, it was not reduced to the extreme extent seen at 250°C. Due to this, it was determined that the burning point of the abaca fibers was somewhere between 240°C and 250°C.

Thermally treated abaca fiber reinforced potassium geopolymer samples were mechanically tested as before, the results of which can be seen below.

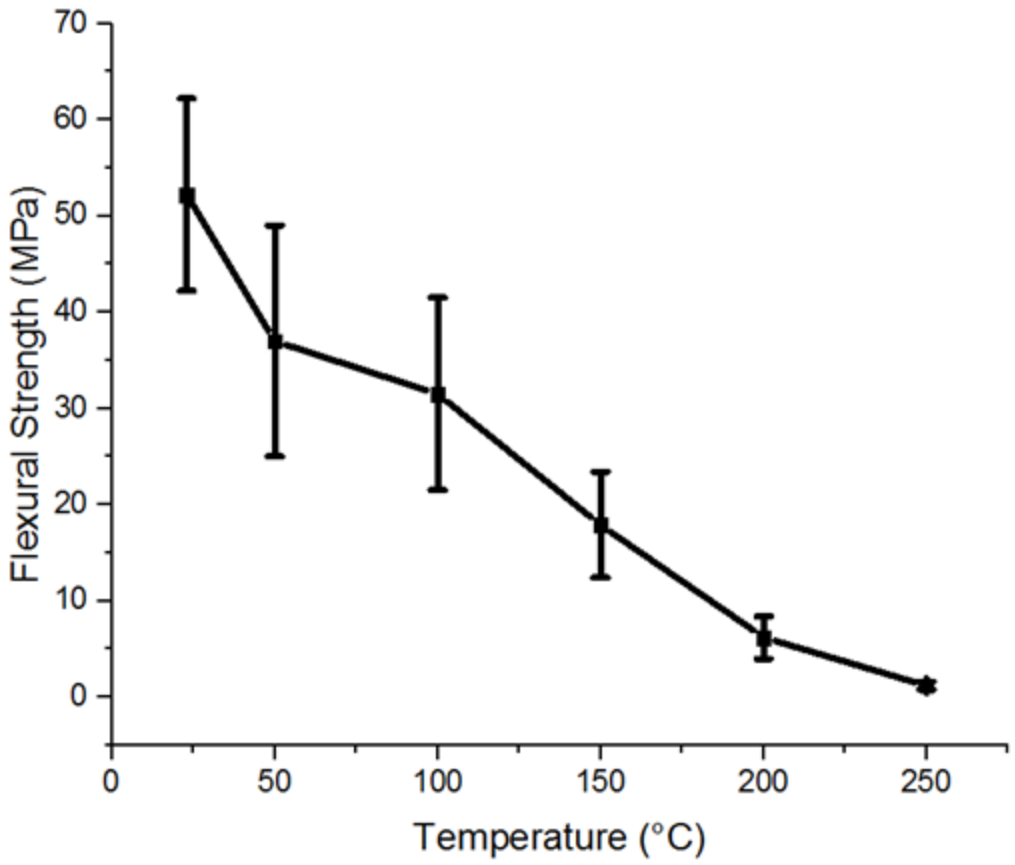

Fig 34. Flexural strength of heat treated abaca-potassium geopolymer composites.

As predicted, an increase in temperature that the abaca fiber reinforced potassium geopolymer composites were exposed to decreased flexural strengths in the samples. This decrease was likely initially caused by dehydration of the potassium geopolymer, and then later exacerbated by the thermal degradation of the biological fiber at elevated temperatures.

As shown in Fig. 34, the composite lost almost all of its structural integrity by the 250°C test, producing flexural strength values of just barely 1 MPa. However, at temperatures experienced in nature, the abaca fiber reinforced potassium geopolymer composite still managed impressive flexural strengths of over 35 MPa.

3.3.4 Weibull Statistical Analysis of Data

Weibull statistical analysis was employed to gain a better understanding of the mechanical data obtained from each sample set. As described in the introduction, three graphs were obtained for each sample group: a scatter plot of ln(ln(1/(1-F))) vs. ln(σ_f), a 95% confidence interval probability plot, and a histogram of the samples in that group. Shown below are three examples of those three graphs: one group from the untreated samples, one group from the durability testing, and one group for the heat treatment testing. The graphs for all sample groups can be found in the Appendix.

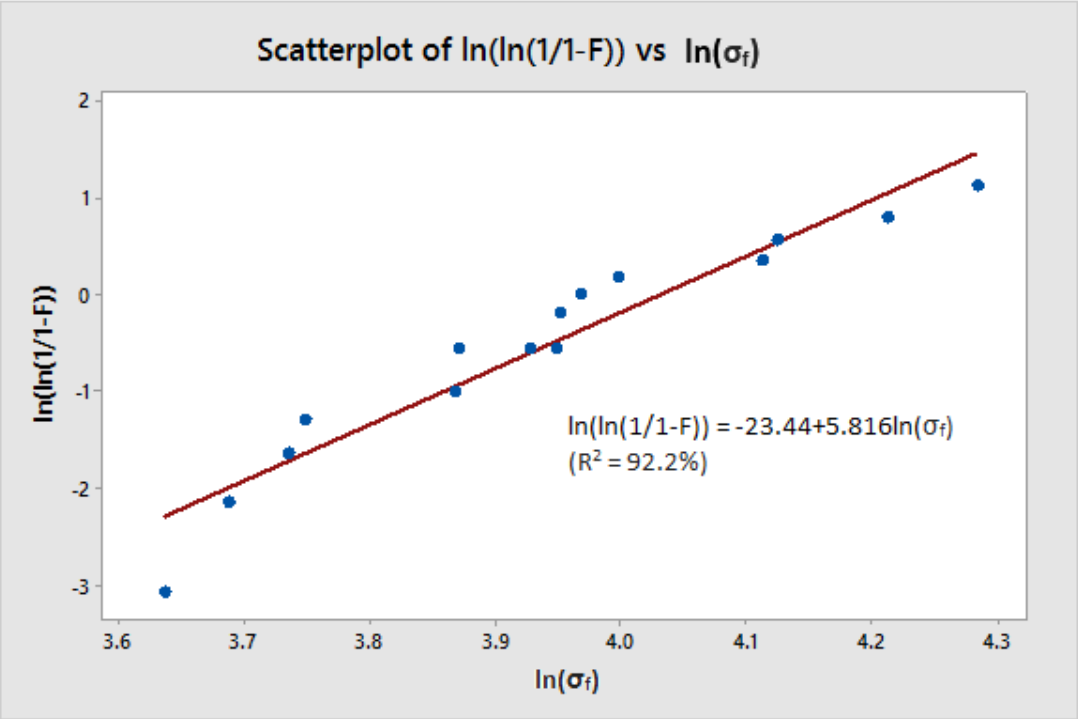

Fig. 35. Plot of ln(ln(1/(1-F))) vs. ln(σ_f) for 8 wt% abaca-reinforced potassium geopolymer.

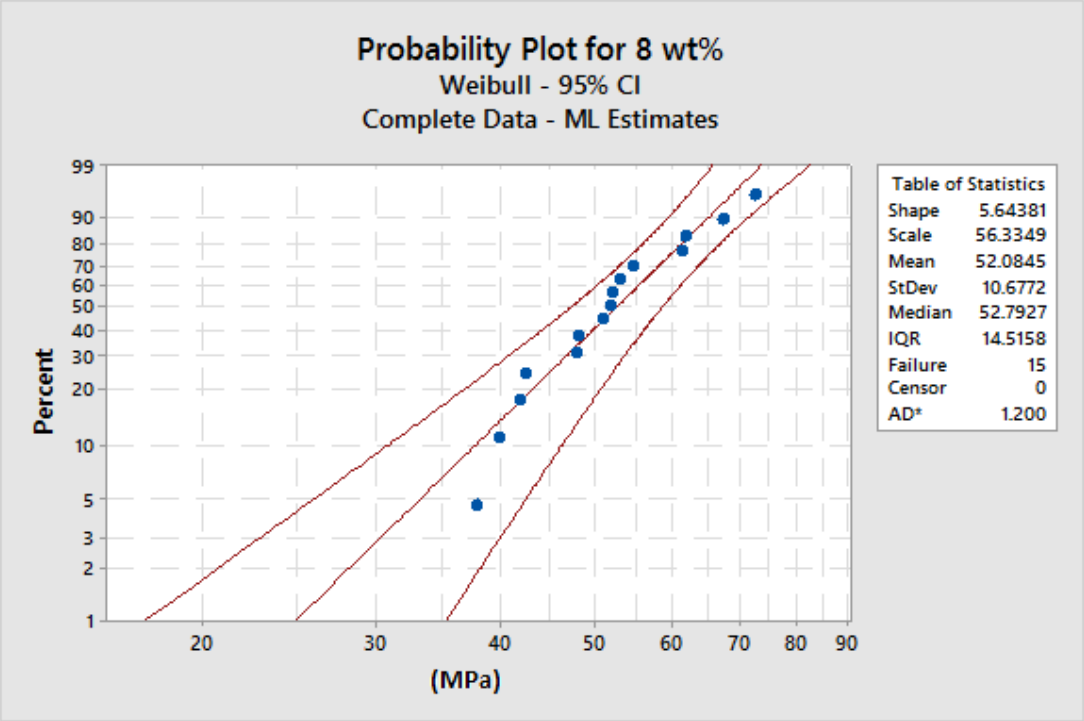

Fig. 36. Probability plot of 8 wt% abaca-reinforced potassium geopolymer.

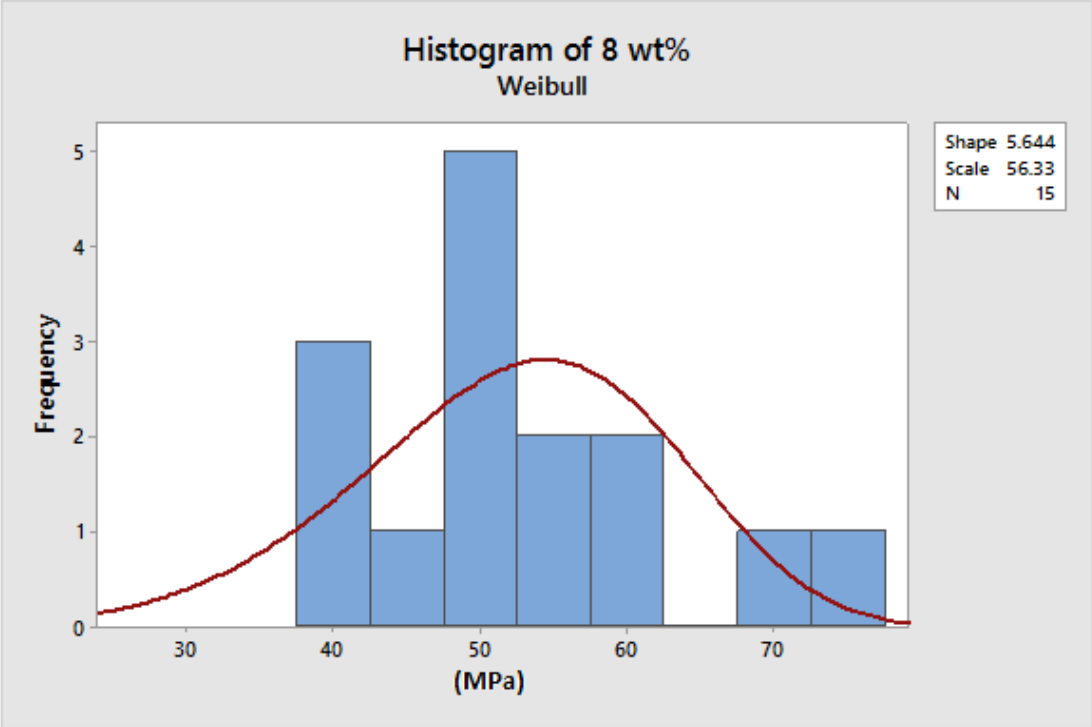

Fig. 37. Histogram of 8 wt% abaca-reinforced potassium geopolymer.

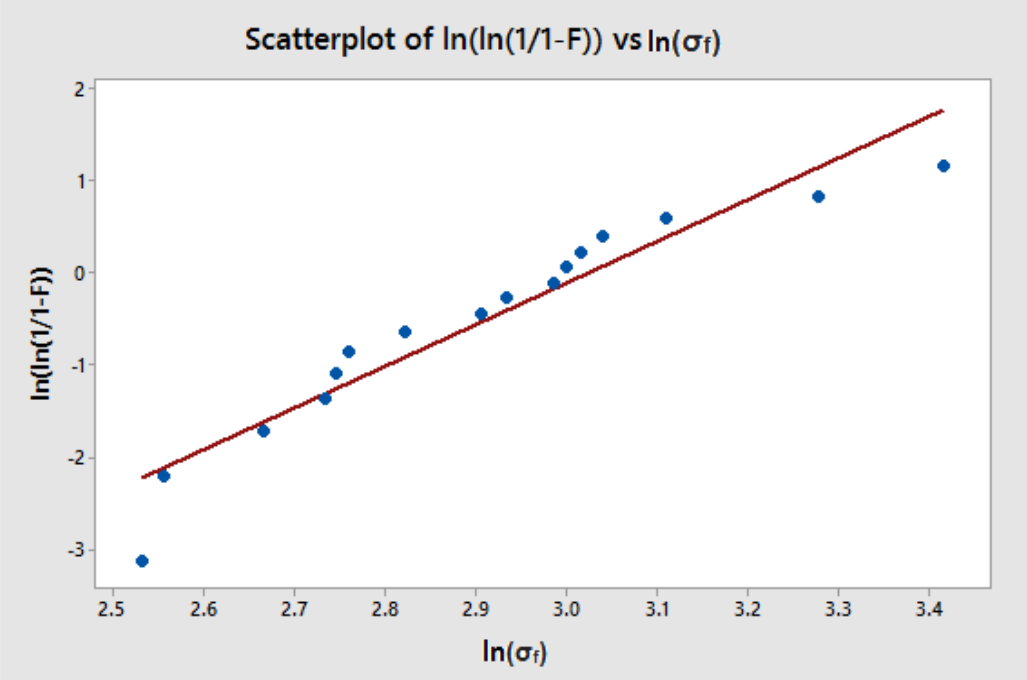

Fig. 38. Plot of ln(ln(1/(1-F))) vs. ln(σ_f) for composite heated to 150°C.

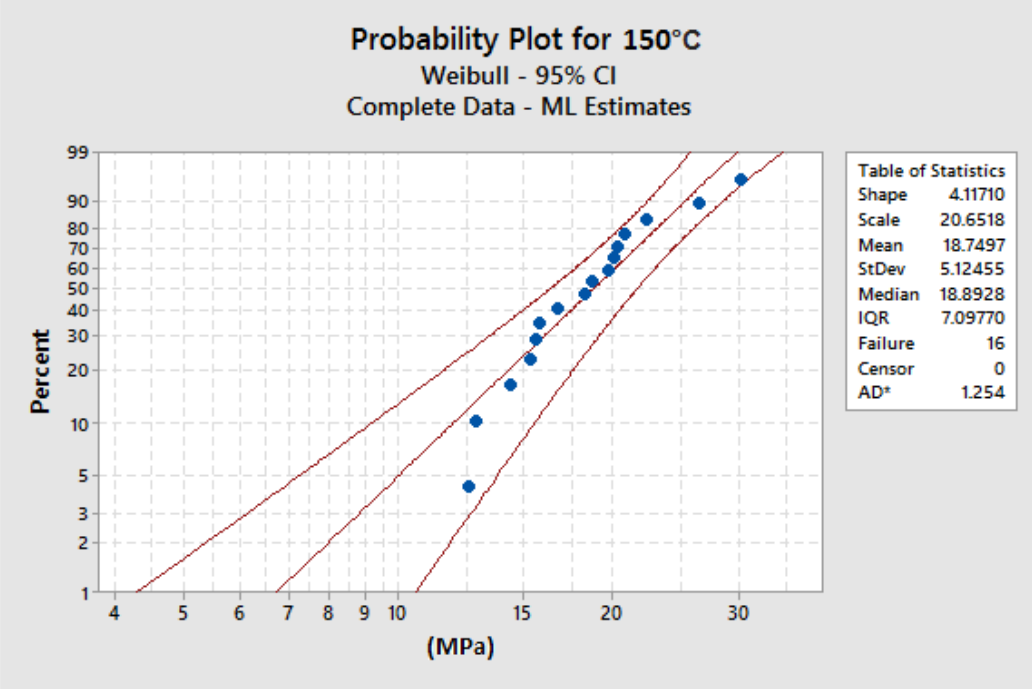

Fig. 39. Probability plot of abaca-reinforced potassium geopolymer heated to 150°C.

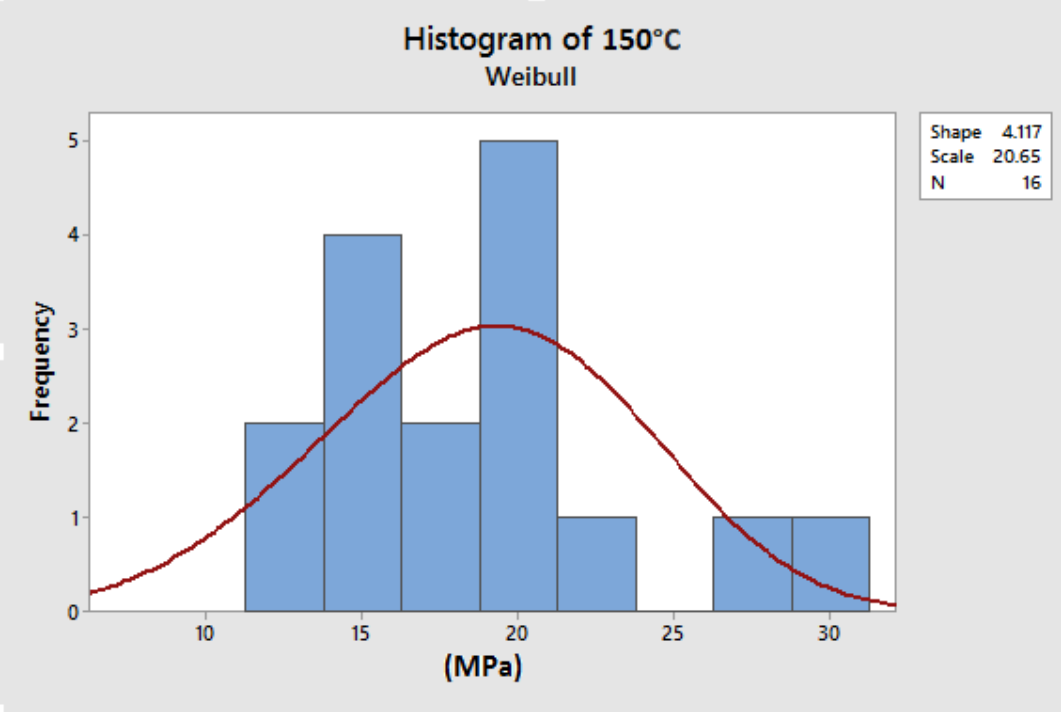

Fig. 40. Histogram of abaca-reinforced potassium geopolymer heated to 150°C.

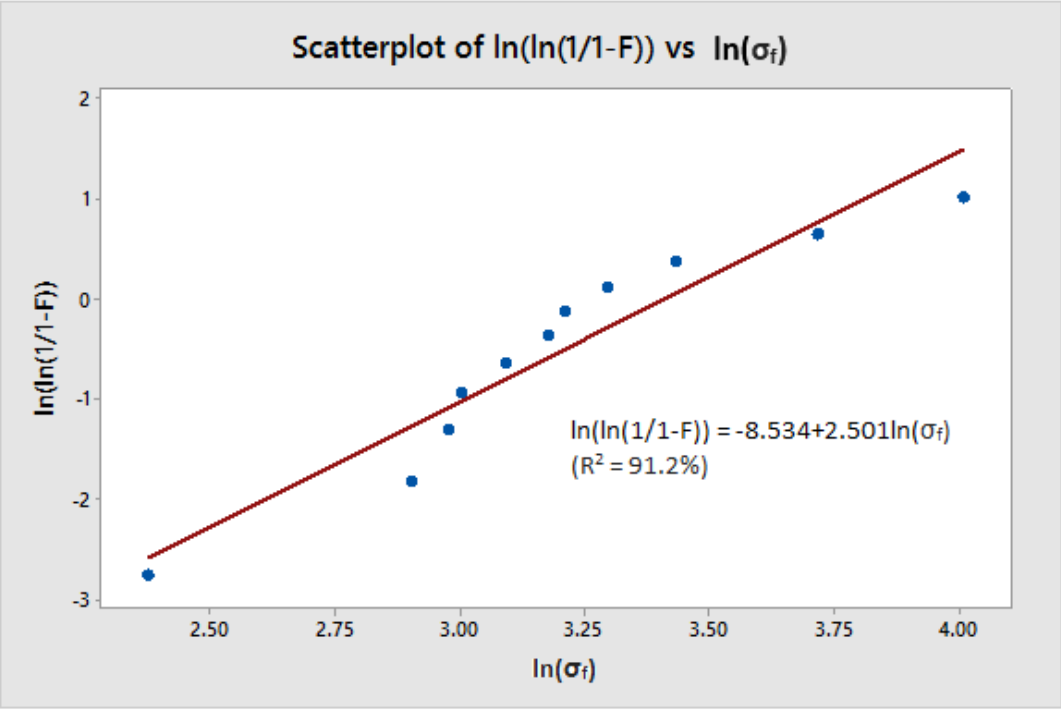

Fig. 41. Plot of ln(ln(1/(1-F))) vs. ln(σ_f) for composite treated with NaOH.

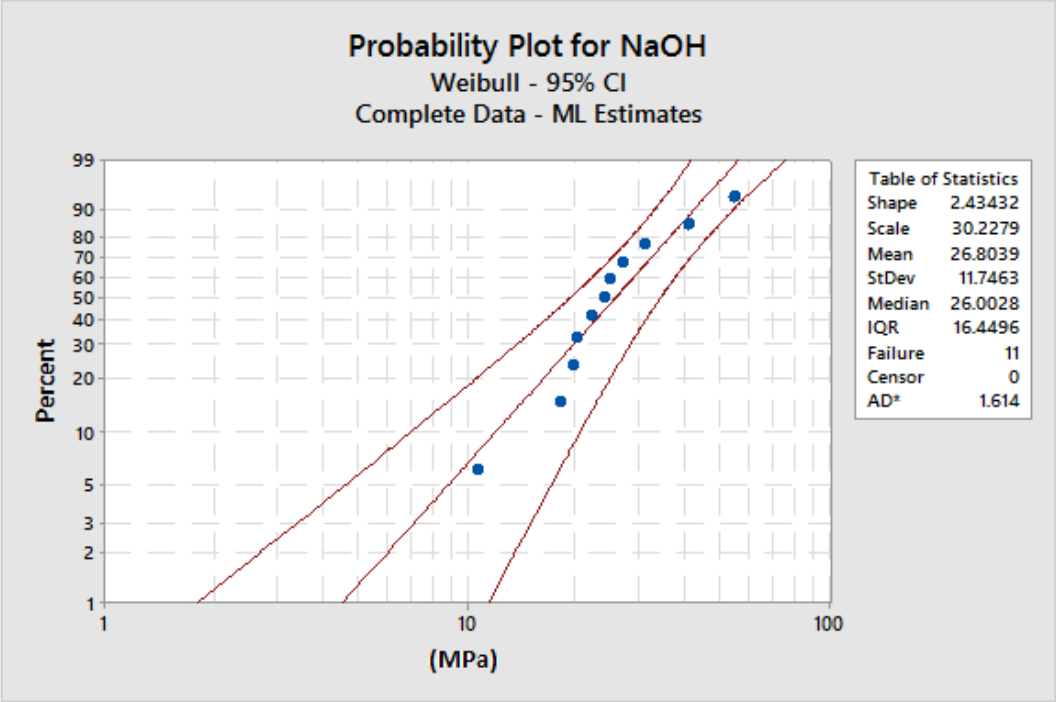

Fig. 42. Probability plot of abaca-reinforced potassium geopolymer treated with NaOH.

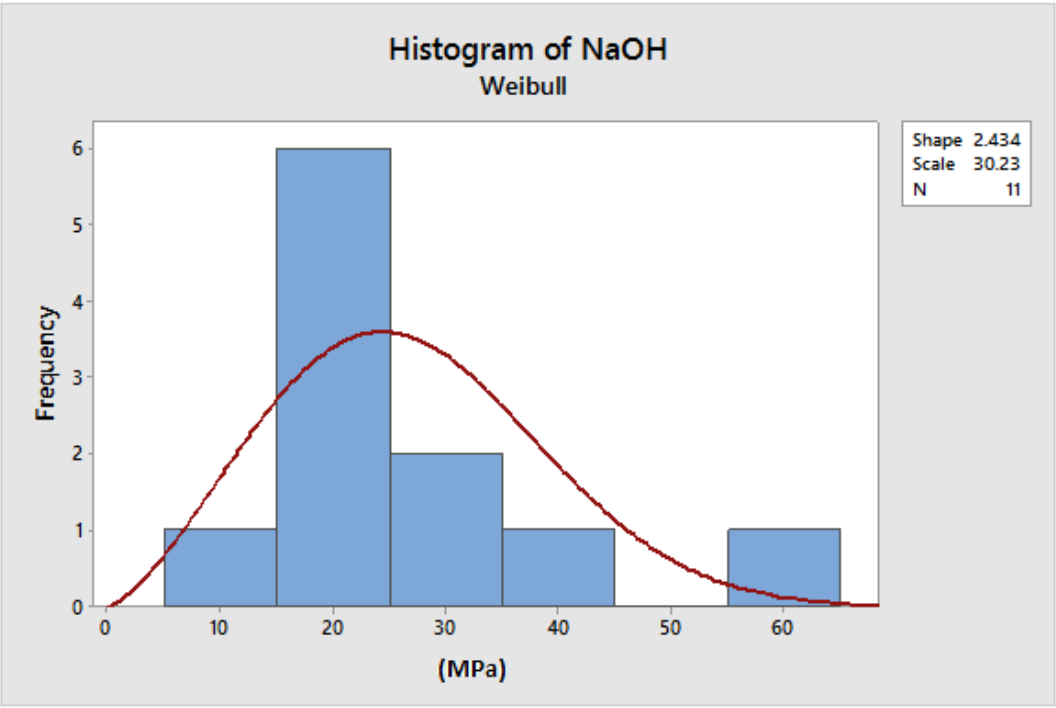

Fig. 43. Histogram of abaca-reinforced potassium geopolymer treated with NaOH.

The data from these graphs were used to make a comprehensive table comparing Weibull modulus, scale parameter, Weibull average, standard deviation and the 95% confidence interval across all sample groups studied, as seen below.

Table 3. Weibull statistics of four-point flexure of abaca fiber reinforced potassium geopolymer.

Sample Group	Weibull Modulus	Scale Parameter (MPa)	Weibull Average (MPa)	Standard Deviation (MPa)	95% Confidence Interval (MPa)
0 wt% Abaca	4.917	8.65	7.94	1.85	7.07, 8.85
2 wt% Abaca	5.323	13.11	12.09	2.61	10.90, 13.42
4 wt% Abaca	4.668	30.47	27.87	6.79	25.11, 31.06
6 wt% Abaca	5.101	37.44	34.42	7.74	30.05, 38.83
8 wt% Abaca	5.816	56.28	52.12	10.39	46.93, 57.80
50°C	3.824	41.05	37.11	10.82	31.42, 44.41
100°C	3.334	34.98	31.39	10.37	25.78, 38.21
150°C	3.435	19.86	17.85	5.74	14.59, 21.84
200°C	3.219	7.13	6.38	2.18	5.16, 7.89
250°C	4.031	1.36	1.23	0.34	1.04, 1.45
NaOH	2.433	30.22	26.80	11.74	20.65, 34.79
Water	3.537	53.55	48.21	15.11	40.00, 58.10
Salt water	3.222	52.84	47.34	16.14	39.03, 57.43
Freeze-Thaw Cycle	6.250	25.65	23.85	4.45	20.95, 27.16

3.3.5 SEM Analysis of Fracture Surfaces

SEM micrographs were taken at four magnifications for the fracture surfaces of one sample from each sample group. A few images of note are presented here, but each SEM micrograph of each fracture surface can be found in the Appendix.

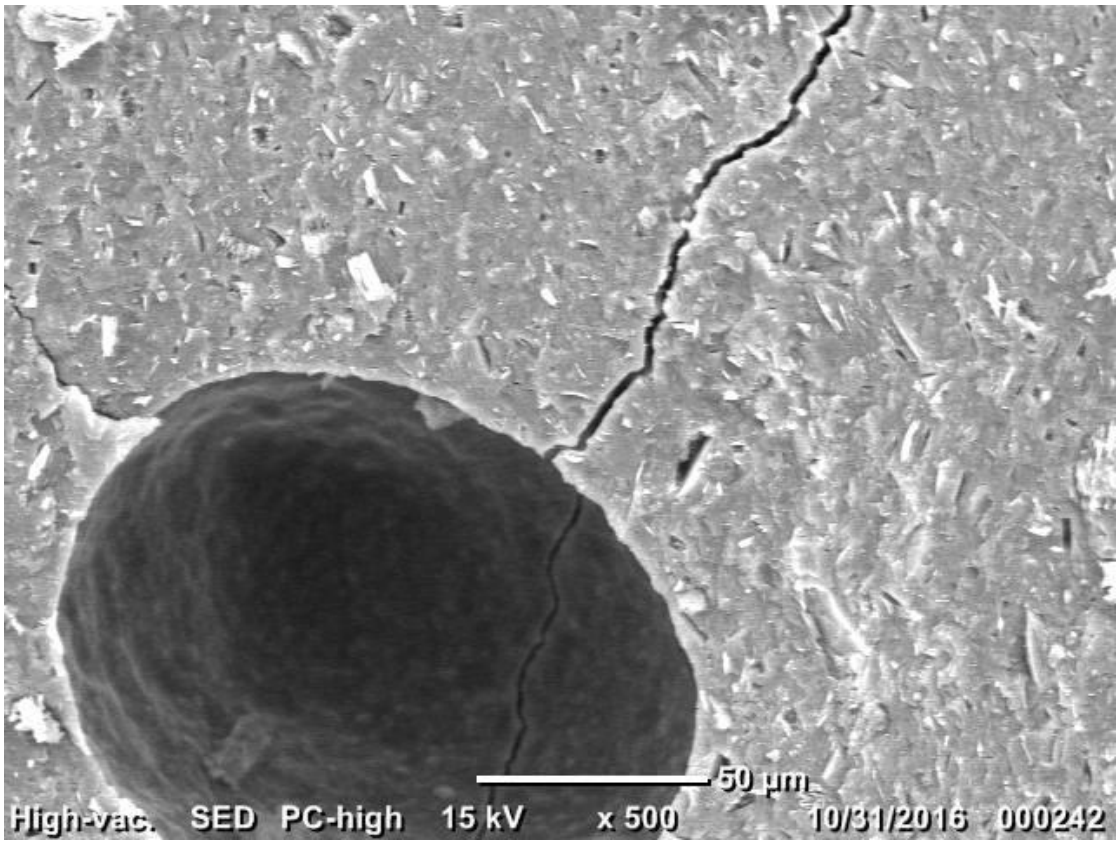

Fig. 44. SEM micrograph of pore in potassium geopolymer at magnification x500.

In Fig. 44, an image of a large defect in an unreinforced potassium geopolymer sample is noted. Imperfections such as this one contributed to lower than theoretical strength values, and were hypothesized to occur more in higher wt% abaca samples as they became less workable and more difficult to mold.

Fig 45. SEM micrograph of a 4 wt% reinforced composite at magnification x100.

Fig. 45 demonstrates that, as in the abaca fiber reinforced sodium geopolymer study, the abaca fibers distributed themselves fairly evenly throughout the composite. This detail was important in mechanical testing, as significant results rely on the material being as homogenous and as uniform as possible.

Fig. 46. SEM micrograph of 8 wt% reinforced composite heated to 300°C, magnification x1000.

In Fig. 46, it is clear that elevated temperatures significantly reduced the diameter of fibers in the composite. Fibers can be seen to have shrunk in from the walls of the matrix, which provides an explanation as to why the composite had an essentially negligible flexural strength after being exposed to such temperatures.

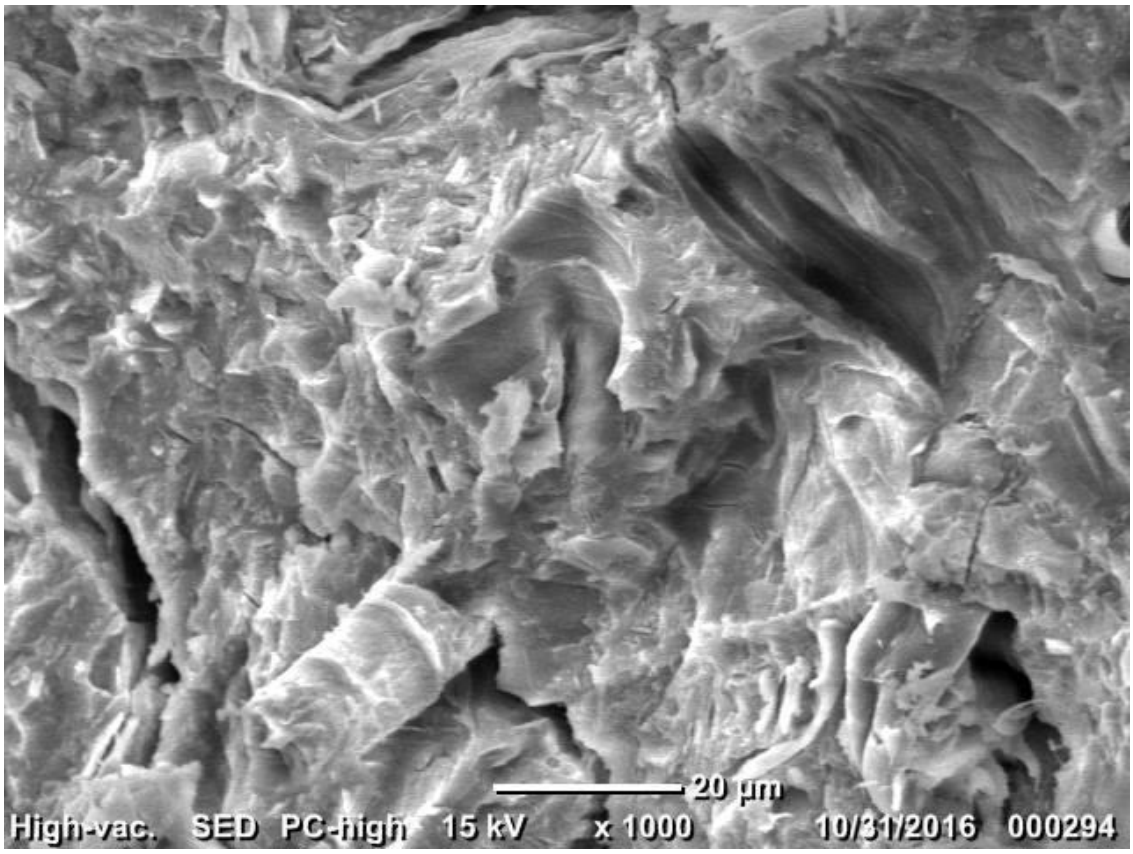

Fig. 47. SEM micrograph of an 8 wt% composite treated with H_2SO_4, magnification x1000.

Finally, Fig. 47 shows the result of sulfuric acid attack on the potassium geopolymer. The large crack around the fiber in the figure likely propagated due to weakened potassium geopolymer that had begun to react with the sulfuric acid to create alum. Once enough geopolymer had reacted and separated from the abaca fibers, the samples were left mechanically untestable.

3.3.6 XRD Analysis of Potassium Geopolymer

A final short experiment was run in order to confirm that fully reacted potassium geopolymer was indeed prepared during this study. As mentioned in the introduction, XRD of geopolymer that contains fully-reacted metakaolin will have an amorphous hump centered

around a two theta value of 28.5 degrees. A hump that was shifted significantly from that value would indicate that the geopolymer was prepared improperly, and contained partially unreacted metakaolin. XRD analysis of ground potassium geopolymer yielded the following results:

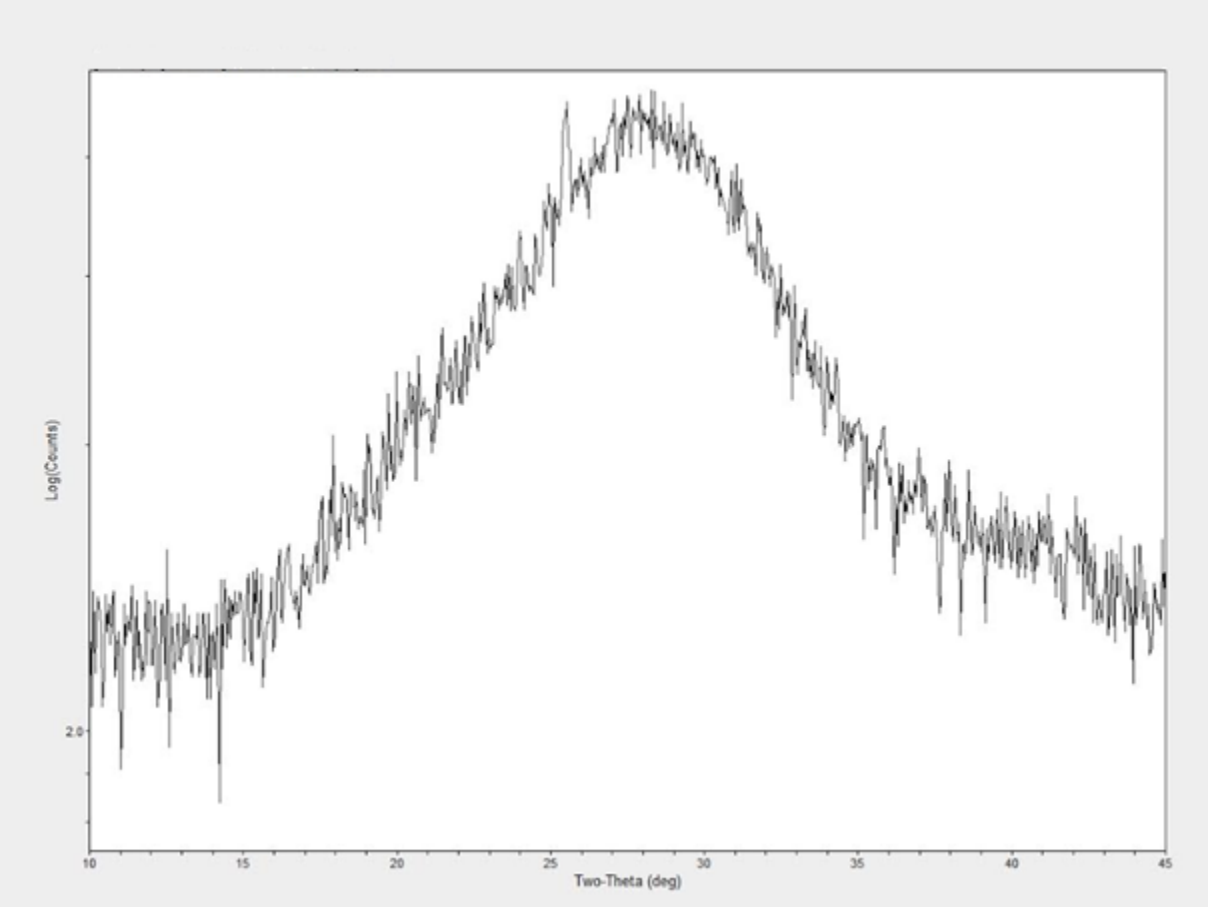

Fig. 48. XRD spectra of pure potassium geopolymer.

As Fig. 48 shows, the amorphous hump is indeed centered about two theta = 28.5 degrees. This indicates that the abaca fiber reinforced potassium geopolymer composites in this study were made with ideal matrix geopolymer.

CHAPTER 4

CONCLUSION

“Biologically reinforced geopolymers” is a broad topic which could be researched at great length. This study managed to explore a few such systems, and characterized their properties and viability as structural ceramic composites.

Cork reinforced sodium geopolymer improved from ~1.25 MPa to ~2.5 MPa (when taken from unreinforced to 60 wt% cork). This composite system, while not a structurally viable material, did yield interesting strain-to-failure results. The highest reinforced group managed average strain-to-failure of 0.9% in flexure, about 9 times greater than expected for a normal brittle ceramic.

Abaca fiber reinforced sodium geopolymer proved to be more viable as a structural ceramic composite. Sodium-based geopolymer composites at the limit of workability (5.2 wt% abaca fiber) demonstrated flexural strengths above 25 MPa, about 4-5 times stronger than flexural strengths associated with OPCs. An attempt to infuse even more abaca fibers into geopolymer led to the use of potassium geopolymer, known to be much less viscous than its sodium counterpart.

Abaca fiber reinforced potassium geopolymer yielded an average flexural strength of 52 MPa at 8 wt% abaca fiber, a vast improvement over OPCs. These same composites demonstrated good water and saltwater durability, decent NaOH and freeze cycle durability, and poor H_2SO_4 durability. Additionally, these composites exhibited good strength retention at temperatures experienced in nature. However, the composite did show a steady decrease in flexural strength at more extreme temperatures due to dehydration and thermal degradation, eventually losing all structural integrity by 300°C.

Several possible avenues for future work exist within this study. To increase the strengths of the abaca fiber reinforced potassium geopolymer composites, more abaca fiber could be added in a variety of ways. One such method might be by employing injection molding methods, which would be doubly effective: injection molding would shear the shear-thinning potassium geopolymer, lowering its viscosity and allowing more abaca fibers to be incorporated into the composite. Injection molding would also help eliminate macroscale defects associated with the current layup of the composite into Delrin molds.

Another area requiring more research is the testing of larger samples. If this composite is to reach commercial applications in structures, it has to be proven to be effective at larger sizes when critical flaws are more statistically likely. Confirmation of elevated strengths at larger sample sizes would improve confidence in this composite as a viable structural ceramic.

Biologically reinforced geopolymers certainly have potential as a green structural alternative to OPCs. Abaca fiber reinforced potassium geopolymer, while still in its infancy as a characterized material, is at the forefront of biologically reinforced geopolymers with potential as a commercial structural material.

CHAPTER 5

REFERENCES

1. J. Davidovits, "Mineral Polymers and Methods of Making Them"; U.S. Patent 4,349,386, September 14, (1982).

2. J. Davidovits, "Geopolymers - Inorganic Polymeric New Materials," J. Therm. Anal. **37** 1633-1656 (1991).

3. J. Davidovits, "Geopolymer Chemistry and Properties"; pp.25-48 in Geopolymer'88 First European Conference on Soft Mineralogy, Vol.1 Edited by J. Davidovits and J. Orlinski. Geopolymer Institute and Technical University, Compiegne, France, (1988).

4. J. Davidovits, Geopolymer Chemistry and Applications, 4th Edition (2015), published by the Geopolymer Institute, St. Quentin, France.

5. V. F. F. Barbosa, and K. J. D. MacKenzie, "Synthesis and Thermal Behaviour of Potassium Sialate Geopolymers," Materials Letters, **57**, 1477–82 (2003).

6. W. M. Kriven, J. L. Bell and M. Gordon, "Microstructure and Microchemistry of Fully-Reacted Geopolymers and Geopolymer Matrix Composites," Ceramic Transactions vol. **153**, 227-250 (2003).

7. P. Duxson, J. L. Provis, G. C. Lukey, S. W. Mallicoat, W. M. Kriven and J. S. J. van Deventer, "Understanding the Relationship between Geopolymer Composition, Microstructure and Mechanical Properties," Colloids and Surfaces A – Physicochemical and Engineering Aspects **269** [1-3] 47-58 (2005).

8. W. M. Kriven, J. L. Bell, S. W. Mallicoat and M. Gordon, "Intrinsic Microstructure and Properties of Metakaolin-Based Geopolymers," Proc. Int. Workshop on Geopolymer Binders – Interdependence of Composition, Structure and Properties, Weimar, Germany. Published by the Geopolymer Institute, St. Quentin, France 71-86 (2007).

9. J. L. Bell, P. Sarin, J. L. Provis, R. P. Haggerty, P. E. Driemeyer, P. J. Chupas, J. S. J. van Deventer and W. M. Kriven, "Atomic Structure of a Cesium Aluminosilicate Geopolymer: A Pair Distribution Function Study," Chemistry of Materials, **20** [14] 4768-4776 (2008).

10. J. L. Bell, P. Sarin, P. E. Driemeyer, R. P. Haggerty, P. J. Chupas and W. M. Kriven, "X-ray Pair Distribution Function Analysis of Potassium Based Geopolymer," J. Materials Chemistry, **18** [48], 5974 - 5981 (2008).

11. W. M. Kriven, "Inorganic Polysialates or "Geopolymers," American Ceramic Society Bulletin, **89** [4] 31-34 (2010).

12. Geopolymer-based Composites," W. M. Kriven, in Vol. 5, Ceramics and Carbon Matrix Composites, edited by Marina Ruggles-Wrenn. Part of an 8 volume set of books entitled Comprehensive Composite Materials II, Peter Beaumont and Carl Zweben, Co-editors-in-chief. Published by Elsevier, Oxford, UK, in press (2017).

13. V. F. F. Barbosa, K. J. D. MacKenzie, "Thermal Behavior of Inorganic Geopolymers and Composites Derived from Sodium Polysialate," Mater. Res. Bull, 38, 319-331 (2003).

14. D. S. Roper, G. P. Kutyla and W. M. Kriven, "Properties of Granite Powder Reinforced Geopolymer Composites," Cer. Eng. and Sci. Proc., **36** [8] 3-10 (2015).

15. ASTM C1161-13, Standard Test Method for Flexural Strength of Advanced Ceramics at Ambient Temperature, ASTM International, West Conshohocken, PA, 2013, DOI: 10.1520/C1161

16. Durability of Fly Ash Based Geopolymer Concrete Against Sulphuric Acid Attack: International Conference On Durability of Building Materials and Components, Lyon, France 17-20 April (2005).

17. M. Hüsnü Dirikolu, Alaattin Aktas and Burak Birgören, "Statistical Analysis of Fracture Strength of Composite Materials Using Weibull Distribution," Turkish J. Eng. Env. Sci ., 26 45-48 (2002).

18. Ross P. Williams, Robert D. Hart, and Arie van Riessen, "Quantification of the Extent of Reaction of Metakaolin-Based Geopolymers Using X-Ray Diffraction, Scanning Electron Microscopy, and Energy-Dispersive Spectroscopy," J. Am. Ceram. Soc., **94** [8] 2663–2670 (2011).

19. D. S. Roper, G. P. Kutyla and W. M. Kriven, "Properties of Cork Particle Reinforced Sodium Geopolymer Composites", Cer. Eng. and Sci. Proc., **37** [7] 79-82 (2016).

20. Faiz Uddin Ahmed Shaikh, "Mechanical and Durability Properties of Fly Ash Geopolymer Concrete Containing Recycled Coarse Aggregates", International Journal of Sustainable Built Environment, **5** [2] 277–287 (2016).

21. Alfred Noufie Mekel, Rudy Soenoko, Wahyono Suprapto and Anindito Purnowidodo, "Tensile Strength of Abaca Strands from Sangihe Talaud Islands", ARPN Journal of Engineering and Applied Sciences, **11** [15] 9487-9490 (2016).

CHAPTER 6

APPENDIX: WEIBULL GRAPHS AND SEM MICROGRAPHS

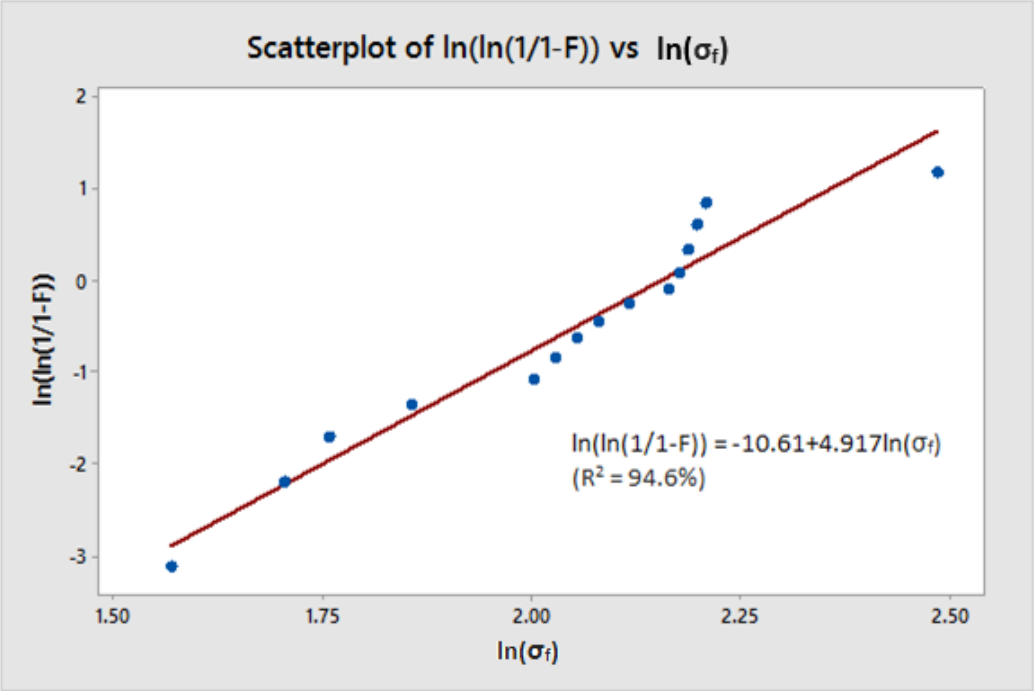

Fig. 49. Scatterplot of ln(ln(1/(1-F))) vs ln(σ) for 0 wt% abaca-potassium geopolymer.

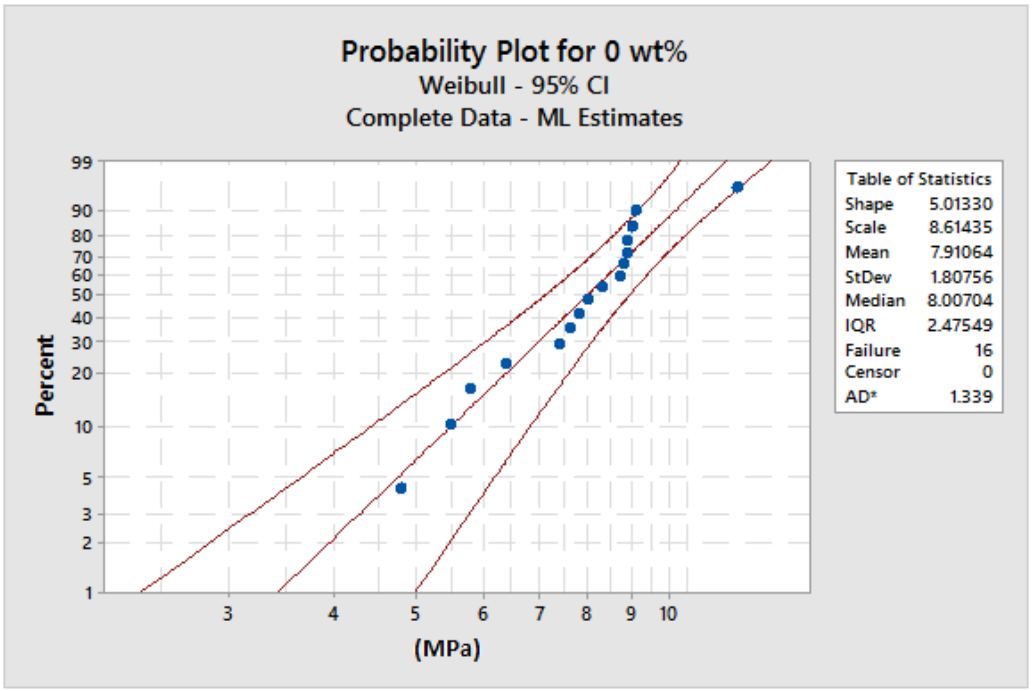

Fig. 50. 95% confidence interval probability plot for 0 wt% abaca-potassium geopolymer.

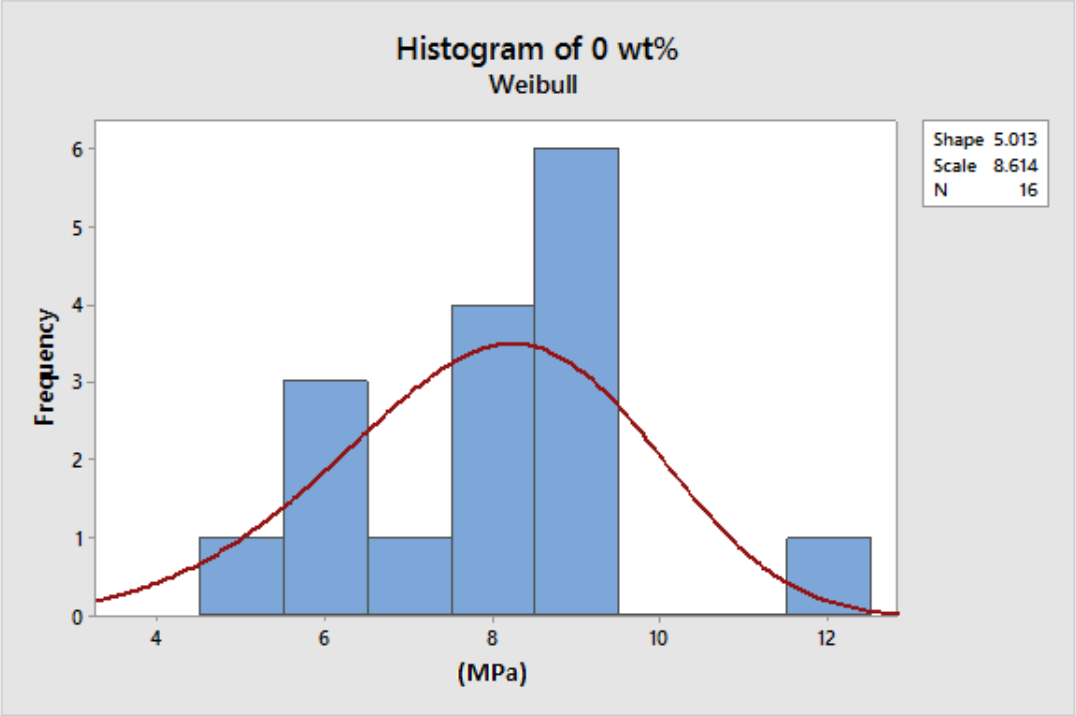

Fig. 51. Weibull fit to histogram for 0 wt% abaca-potassium geopolymer.

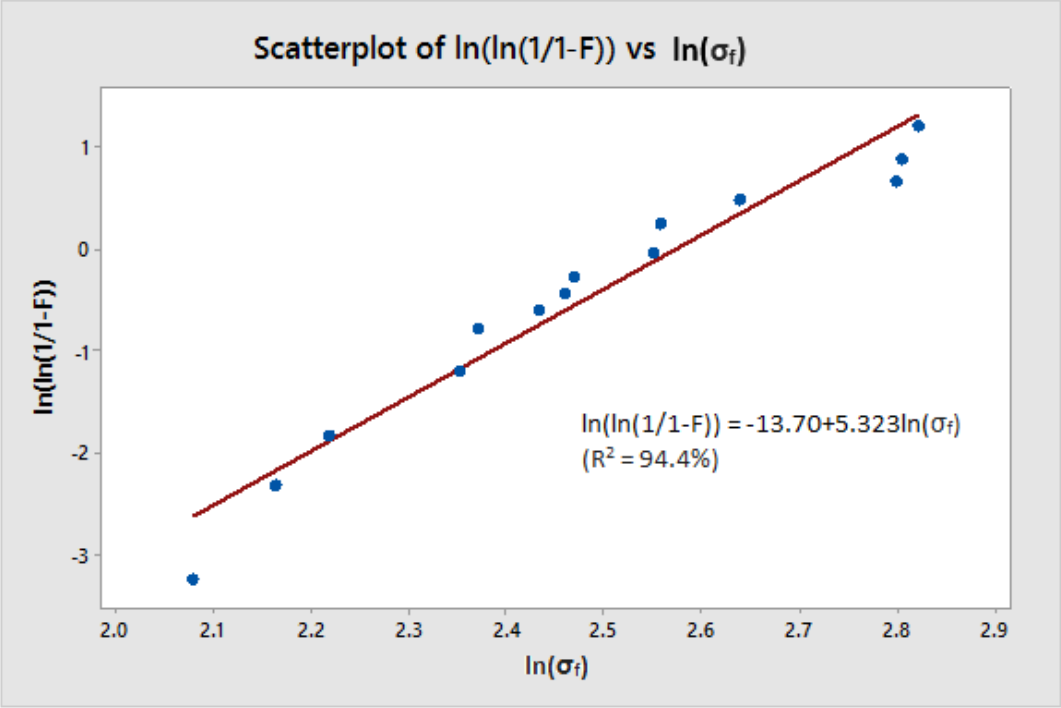

Fig. 52. Scatterplot of ln(ln(1/(1-F))) vs ln(σ) for 2 wt% abaca-potassium geopolymer.

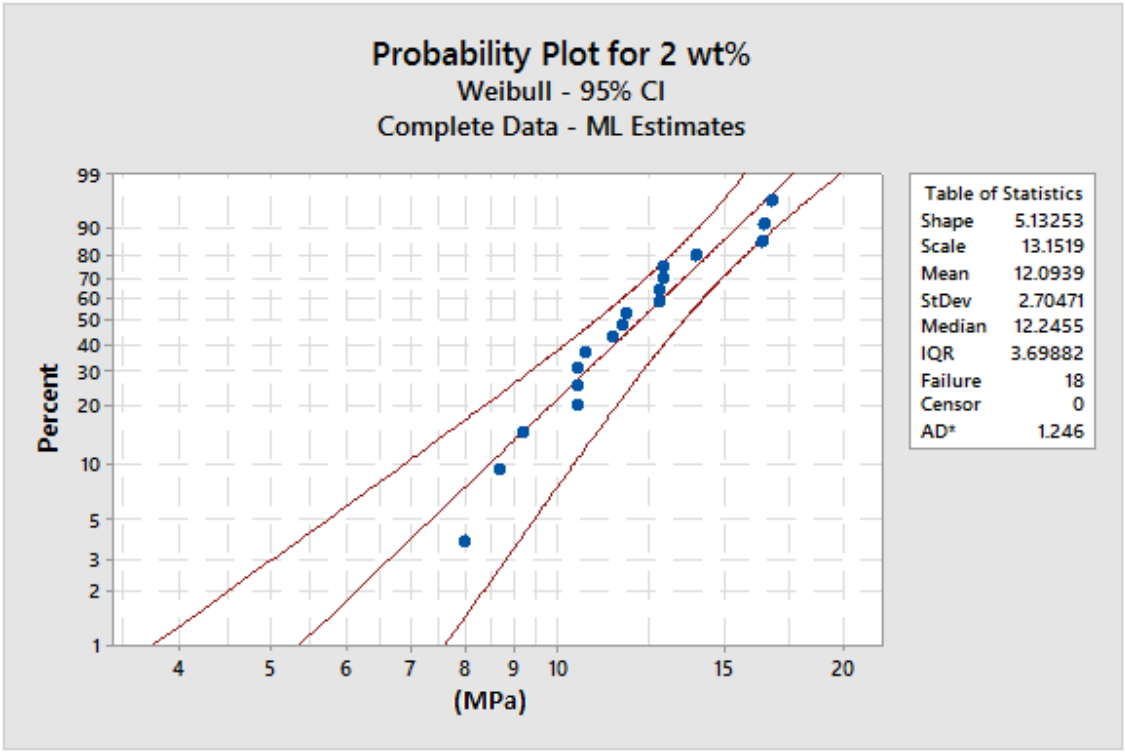

Fig. 53. 95% confidence interval probability plot for 2 wt% abaca-potassium geopolymer.

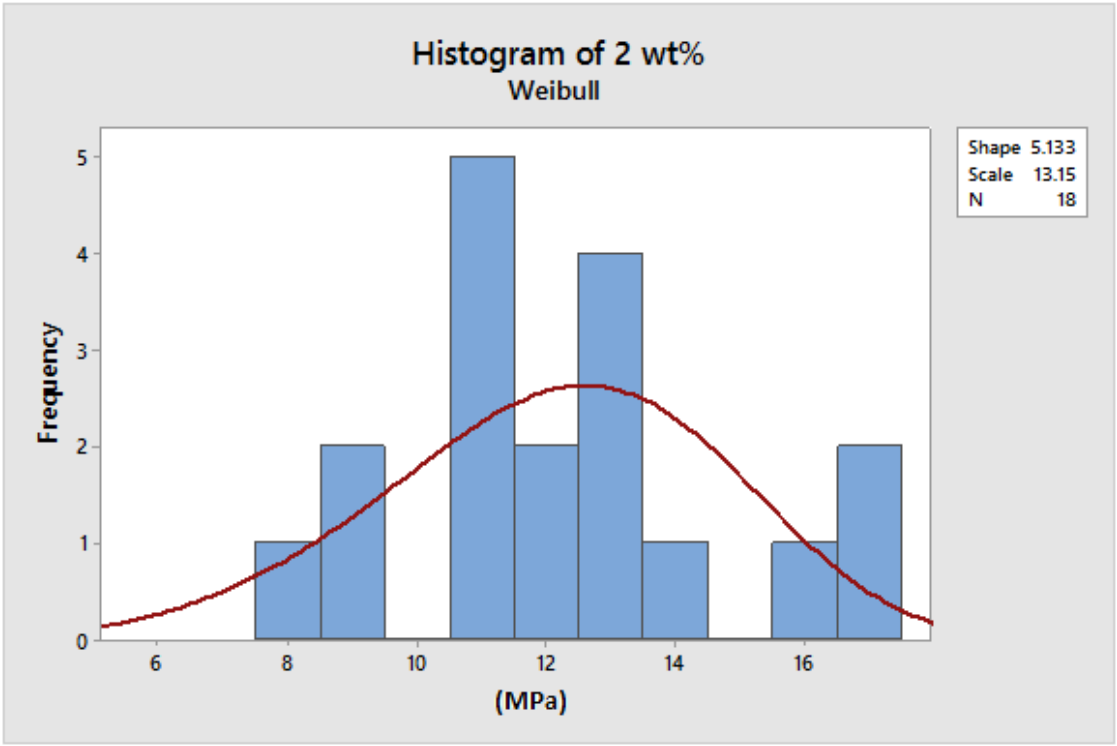

Fig. 54. Weibull fit to histogram for 2 wt% abaca-potassium geopolymer.

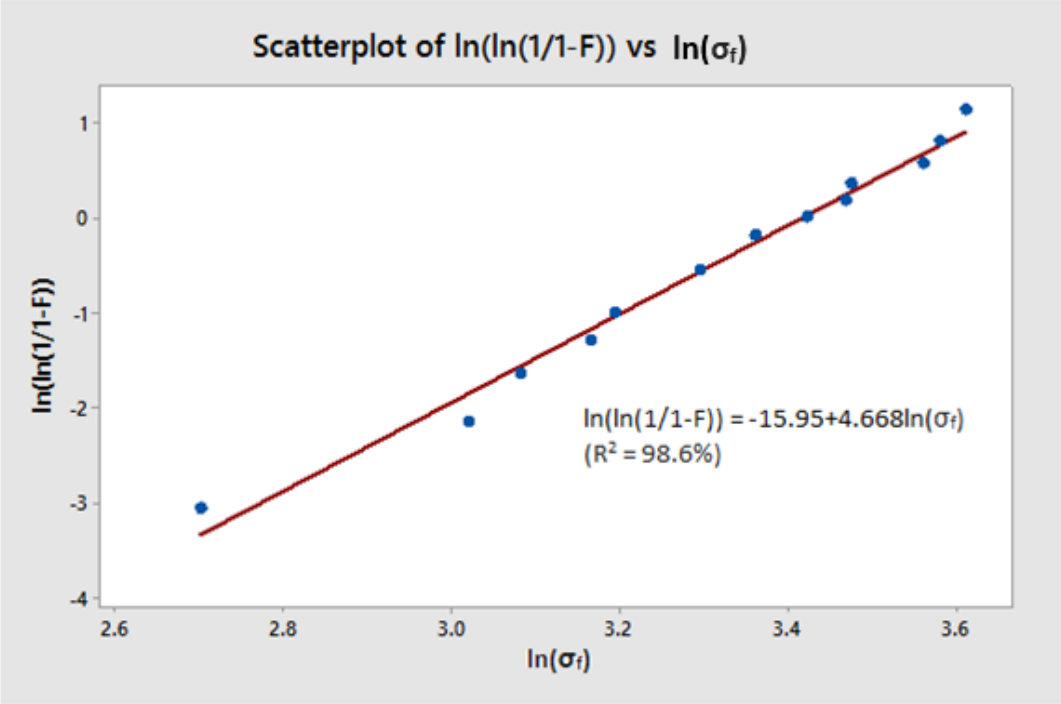

Fig. 55. Scatterplot of ln(ln(1/(1-F))) vs ln(σ) for 4 wt% abaca-potassium geopolymer.

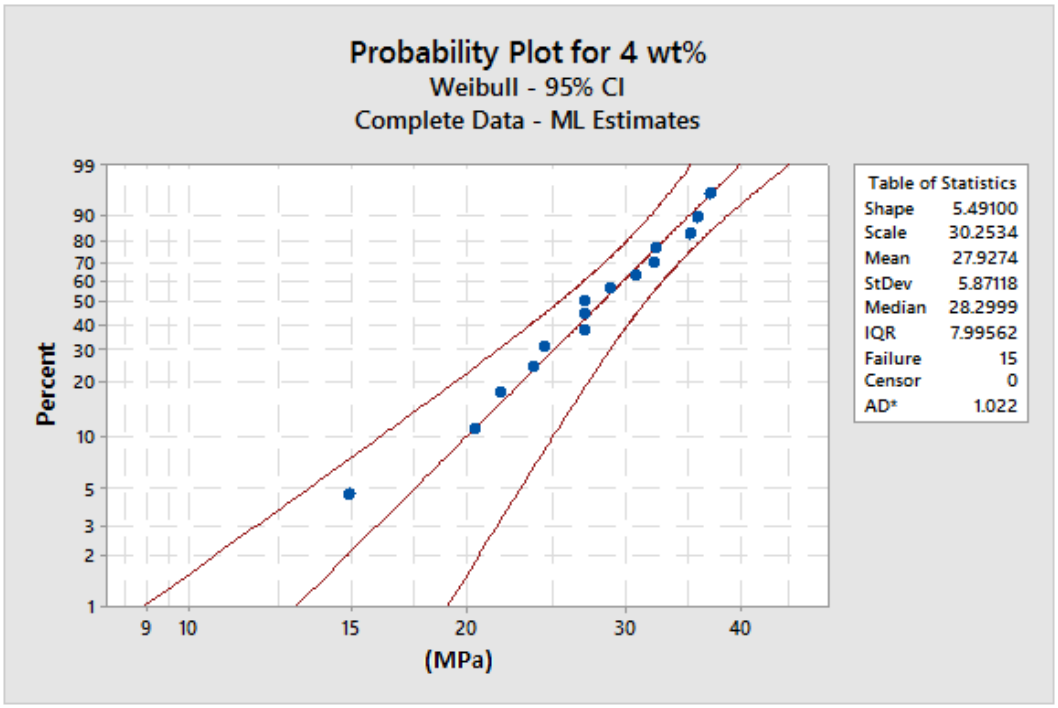

Fig. 56. 95% confidence interval probability plot for 4 wt% abaca-potassium geopolymer.

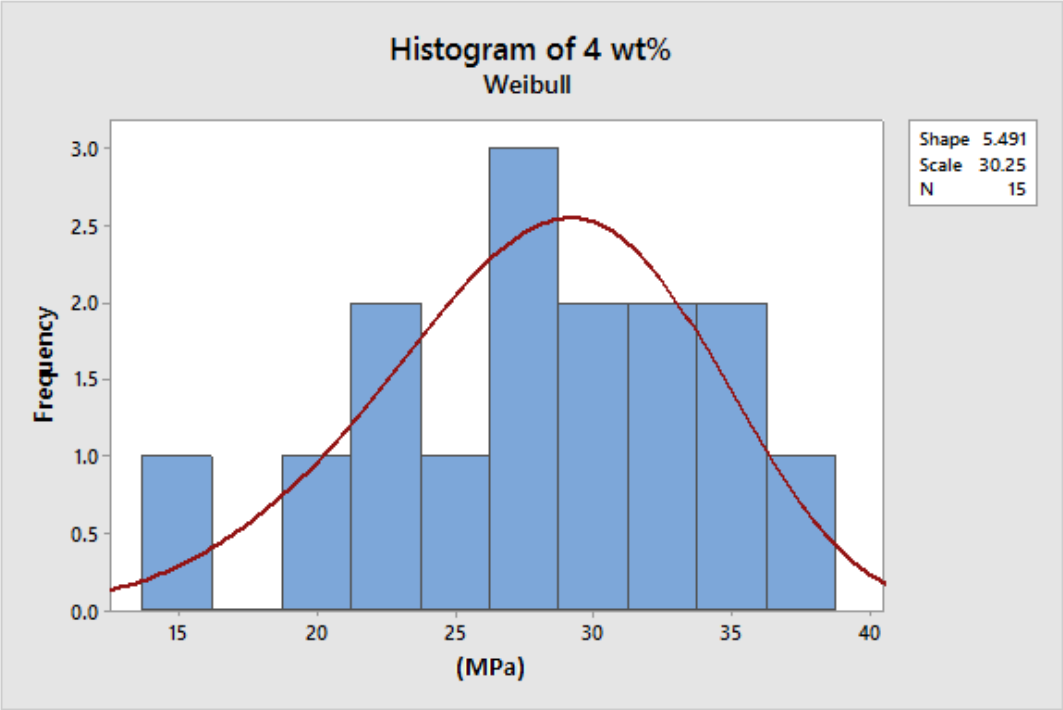

Fig. 57. Weibull fit to histogram for 4 wt% abaca-potassium geopolymer.

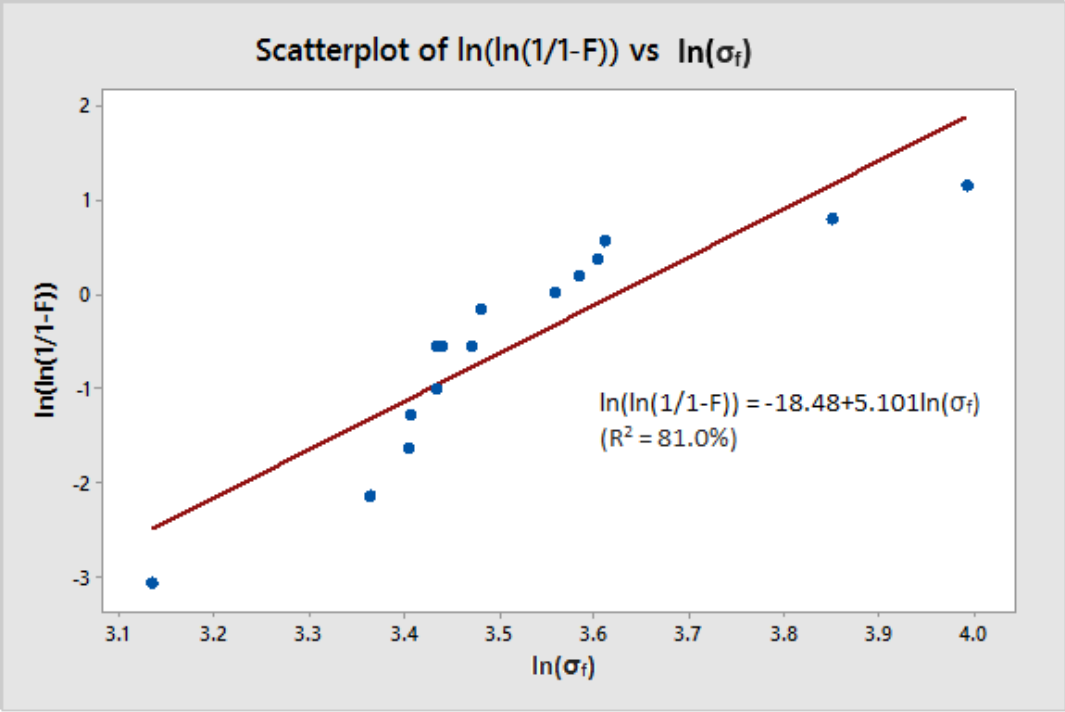

Fig. 58. Scatterplot of ln(ln(1/(1-F))) vs ln(σ) for 6 wt% abaca-potassium geopolymer.

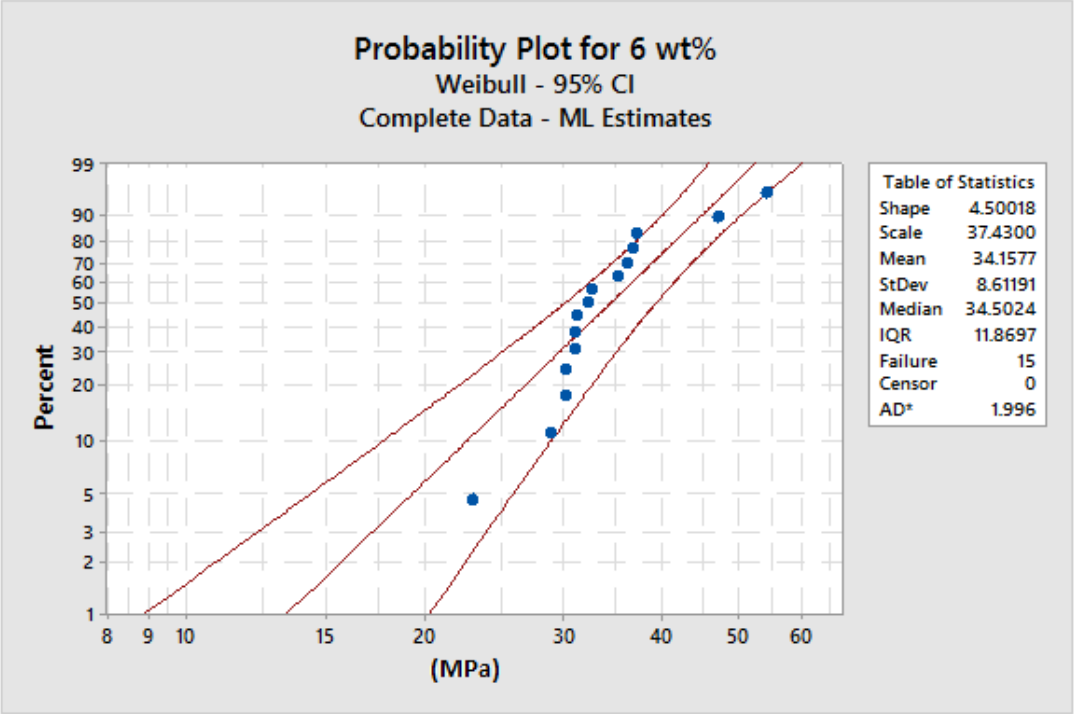

Fig. 59. 95% confidence interval probability plot for 6 wt% abaca-potassium geopolymer.

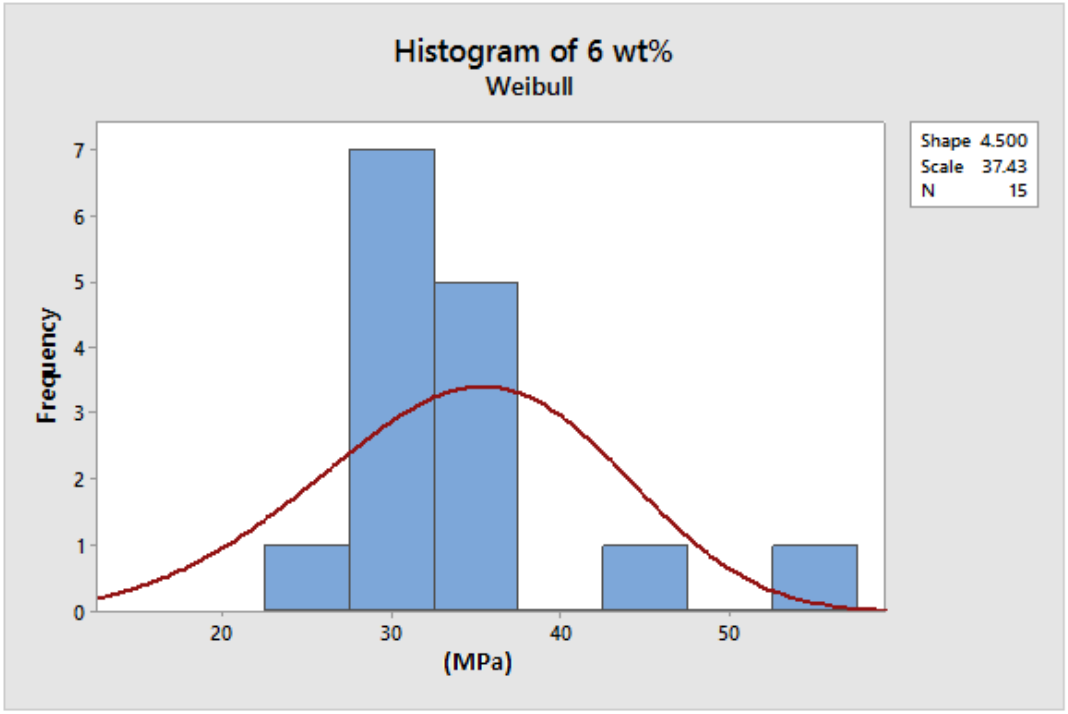

Fig. 60. Weibull fit to histogram for 6 wt% abaca-potassium geopolymer.

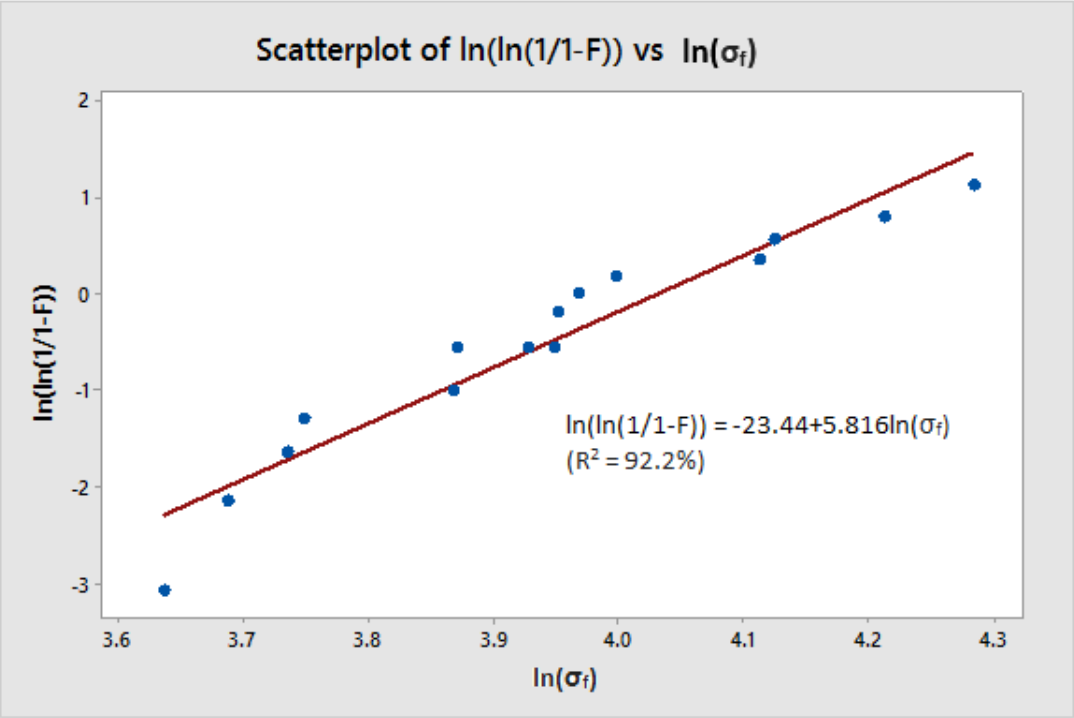

Fig. 61. Scatterplot of ln(ln(1/(1-F))) vs ln(σ) for 8 wt% abaca-potassium geopolymer.

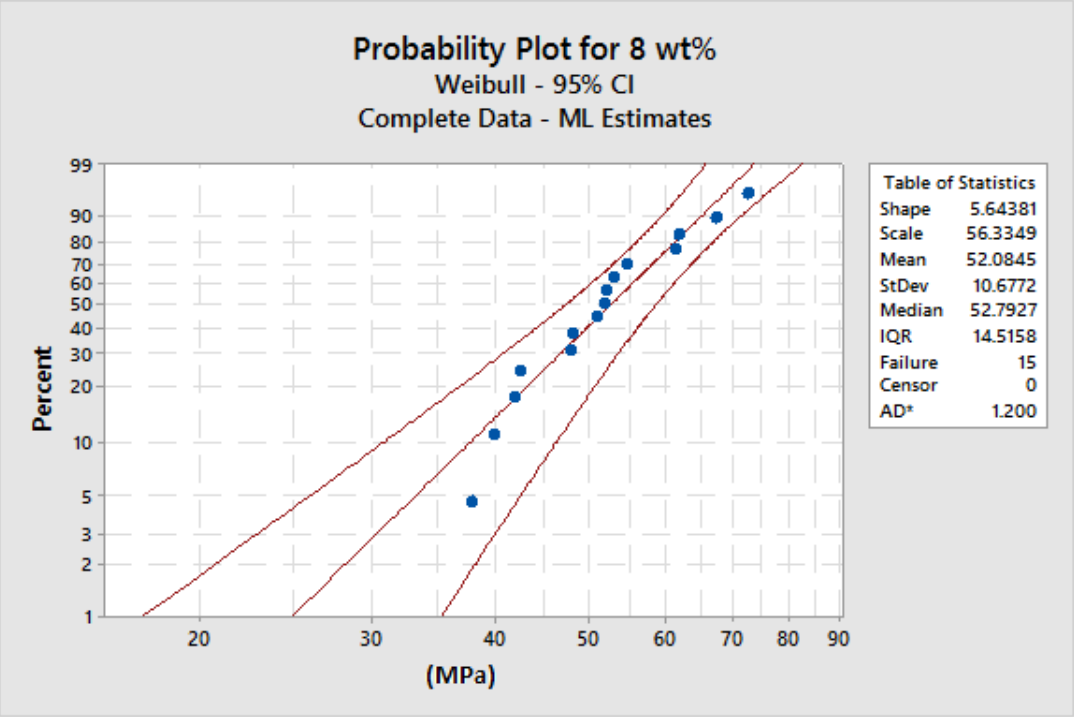

Fig. 62. 95% confidence interval probability plot for 8 wt% abaca-potassium geopolymer.

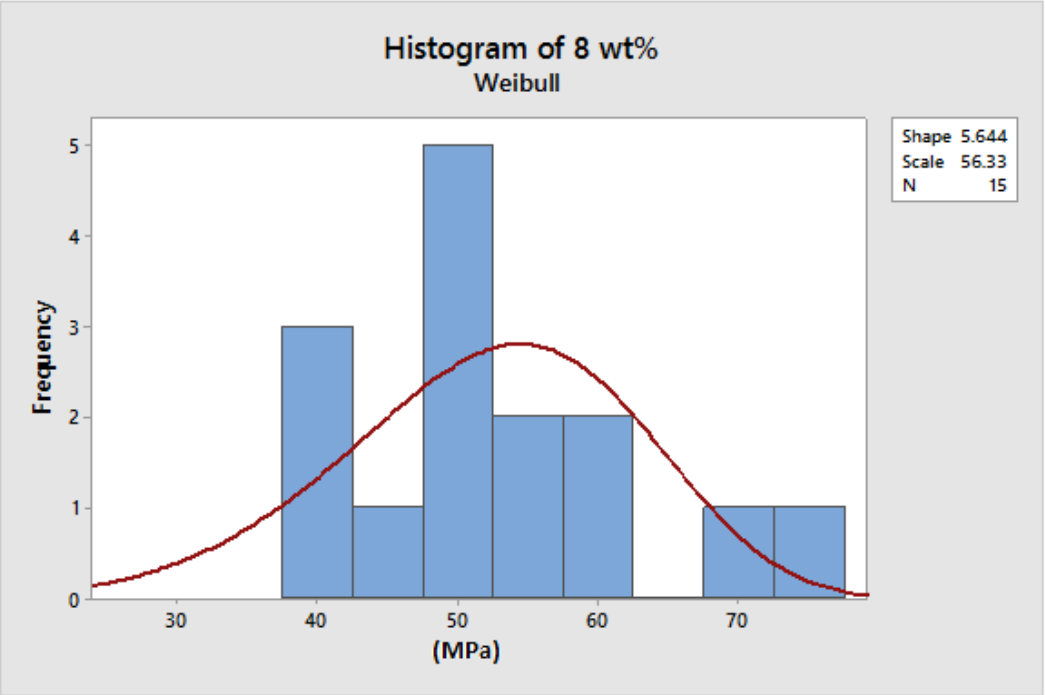

Fig. 63. Weibull fit to histogram for 8 wt% abaca-potassium geopolymer.

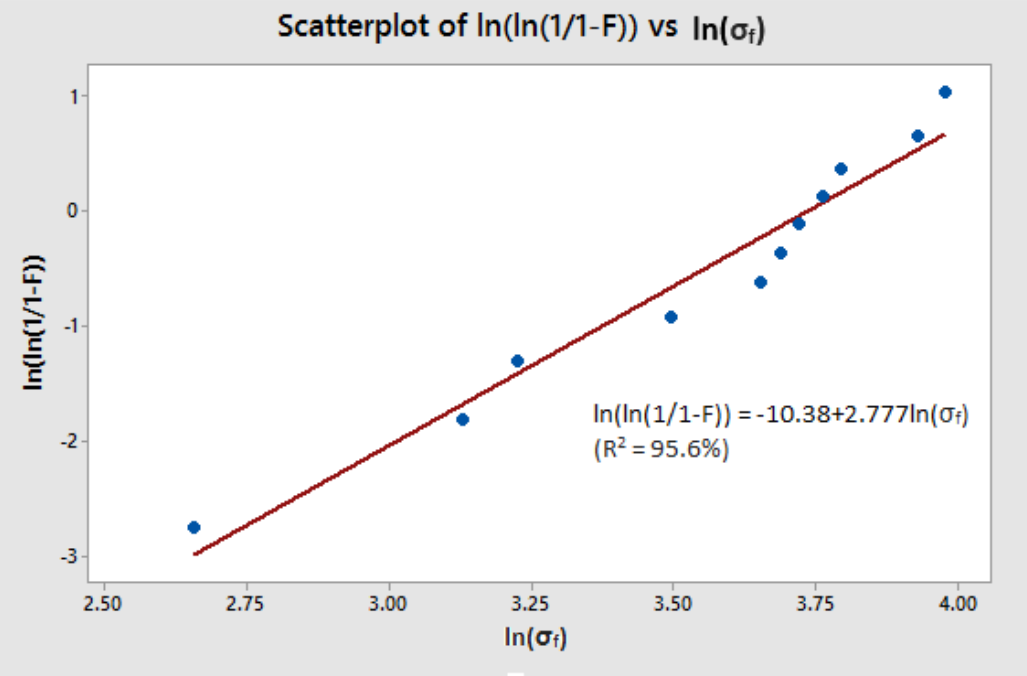

Fig. 64. Scatterplot of ln(ln(1/(1-F))) vs ln(σ) for 50°C heat-treated samples.

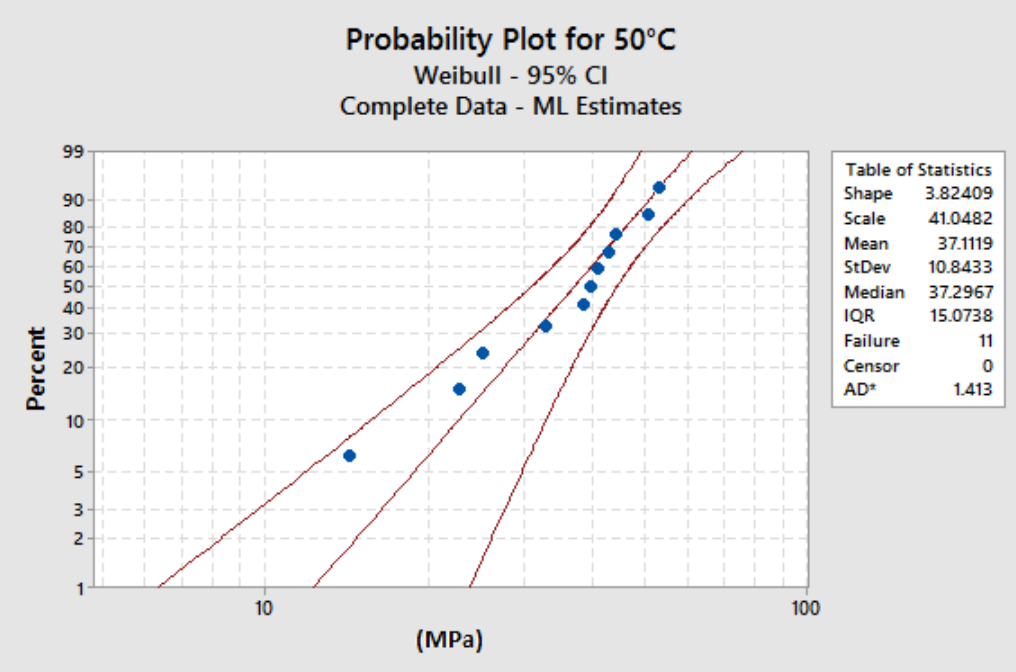

Fig. 65. 95% confidence interval probability plot for 50°C heat-treated samples.

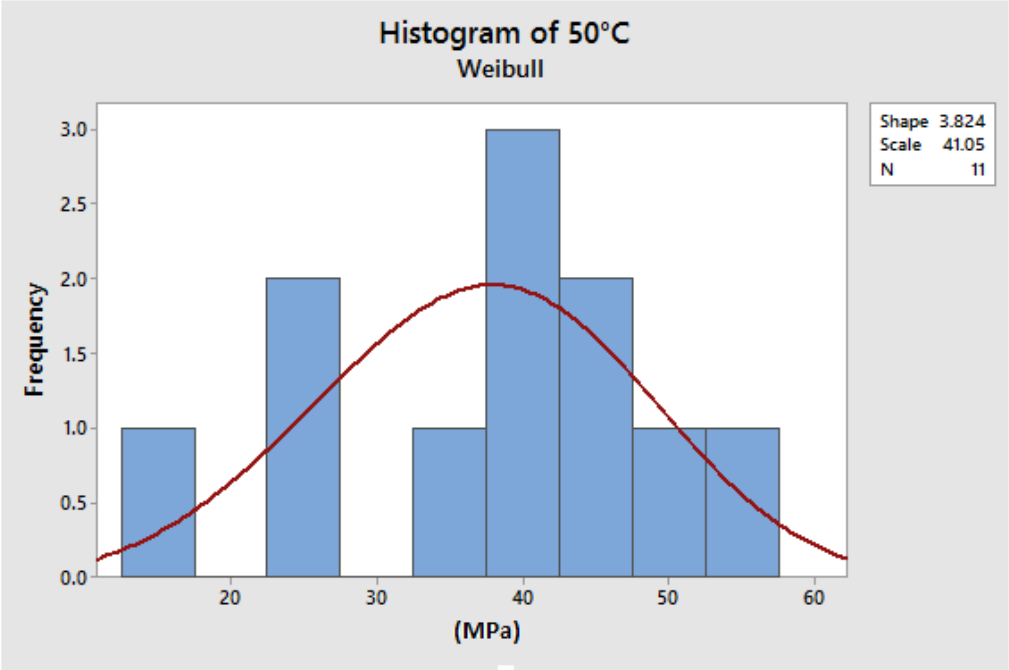

Fig. 66. Weibull fit to histogram for 50°C heat-treated samples.

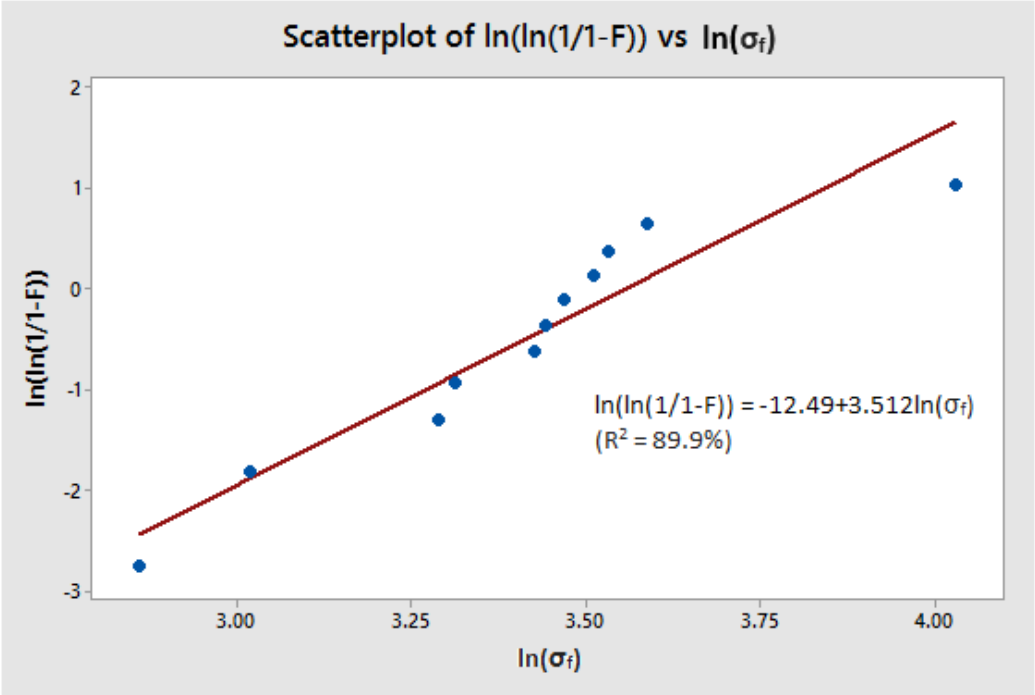

Fig. 67. Scatterplot of ln(ln(1/(1-F))) vs ln(σ) for 100°C heat-treated samples.

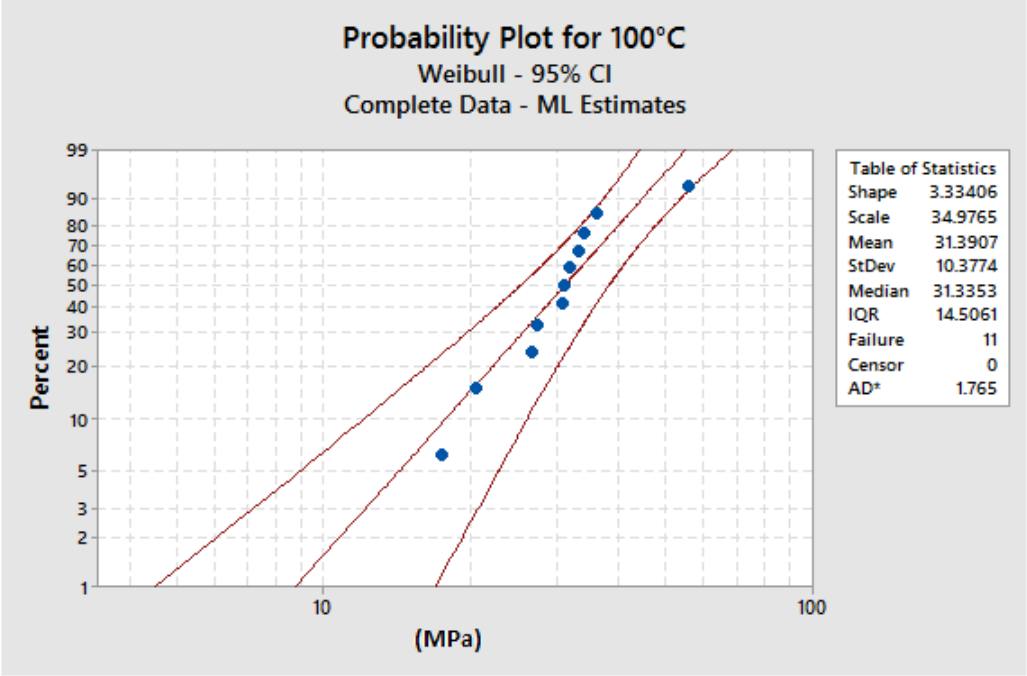

Fig. 68. 95% confidence interval probability plot for 100°C heat-treated samples.

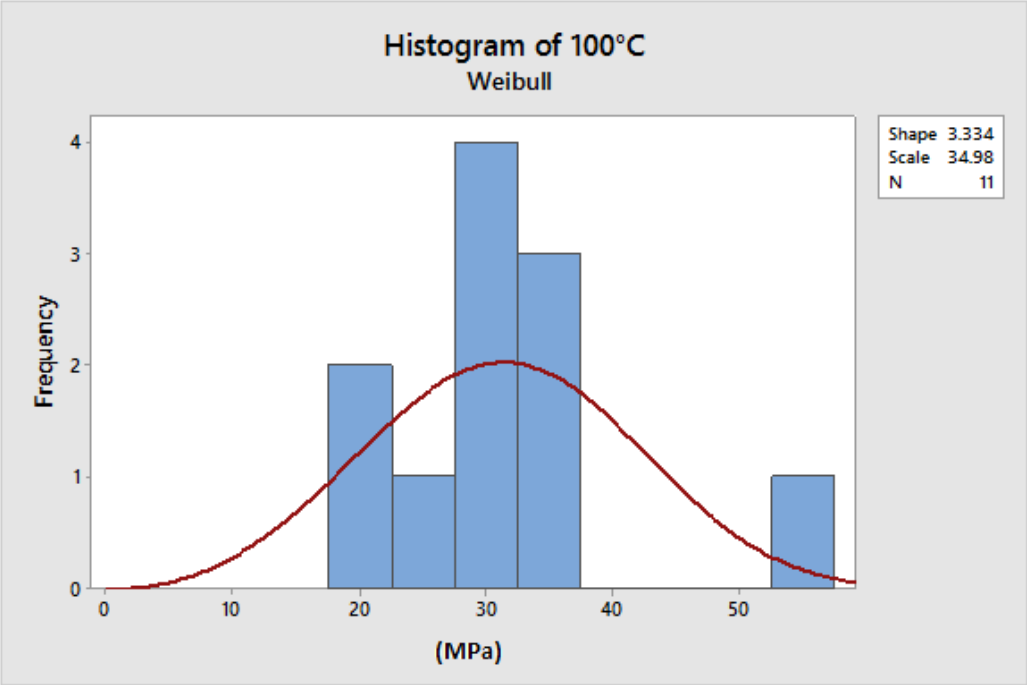

Fig. 69. Weibull fit to histogram for 100°C heat-treated samples.

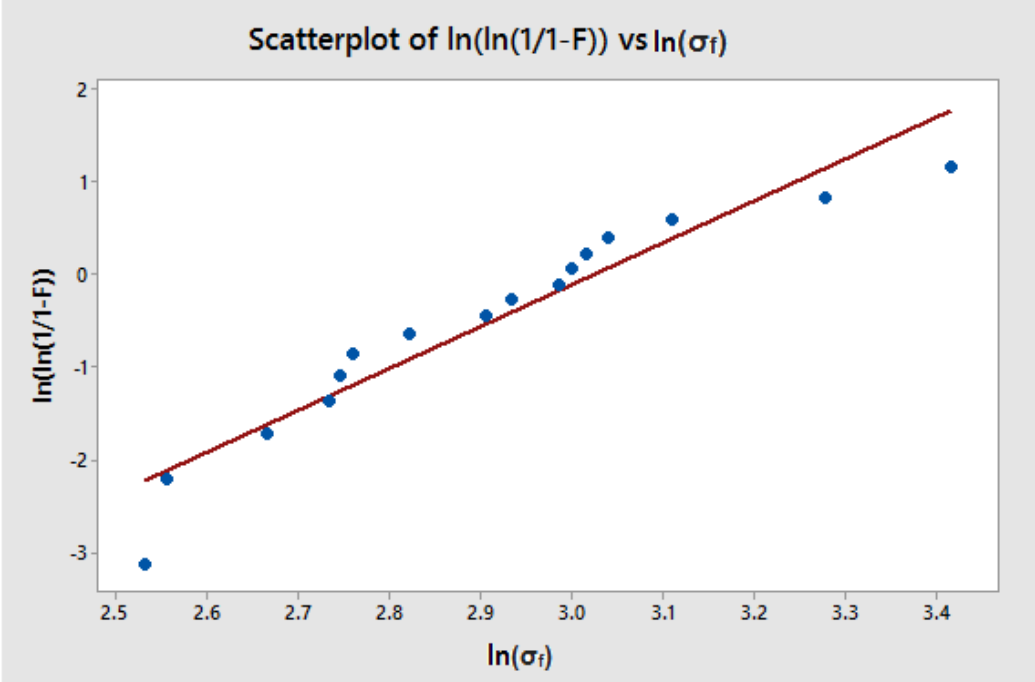

Fig. 70. Scatterplot of ln(ln(1/(1-F))) vs ln(σ) for 150°C heat-treated samples.

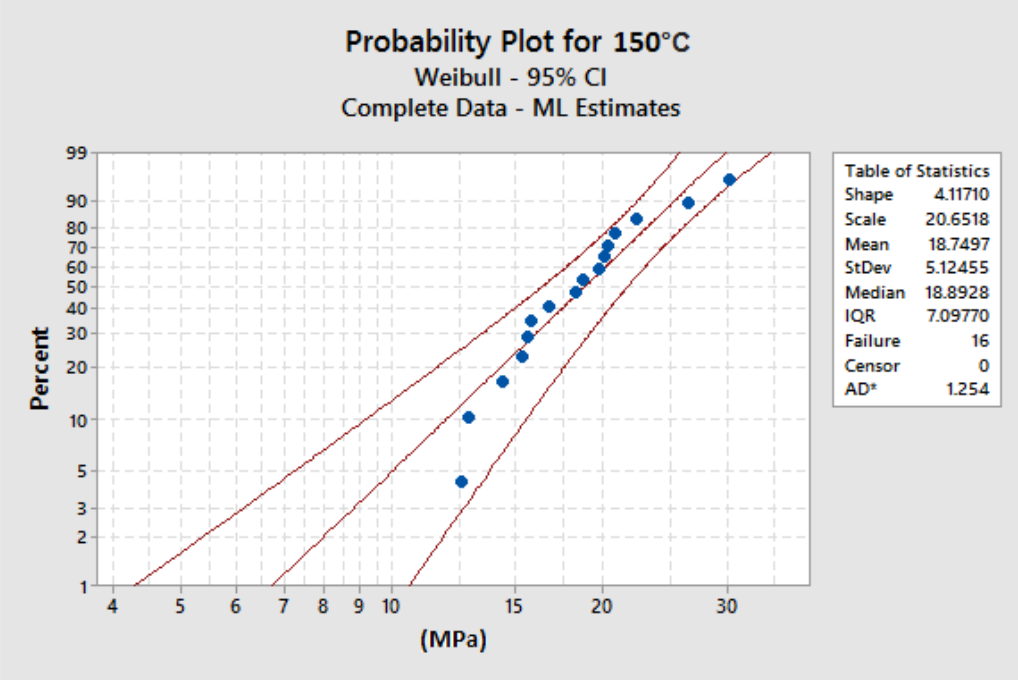

Fig. 71. 95% confidence interval probability plot for 150°C heat-treated samples.

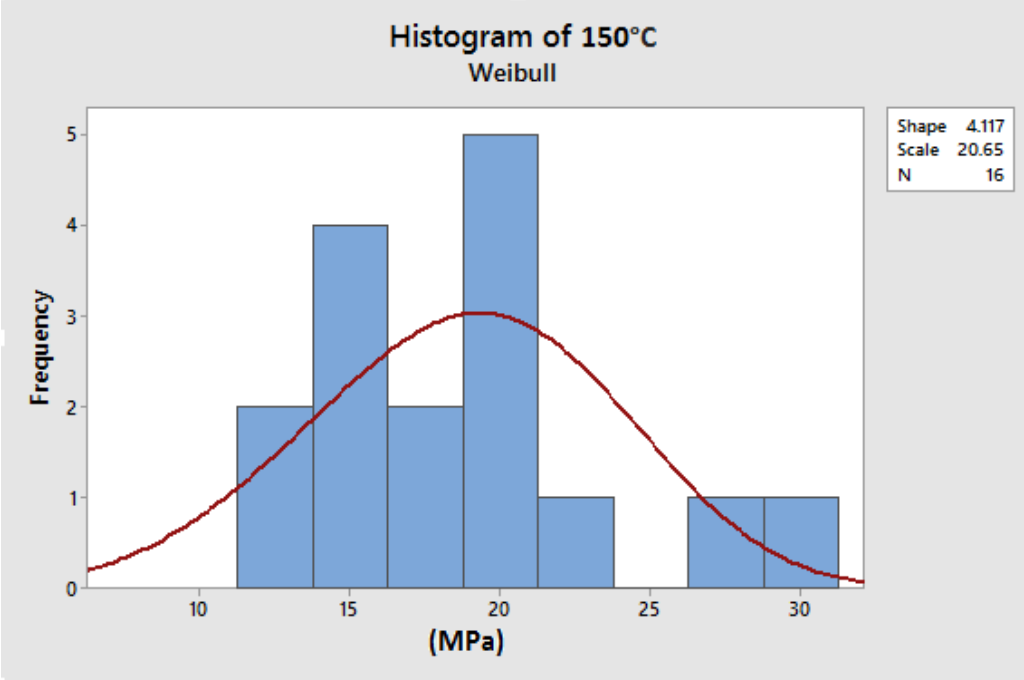

Fig. 72. Weibull fit to histogram for 150°C heat-treated samples.

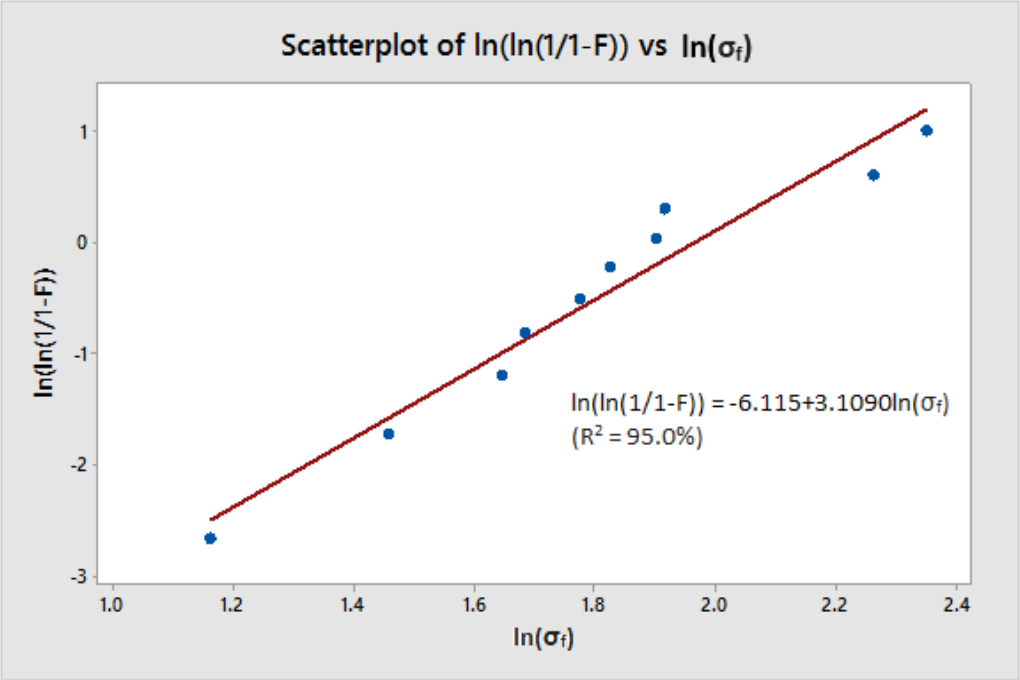

Fig. 73. Scatterplot of ln(ln(1/(1-F))) vs ln(σ) for 200°C heat-treated samples.

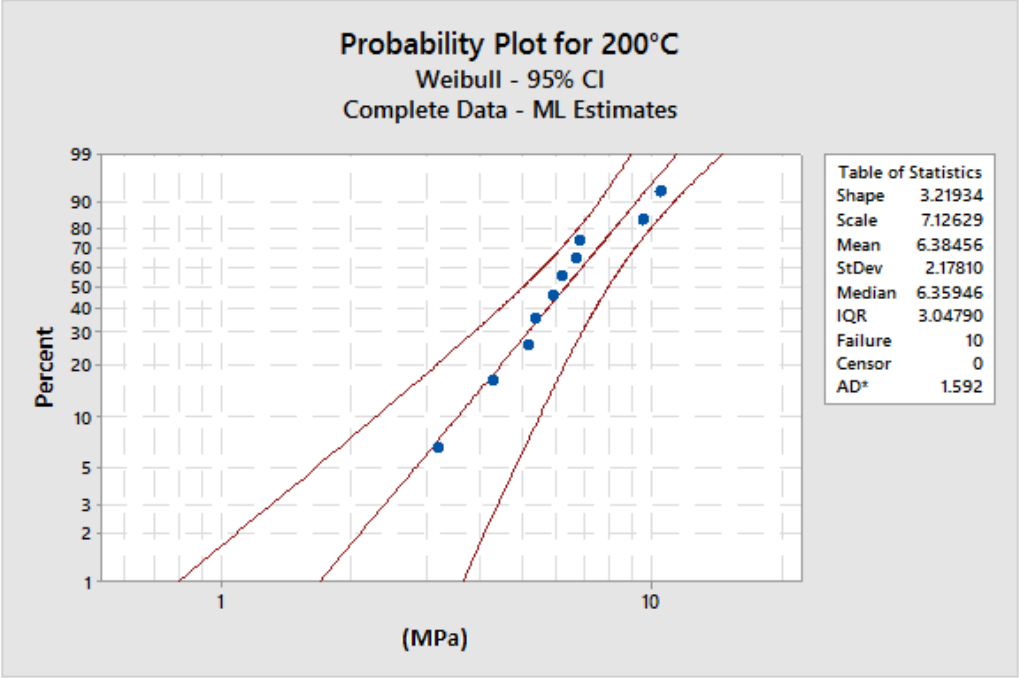

Fig. 74. 95% confidence interval probability plot for 200°C heat-treated samples.

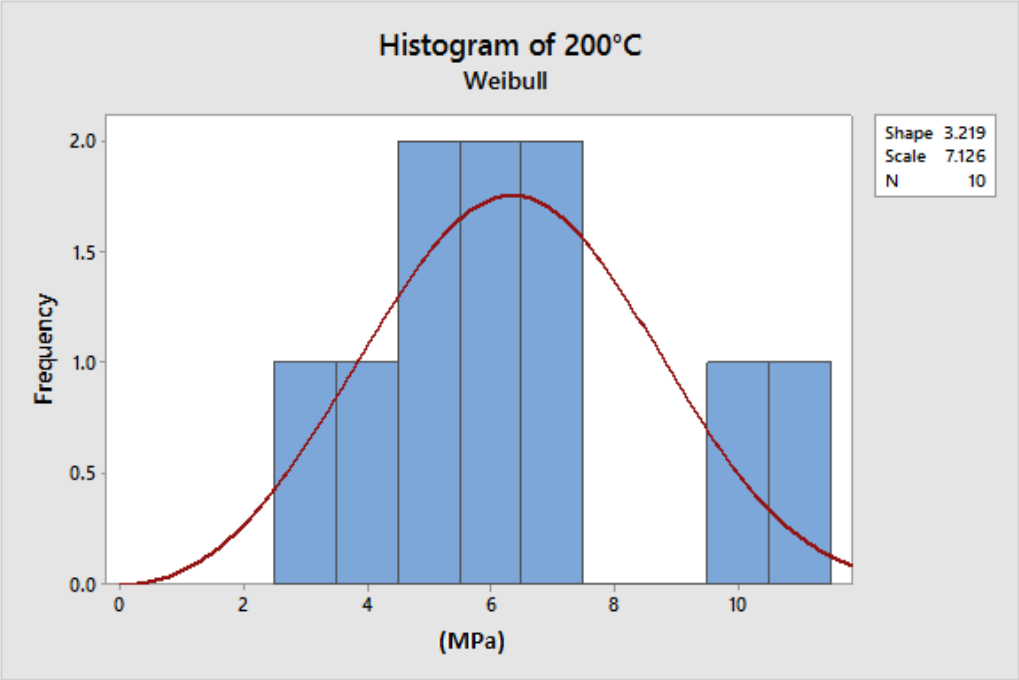

Fig. 75. Weibull fit to histogram for 200°C heat-treated samples.

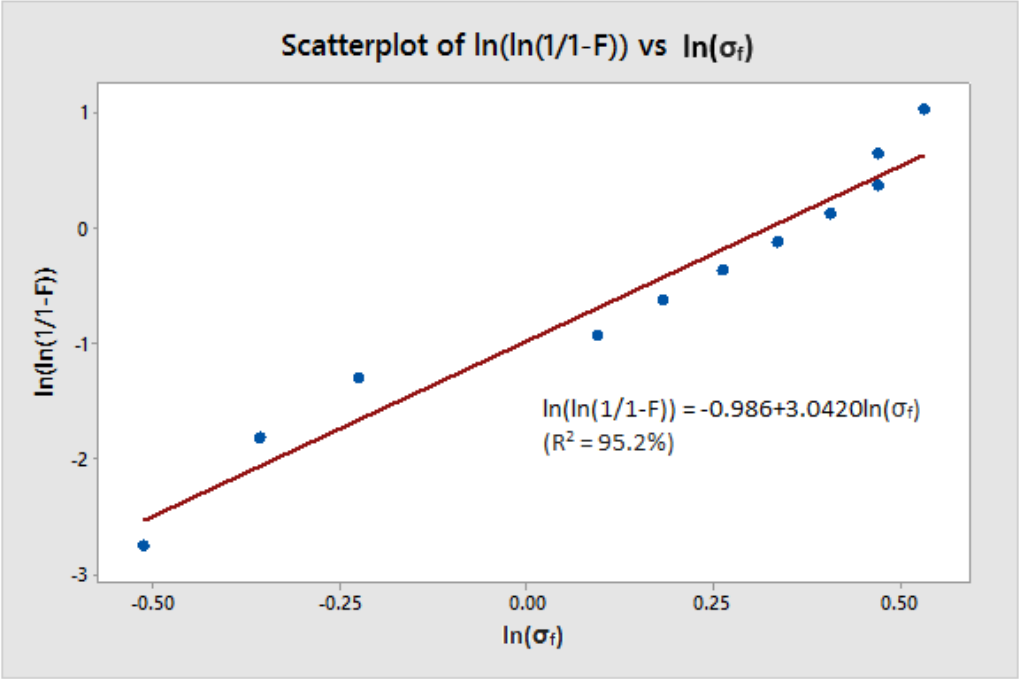

Fig. 76. Scatterplot of ln(ln(1/(1-F))) vs ln(σ) for 250°C heat-treated samples.

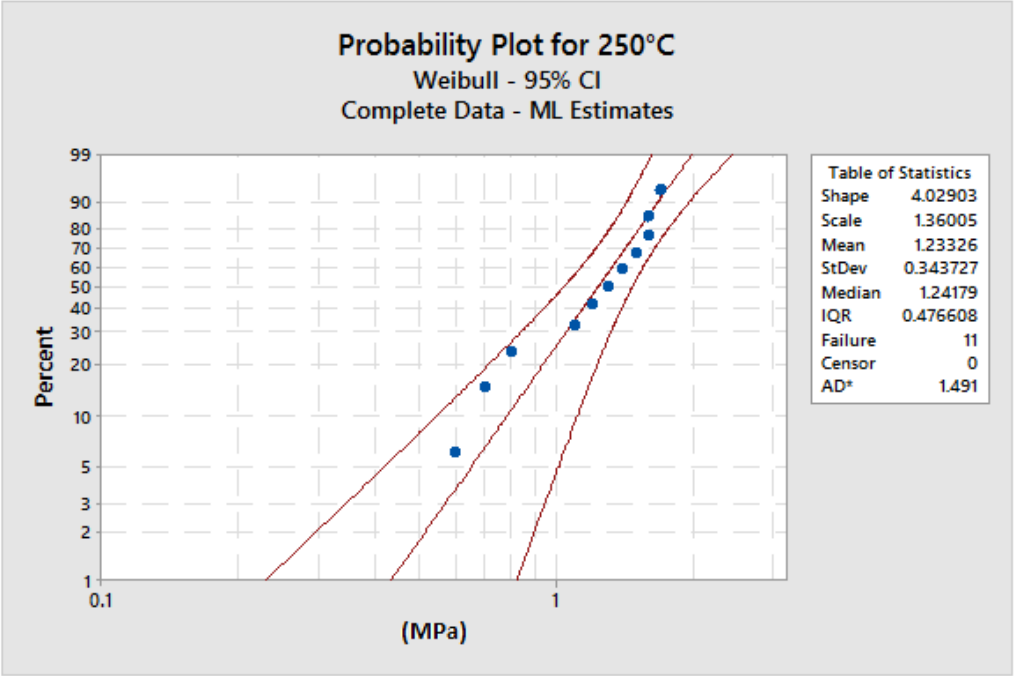

Fig. 77. 95% confidence interval probability plot for 250°C heat-treated samples.

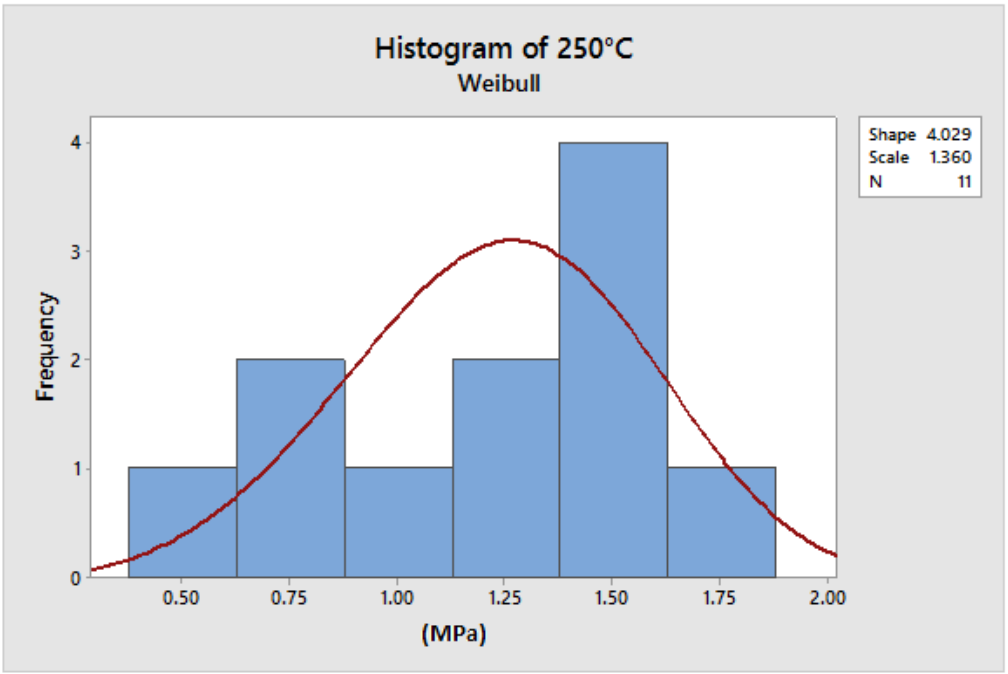

Fig. 78. Weibull fit to histogram for 250°C heat-treated samples.

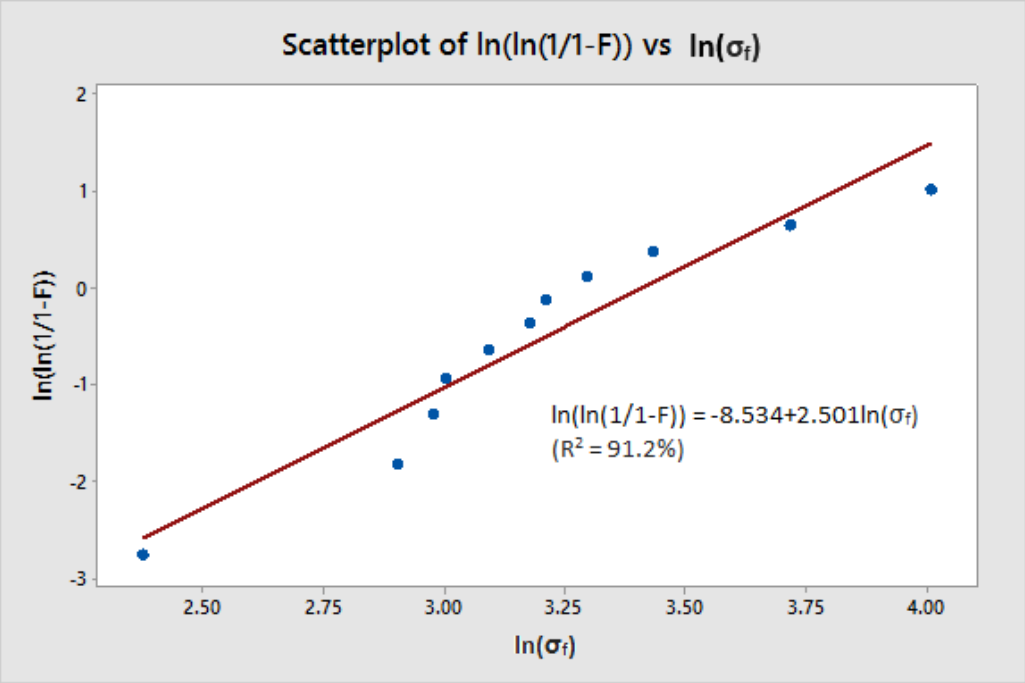

Fig. 79. Scatterplot of ln(ln(1/(1-F))) vs ln(σ) for NaOH durability samples.

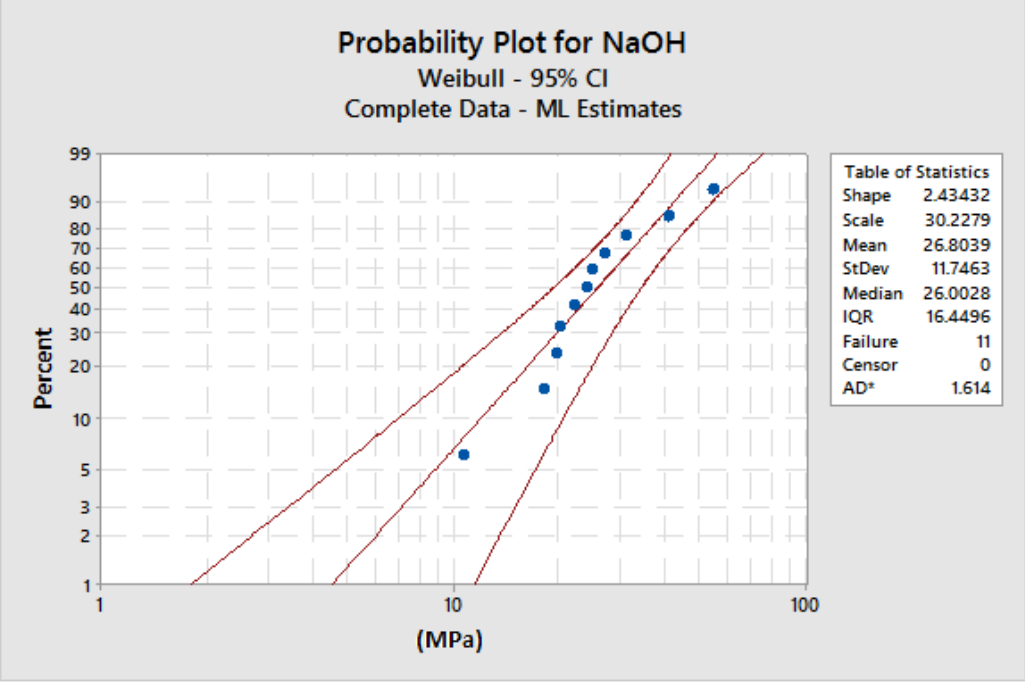

Fig. 80. 95% confidence interval probability plot for NaOH durability samples.

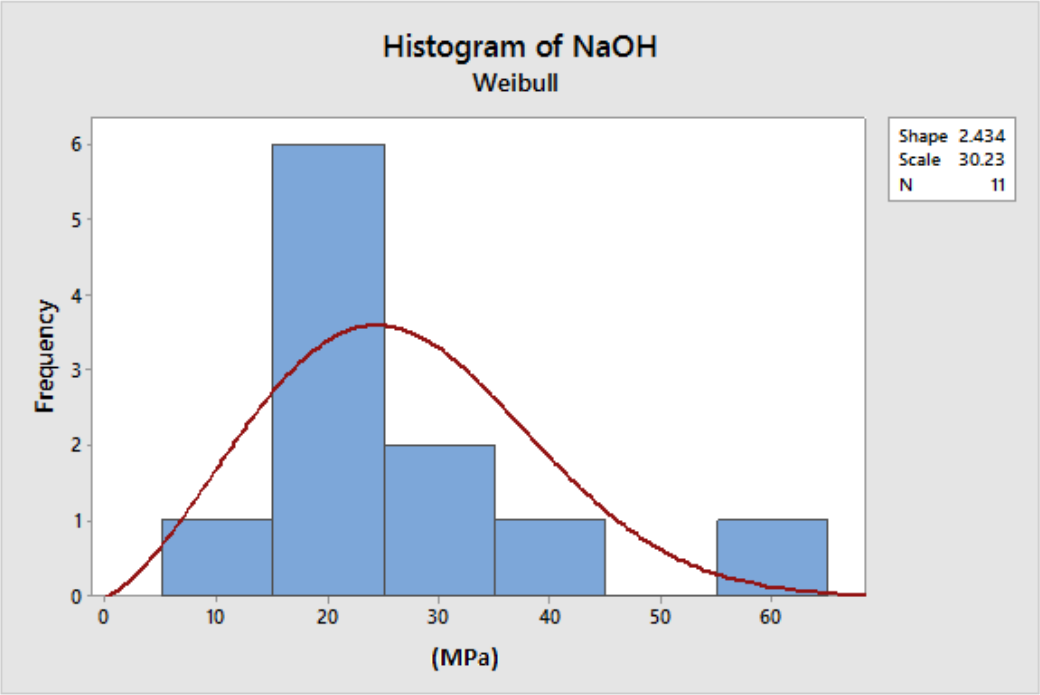

Fig. 81. Weibull fit to histogram for NaOH durability samples.

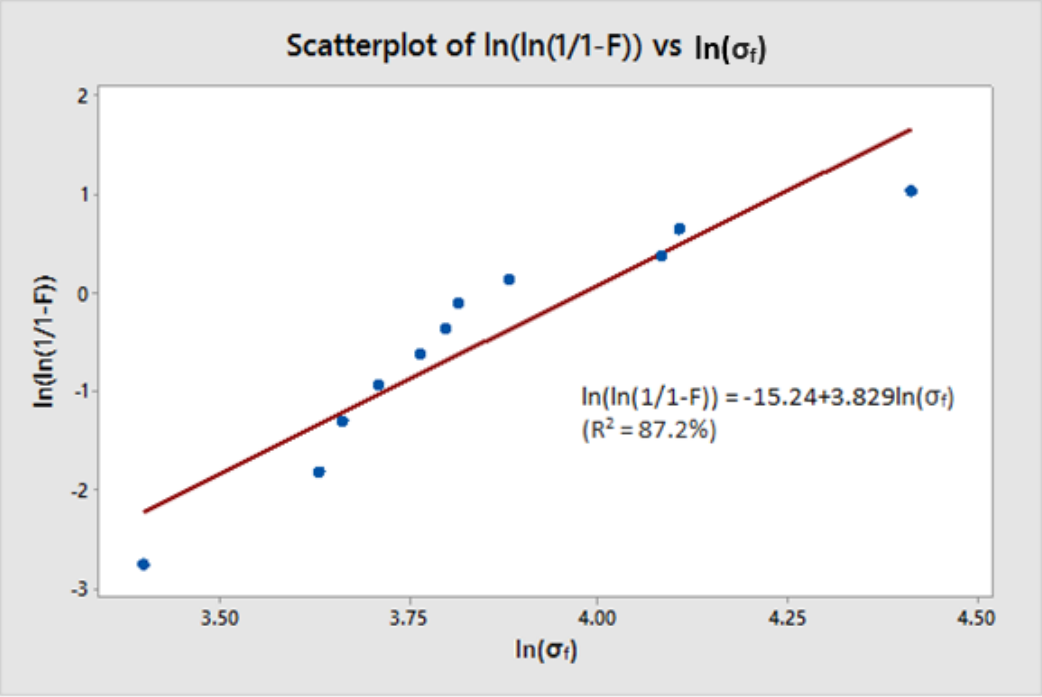

Fig. 82. Scatterplot of ln(ln(1/(1-F))) vs ln(σ) for water durability samples.

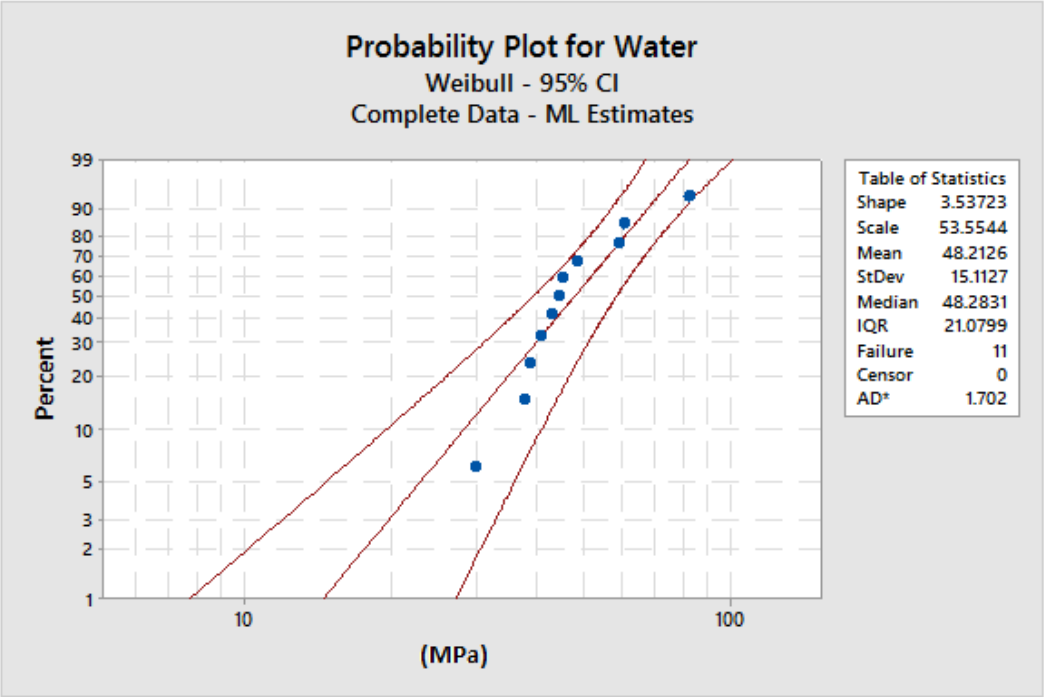

Fig. 83. 95% confidence interval probability plot for water durability samples.

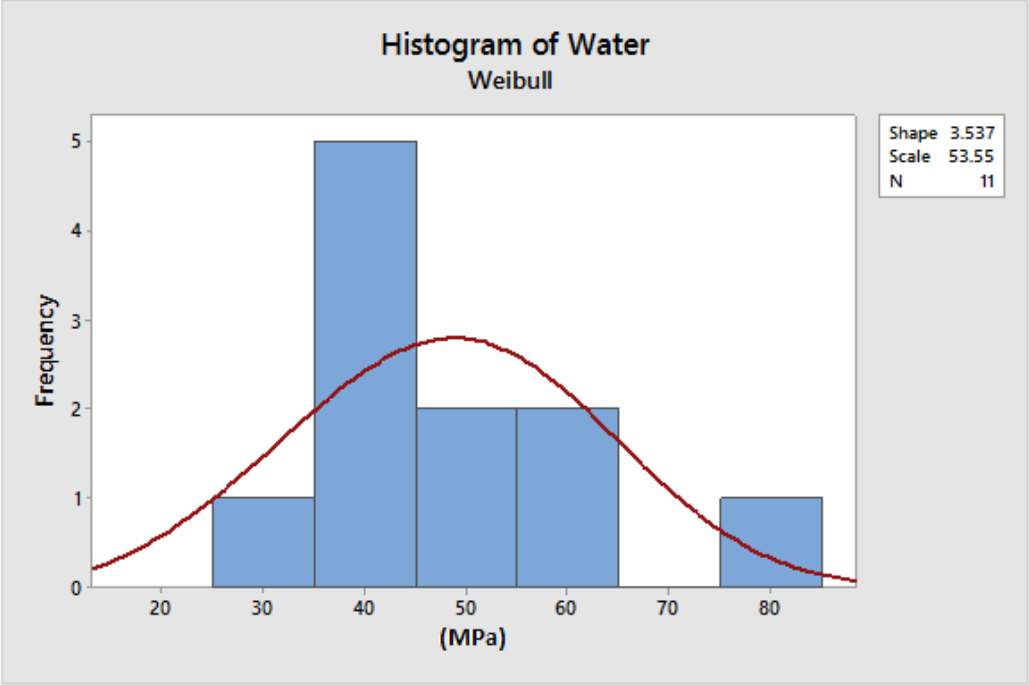

Fig. 84. Weibull fit to histogram for water durability samples.

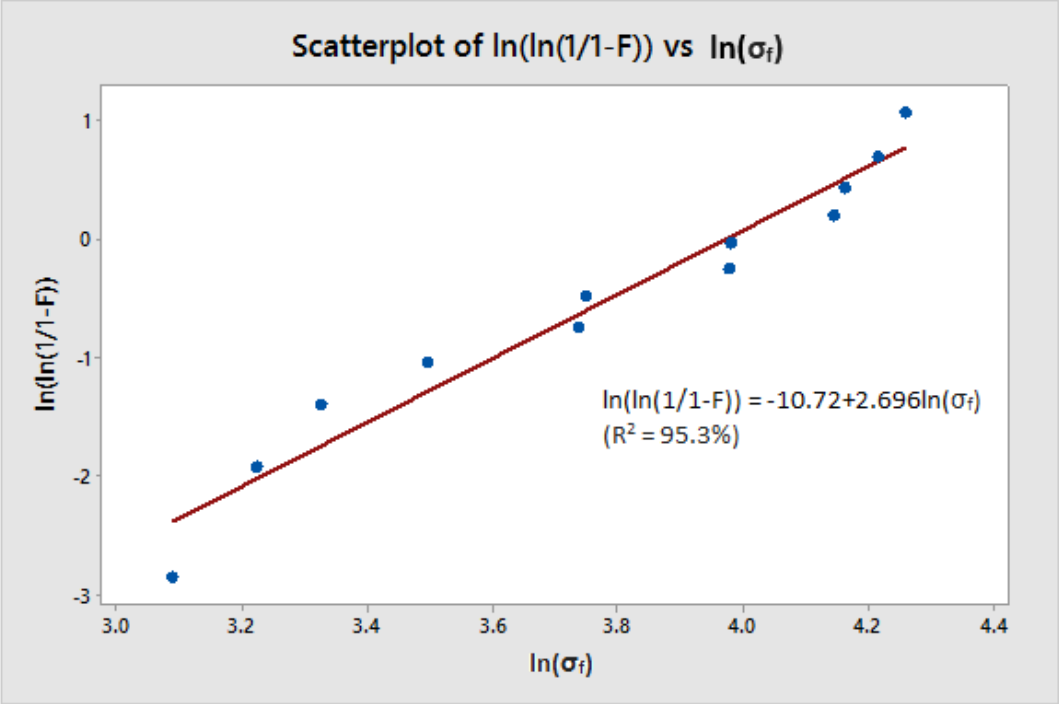

Fig. 85. Scatterplot of ln(ln(1/(1-F))) vs ln(σ) for salt water durability samples.

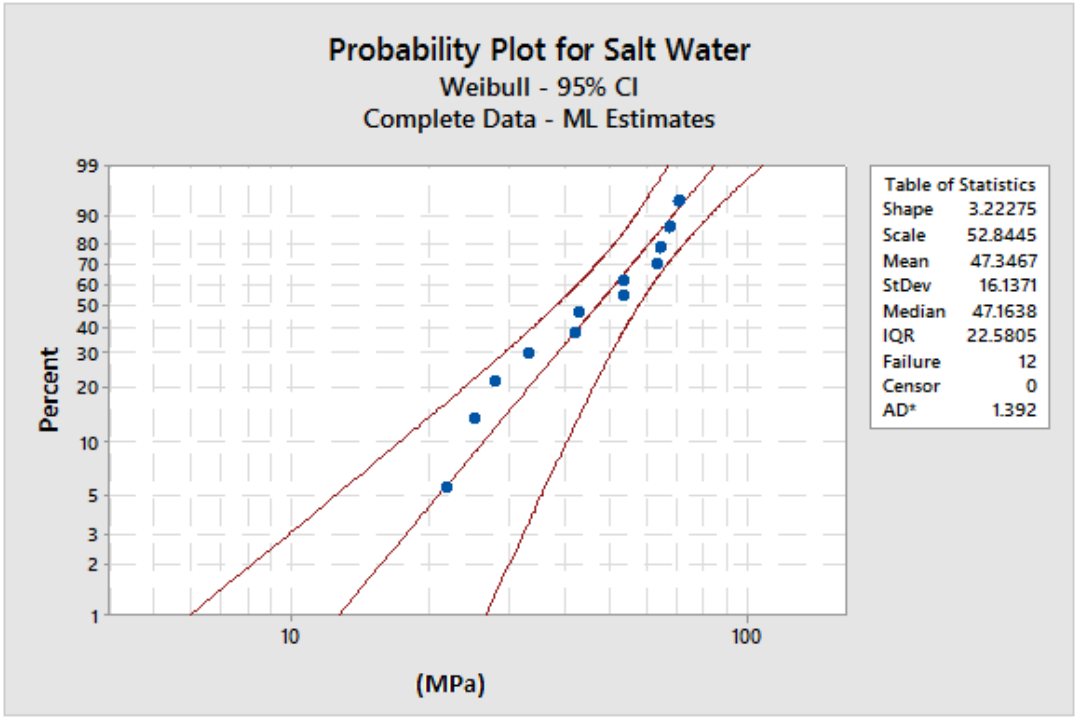

Fig. 86. 95% confidence interval probability plot for salt water durability samples.

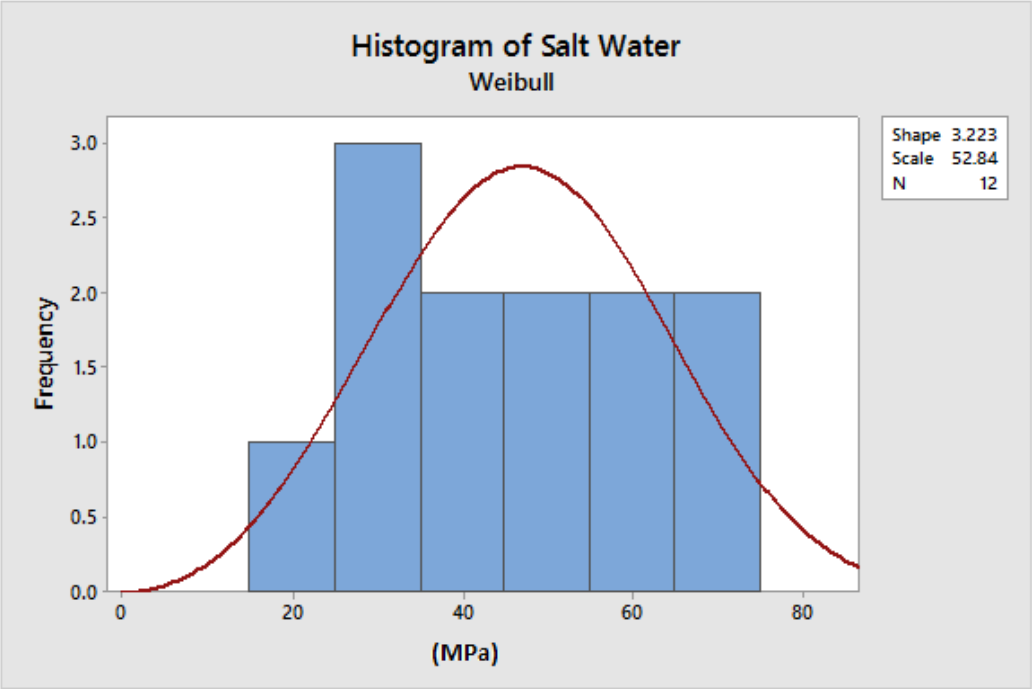

Fig. 87. Weibull fit to histogram for salt water durability samples.

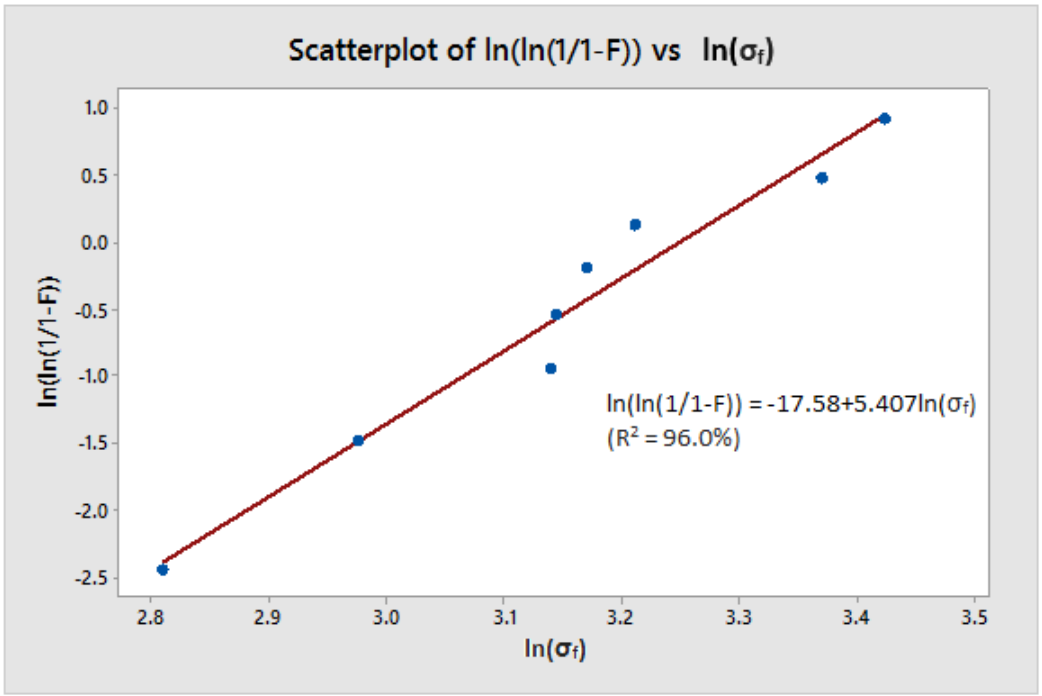

Fig. 88. Scatterplot of ln(ln(1/(1-F))) vs ln(σ) for freeze cycle durability samples.

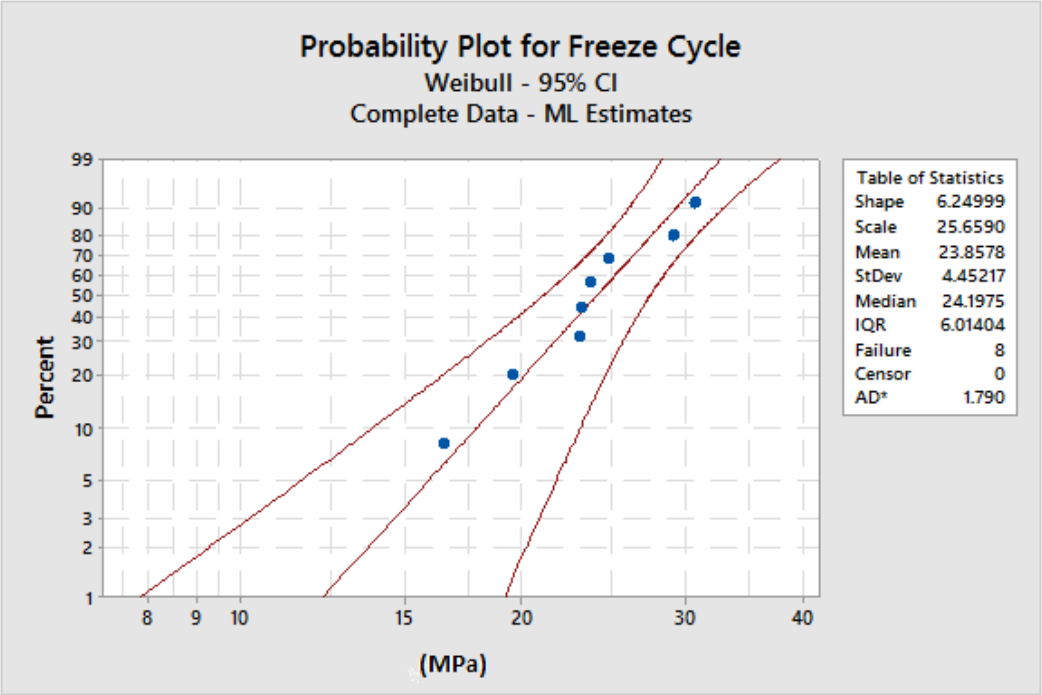

Fig. 89. 95% confidence interval probability plot for freeze cycle durability samples.

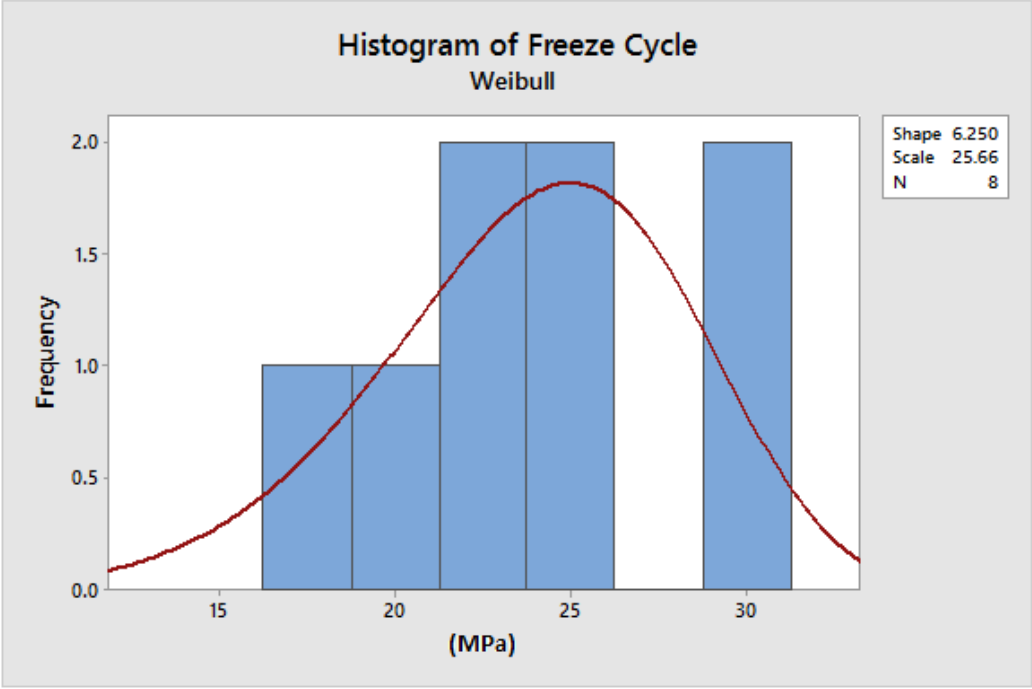

Fig. 90. Weibull fit to histogram for freeze cycle durability samples.

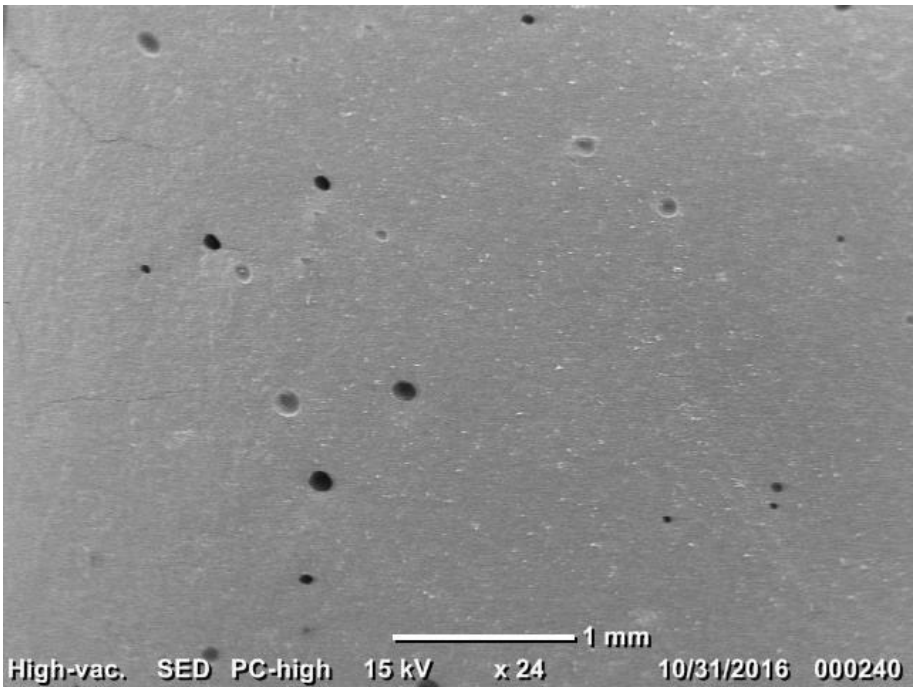

Fig. 91. SEM micrograph of 0 wt% abaca-potassium geopolymer at x24 magnification.

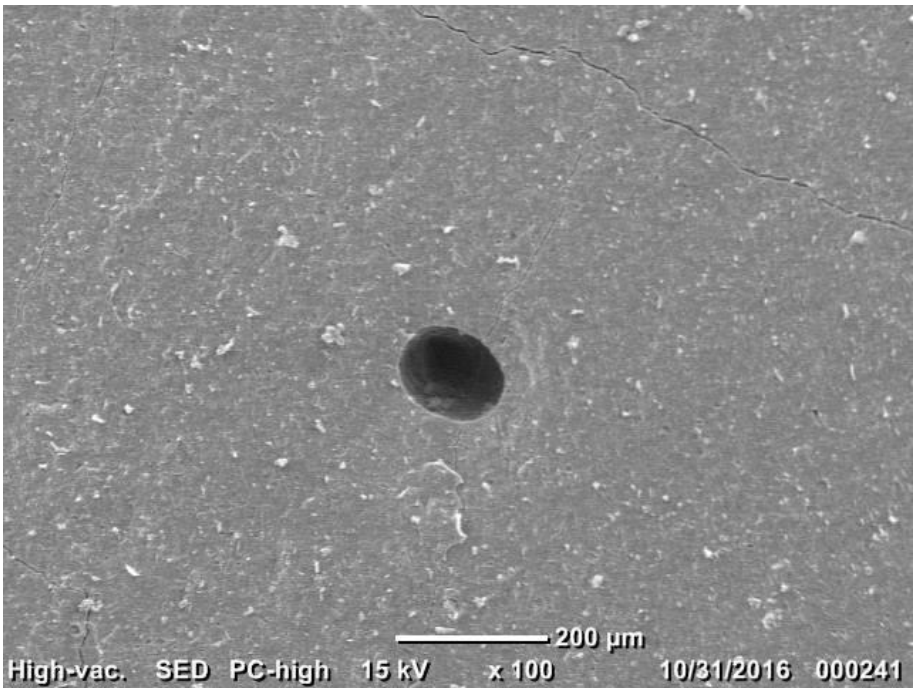

Fig. 92. SEM micrograph of 0 wt% abaca-potassium geopolymer at x100 magnification.

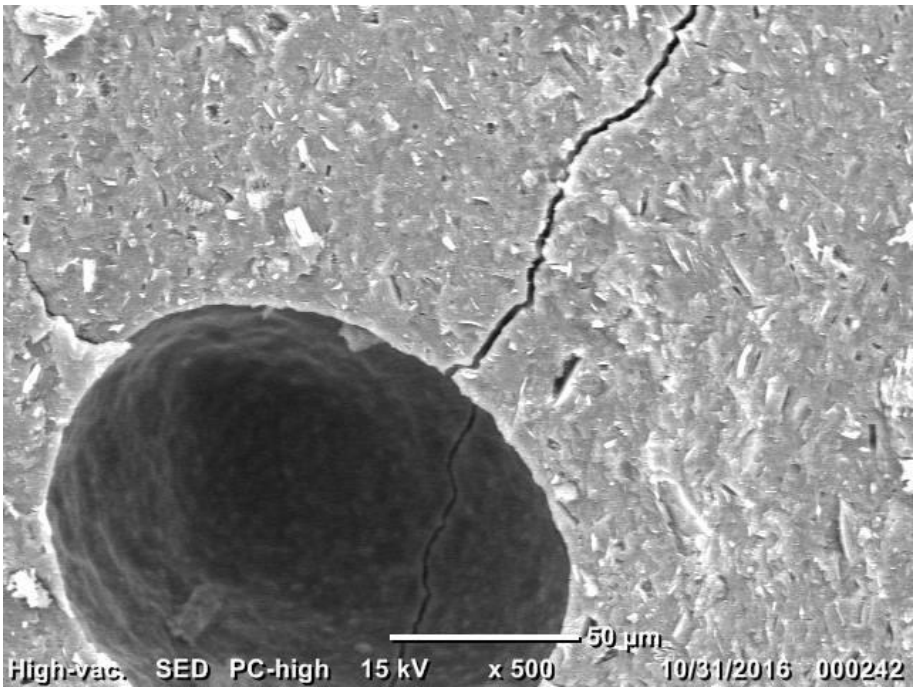

Fig. 93. SEM micrograph of 0 wt% abaca-potassium geopolymer at x500 magnification.

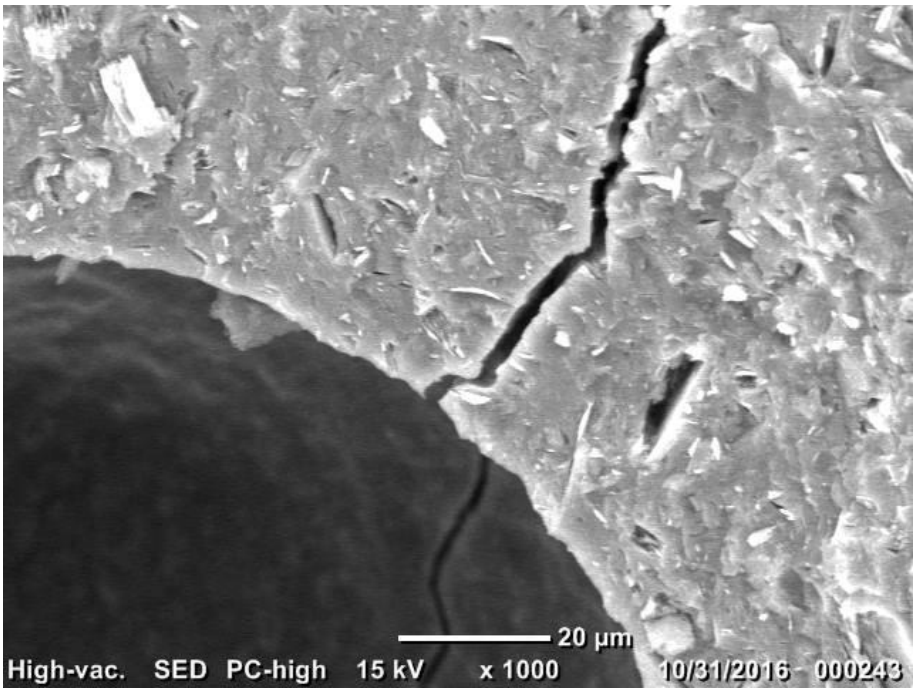

Fig. 94. SEM micrograph of 0 wt% abaca-potassium geopolymer at x1000 magnification.

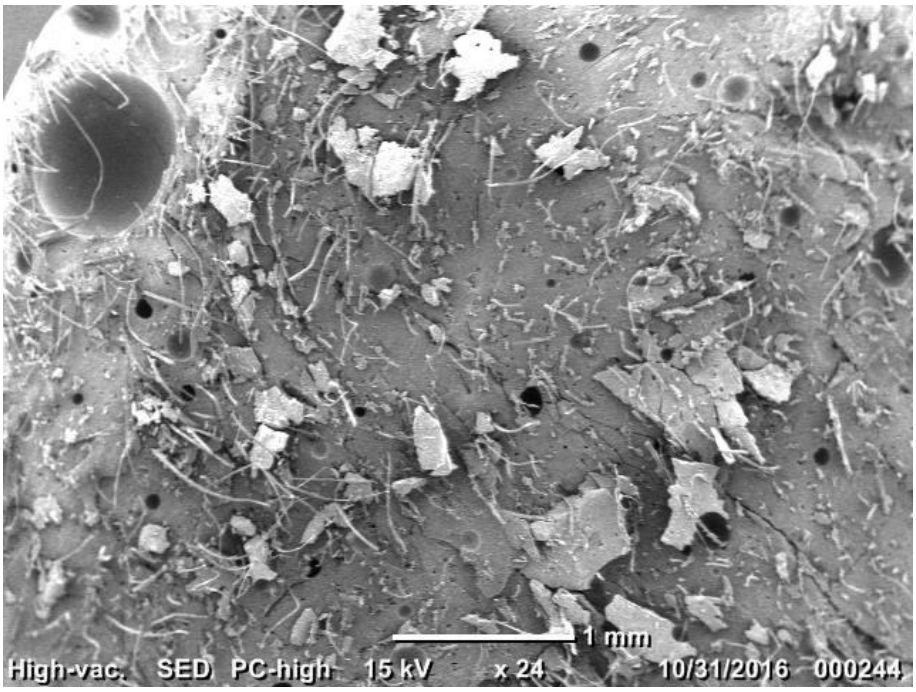

Fig. 95. SEM micrograph of 2 wt% abaca-potassium geopolymer at x24 magnification.

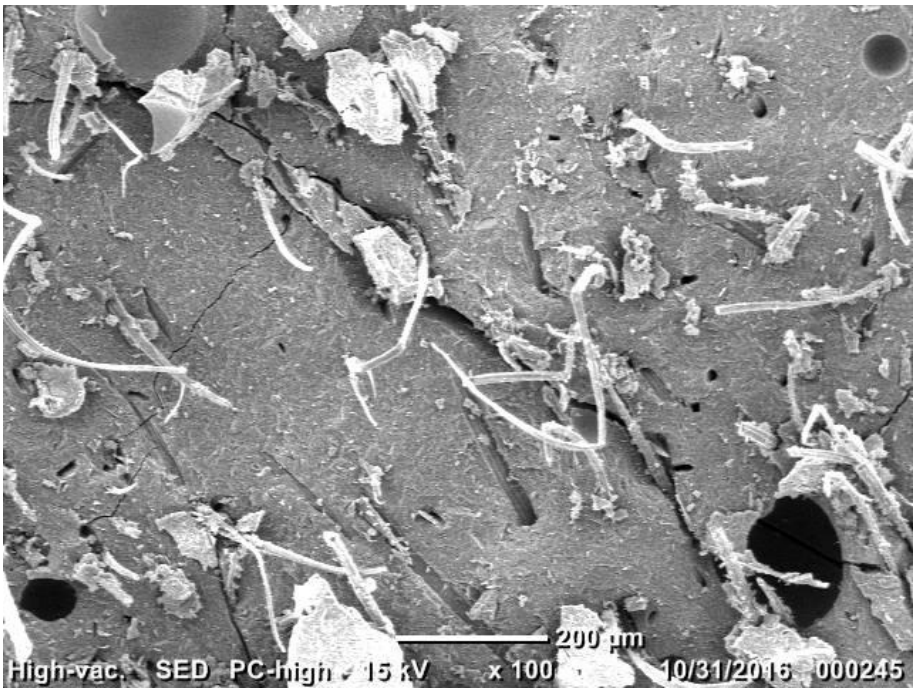

Fig. 96. SEM micrograph of 2 wt% abaca-potassium geopolymer at x100 magnification.

Fig. 97. SEM micrograph of 2 wt% abaca-potassium geopolymer at x500 magnification.

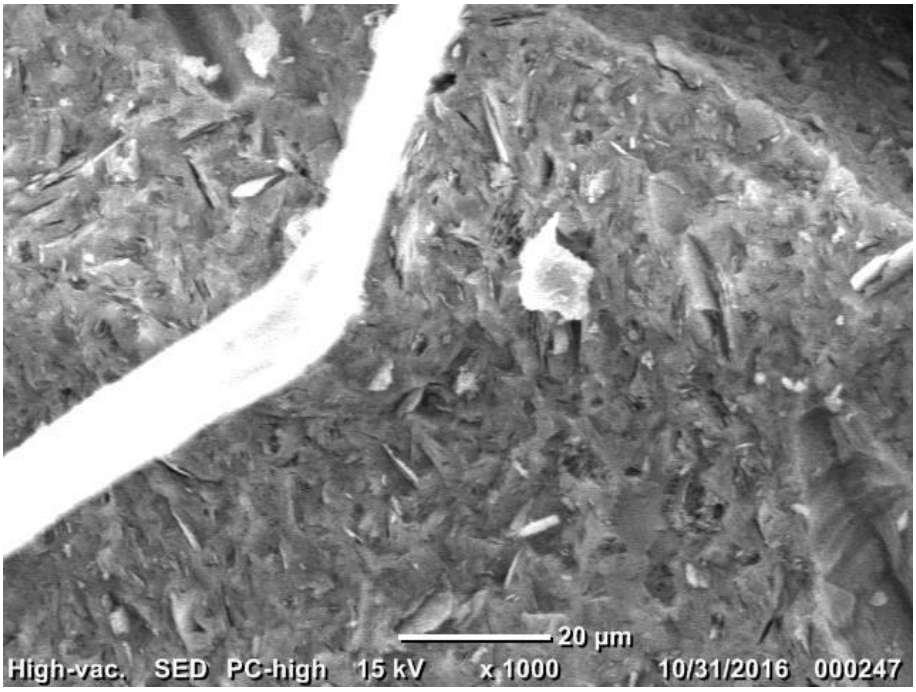

Fig. 98. SEM micrograph of 2 wt% abaca-potassium geopolymer at x1000 magnification.

Fig. 99. SEM micrograph of 4 wt% abaca-potassium geopolymer at x27 magnification.

Fig. 100. SEM micrograph of 4 wt% abaca-potassium geopolymer at x100 magnification.

Fig. 101. SEM micrograph of 4 wt% abaca-potassium geopolymer at x500 magnification.

Fig. 102. SEM micrograph of 4 wt% abaca-potassium geopolymer at x1000 magnification.

Fig. 103. SEM micrograph of 6 wt% abaca-potassium geopolymer at x24 magnification.

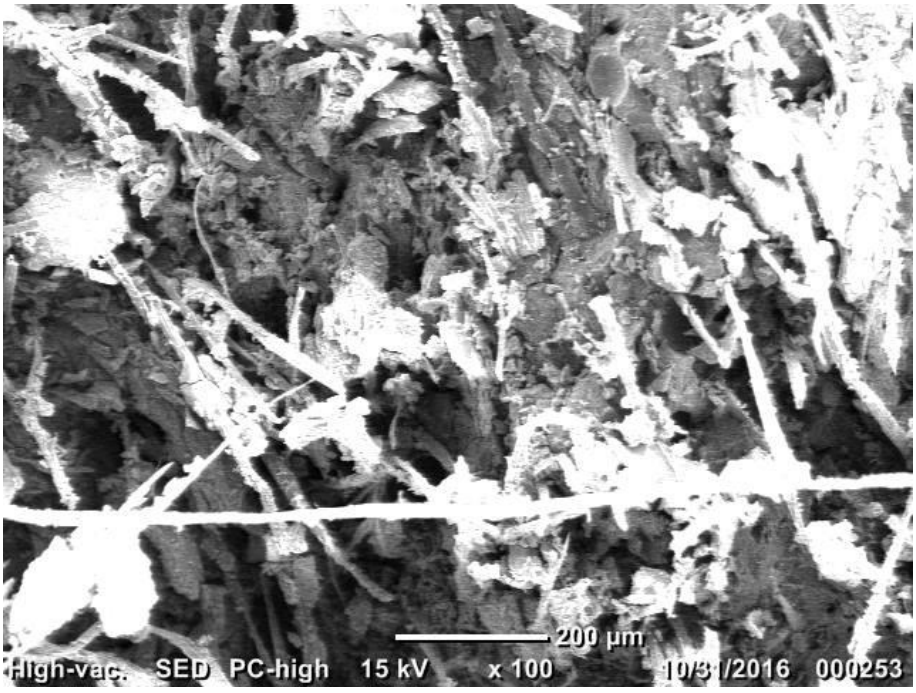

Fig. 104. SEM micrograph of 6 wt% abaca-potassium geopolymer at x100 magnification.

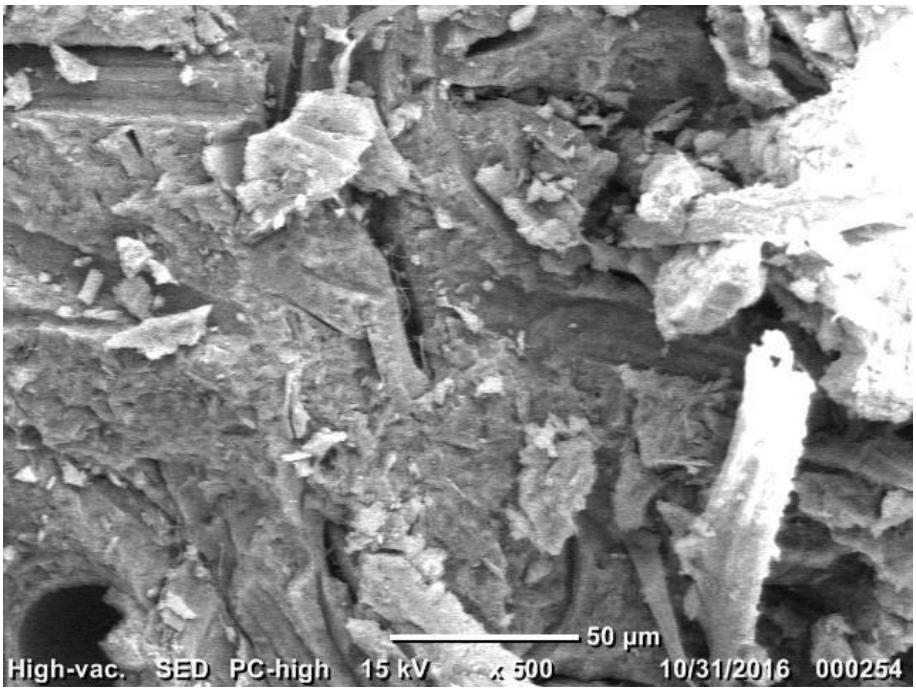

Fig. 105. SEM micrograph of 6 wt% abaca-potassium geopolymer at x500 magnification.

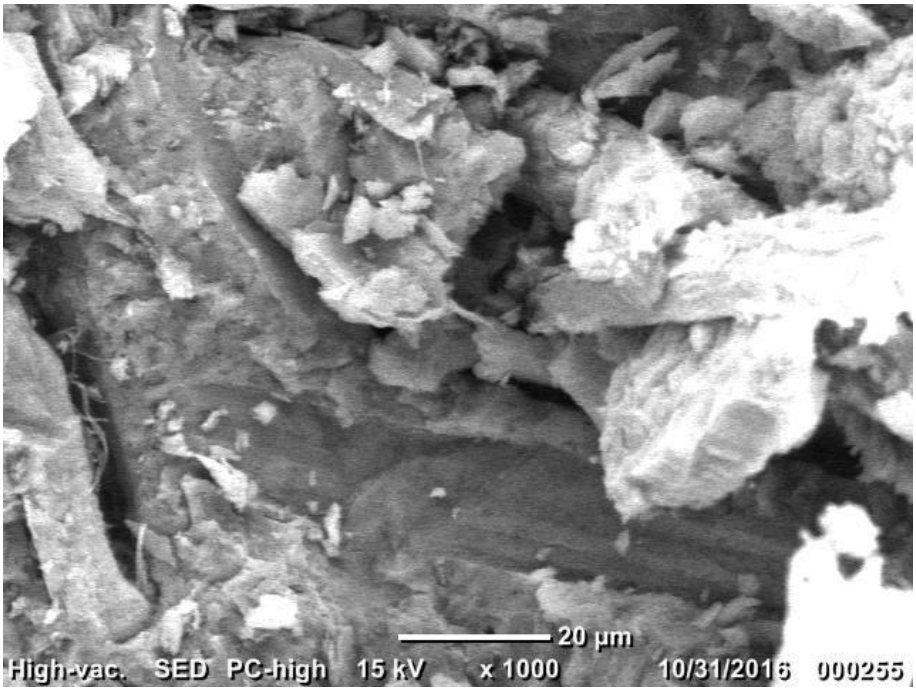

Fig. 106. SEM micrograph of 6 wt% abaca-potassium geopolymer at x1000 magnification.

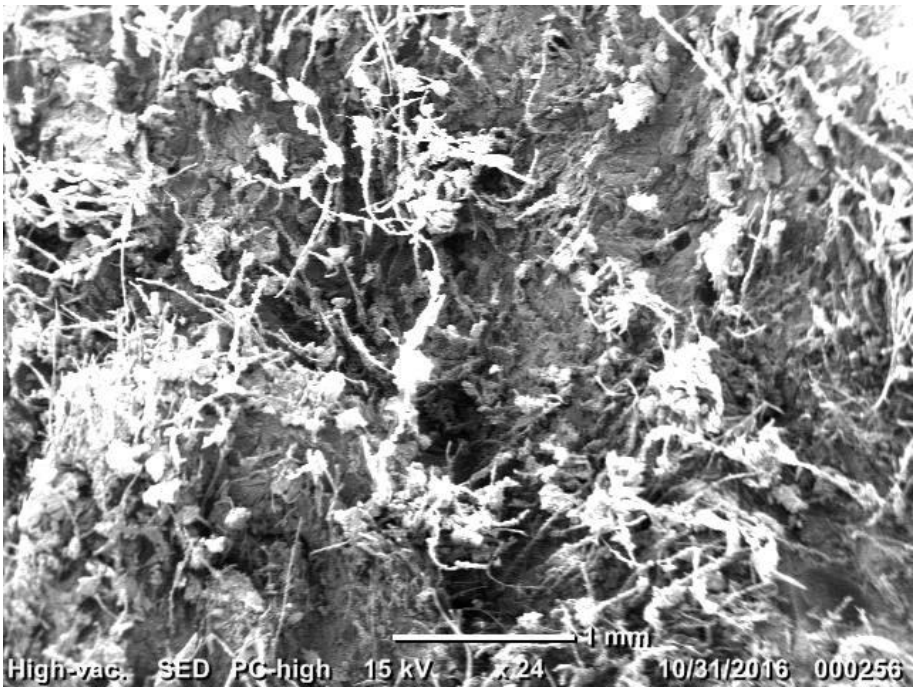

Fig. 107. SEM micrograph of 8 wt% abaca-potassium geopolymer at x24 magnification.

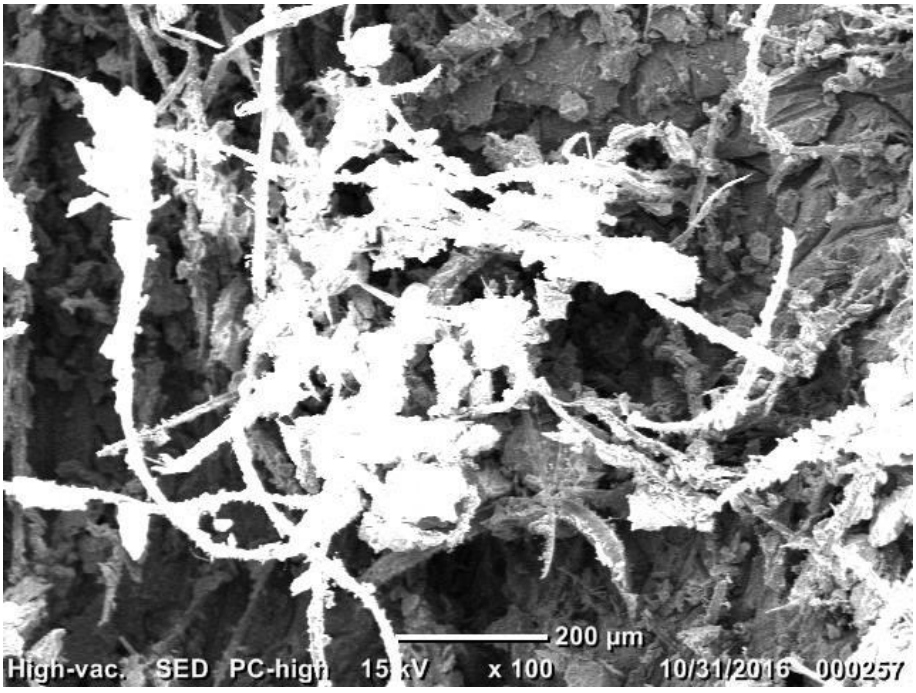

Fig. 108. SEM micrograph of 8 wt% abaca-potassium geopolymer at x100 magnification.

Fig. 109. SEM micrograph of 8 wt% abaca-potassium geopolymer at x500 magnification.

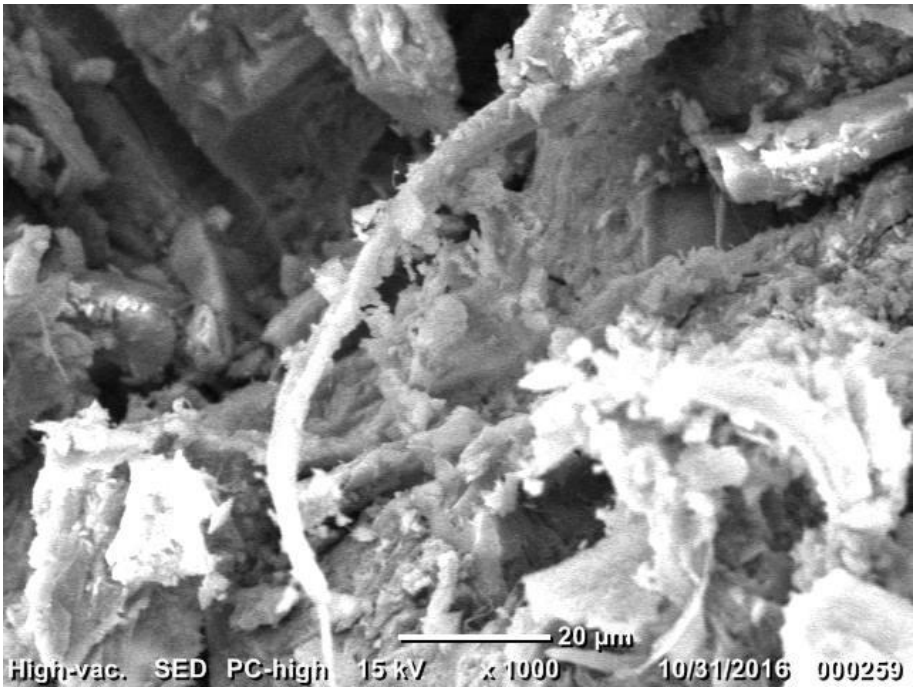

Fig. 110. SEM micrograph of 8 wt% abaca-potassium geopolymer at x1000 magnification.

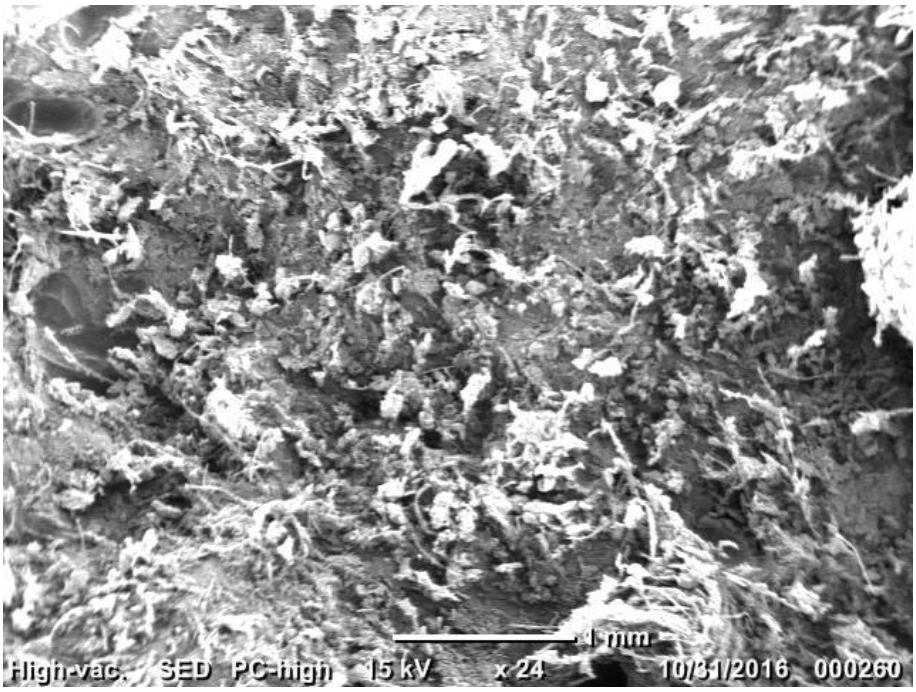

Fig. 111. SEM micrograph of 50°C heat treated sample at x24 magnification.

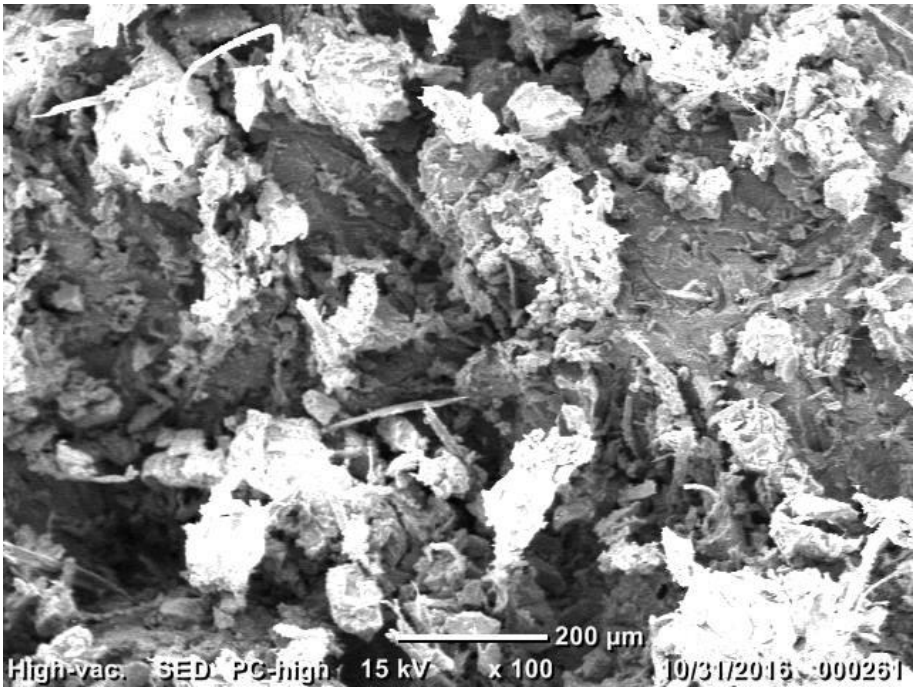

Fig. 112. SEM micrograph of 50°C heat treated sample at x100 magnification.

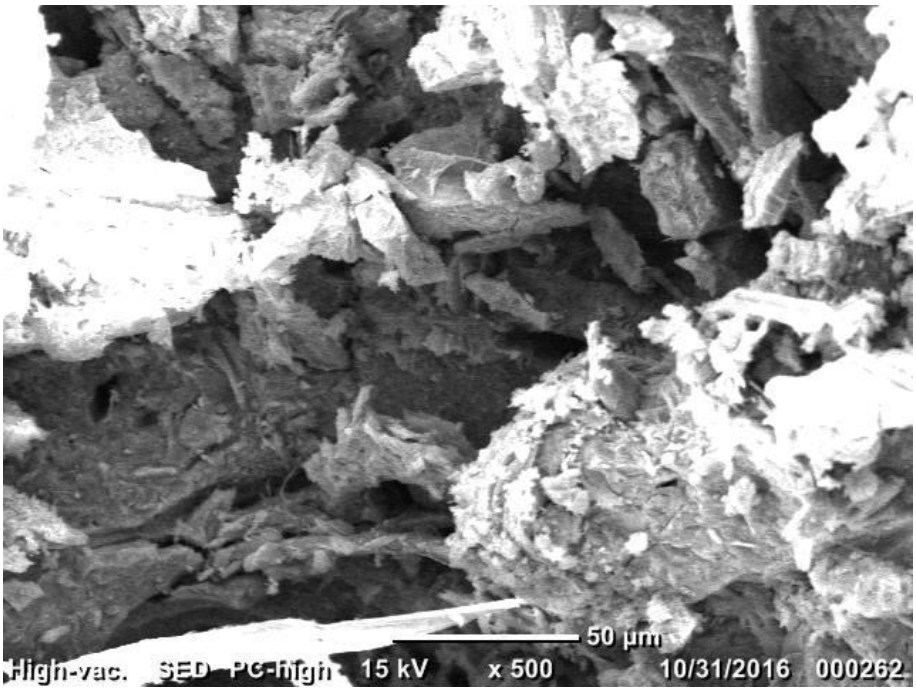

Fig. 113. SEM micrograph of 50°C heat treated sample at x500 magnification.

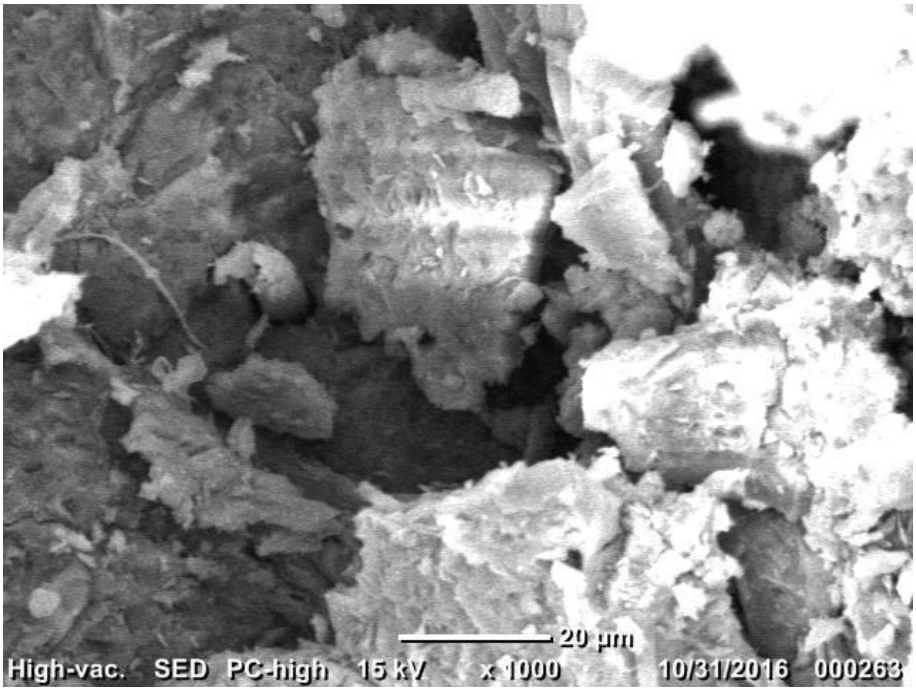

Fig. 114. SEM micrograph of 50°C heat treated sample at x1000 magnification.

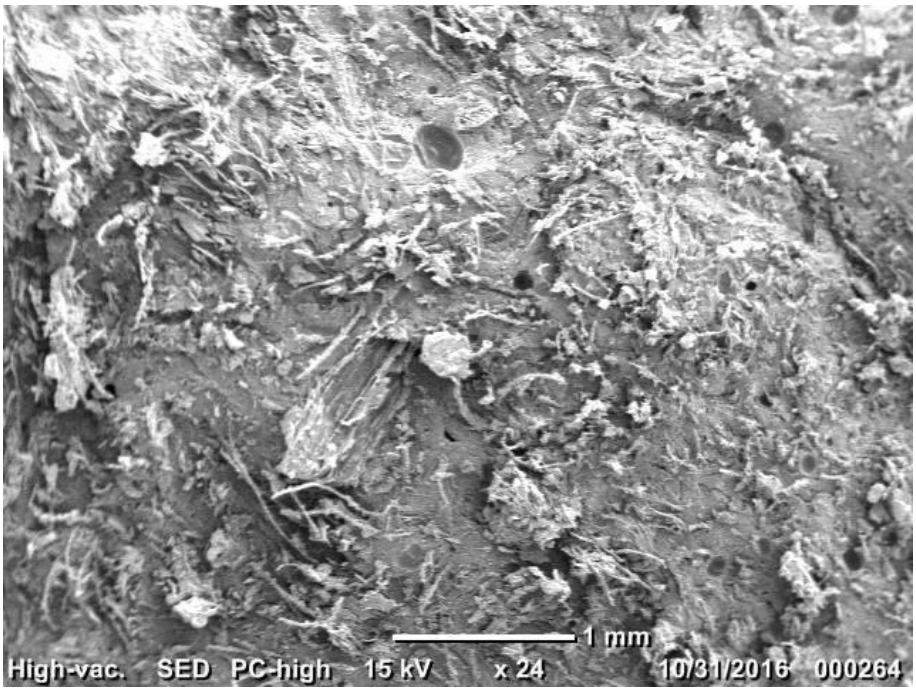

Fig. 115. SEM micrograph of 100°C heat treated sample at x24 magnification.

Fig. 116. SEM micrograph of 100°C heat treated sample at x100 magnification.

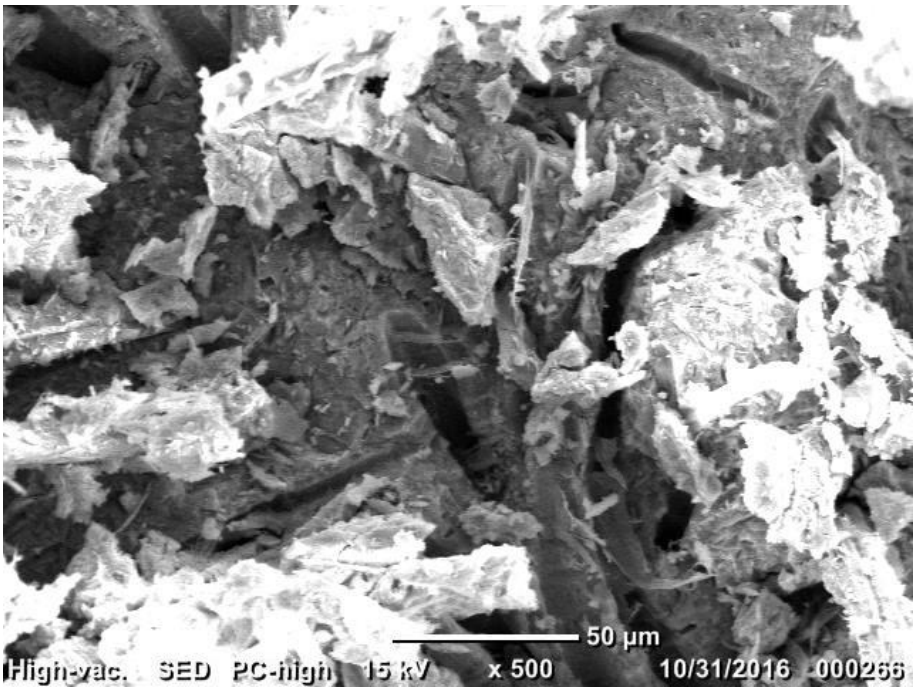

Fig. 117. SEM micrograph of 100°C heat treated sample at x500 magnification.

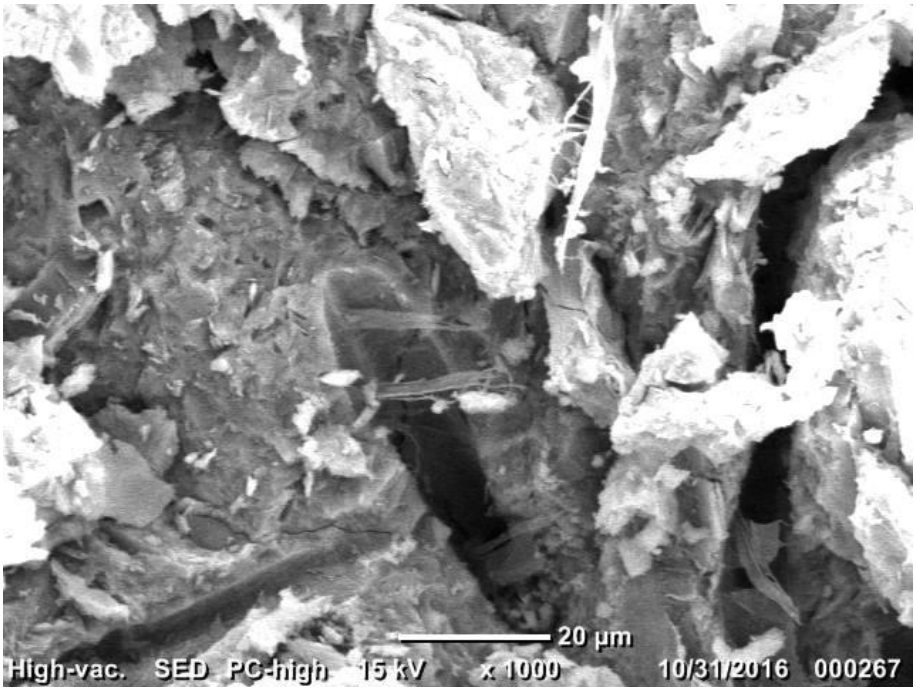

Fig. 118. SEM micrograph of 100°C heat treated sample at x1000 magnification.

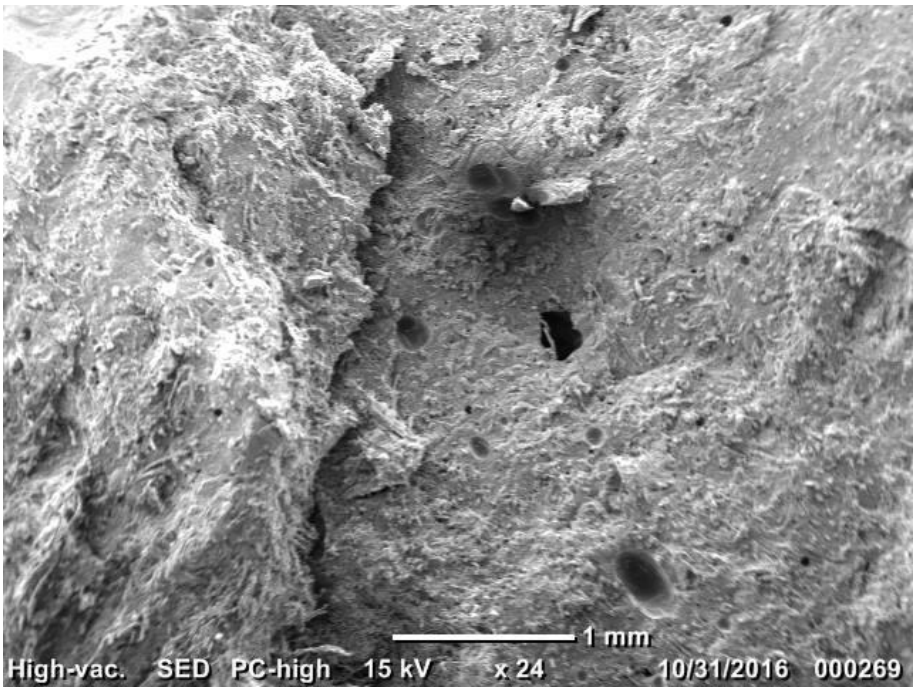

Fig. 119. SEM micrograph of 150°C heat treated sample at x24 magnification.

Fig. 120. SEM micrograph of 150°C heat treated sample at x100 magnification.

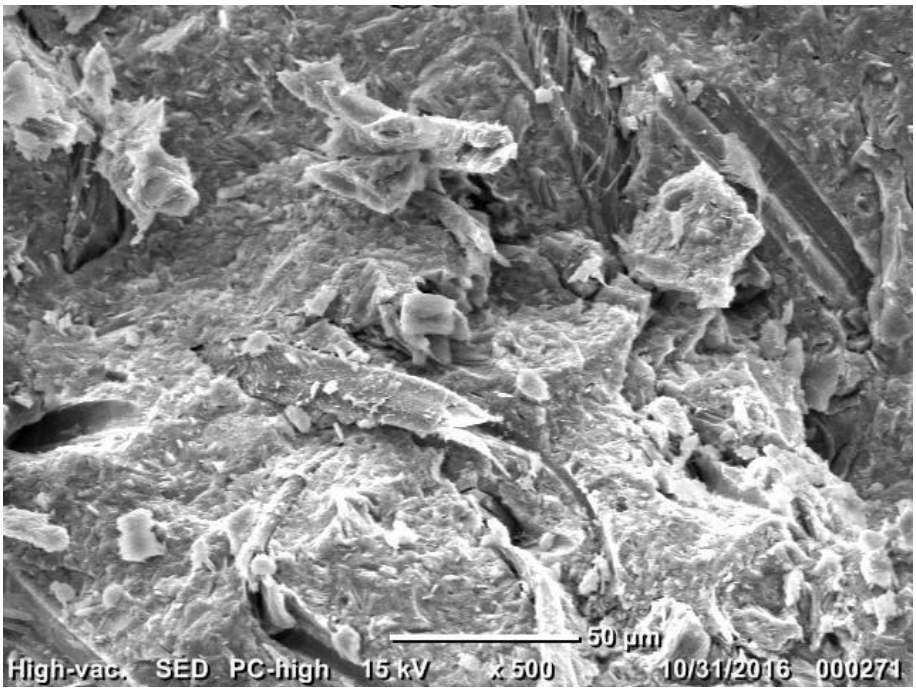

Fig. 121. SEM micrograph of 150°C heat treated sample at x500 magnification.

Fig. 122. SEM micrograph of 150°C heat treated sample at x1000 magnification.

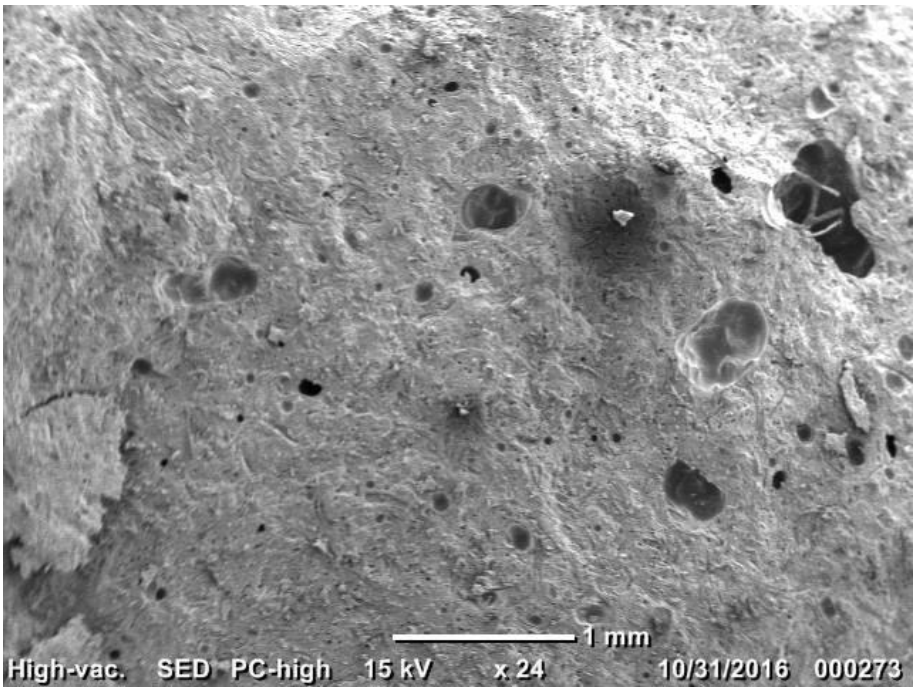

Fig. 123. SEM micrograph of 200°C heat treated sample at x24 magnification.

Fig. 124. SEM micrograph of 200°C heat treated sample at x100 magnification.

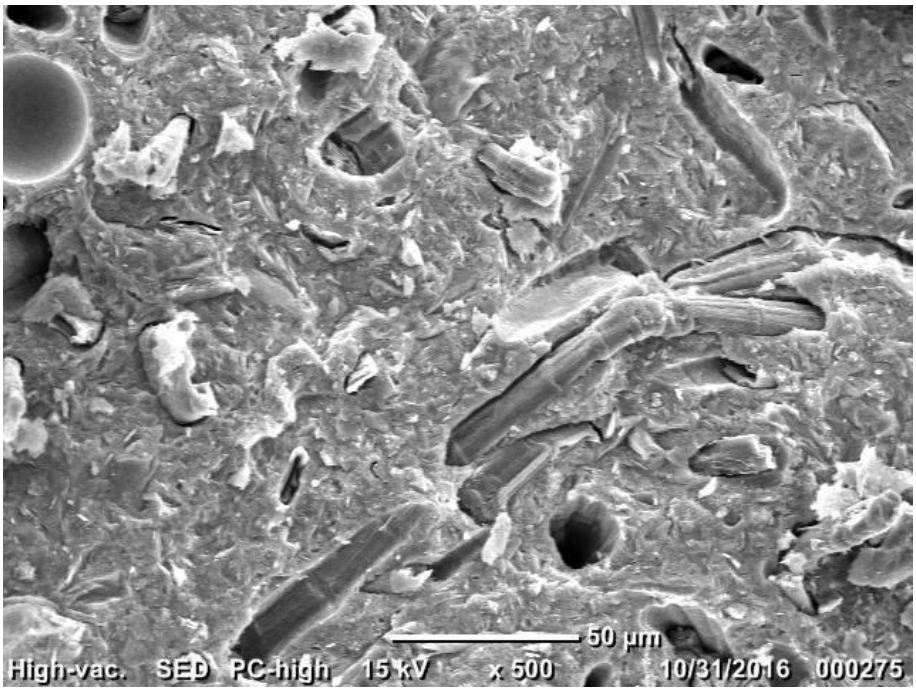

Fig. 125. SEM micrograph of 200°C heat treated sample at x500 magnification.

Fig. 126. SEM micrograph of 200°C heat treated sample at x1000 magnification.

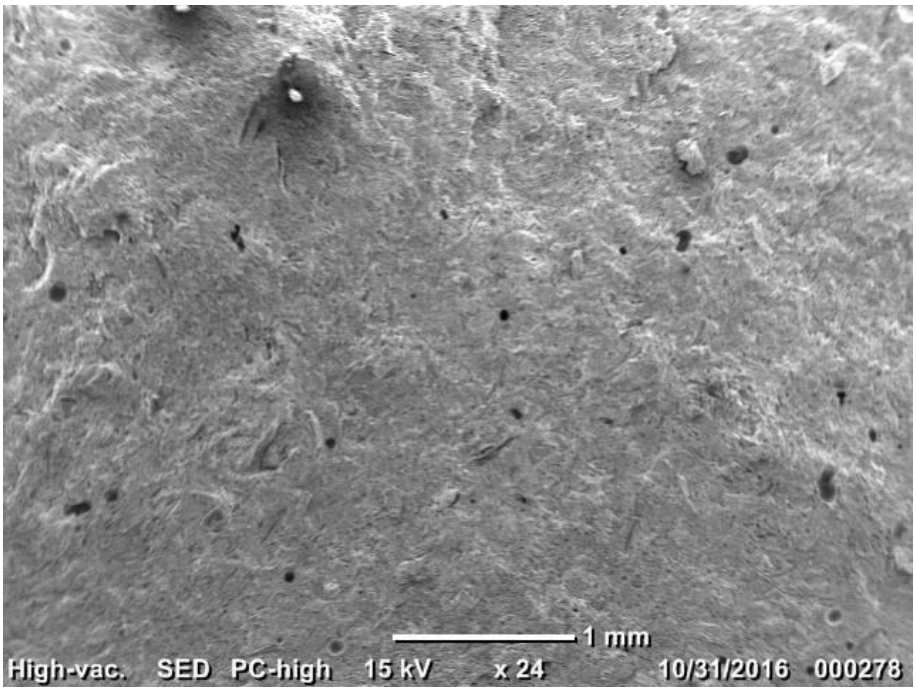

Fig. 127. SEM micrograph of 250°C heat treated sample at x24 magnification.

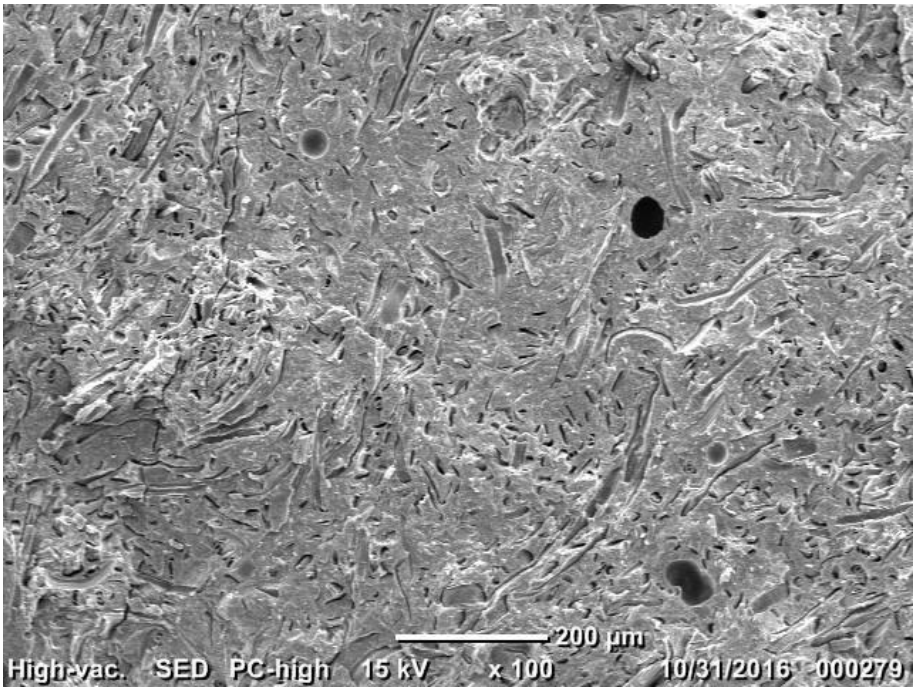

Fig. 128. SEM micrograph of 250°C heat treated sample at x100 magnification.

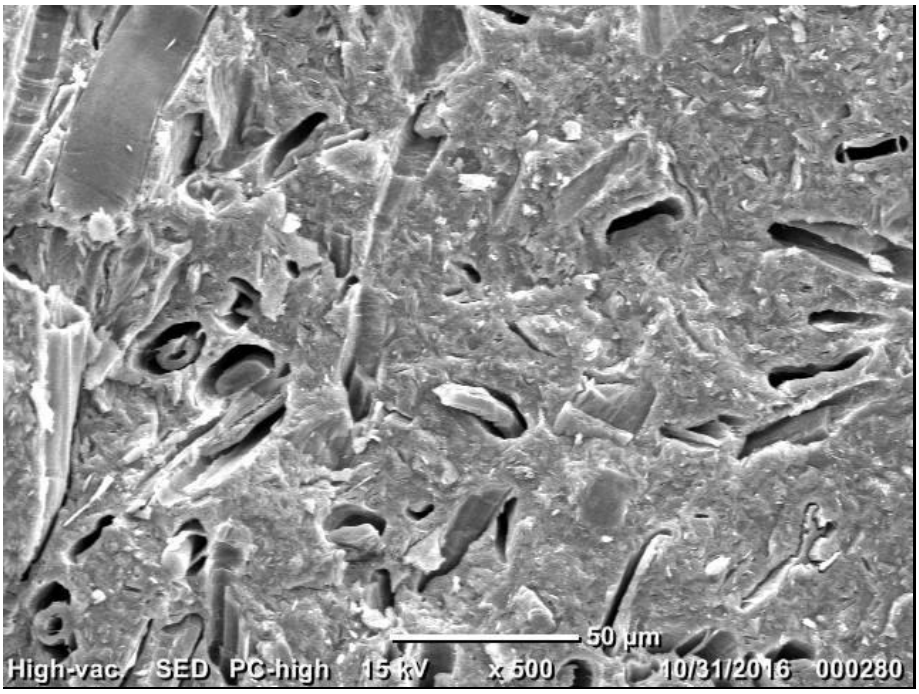

Fig. 129. SEM micrograph of 250°C heat treated sample at x500 magnification.

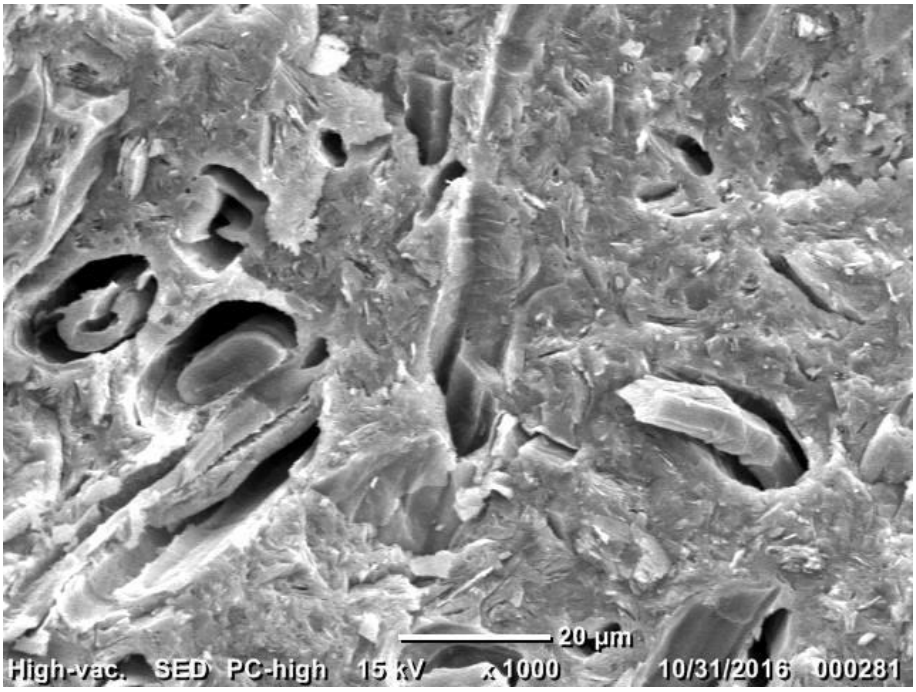

Fig. 130. SEM micrograph of 250°C heat treated sample at x1000 magnification.

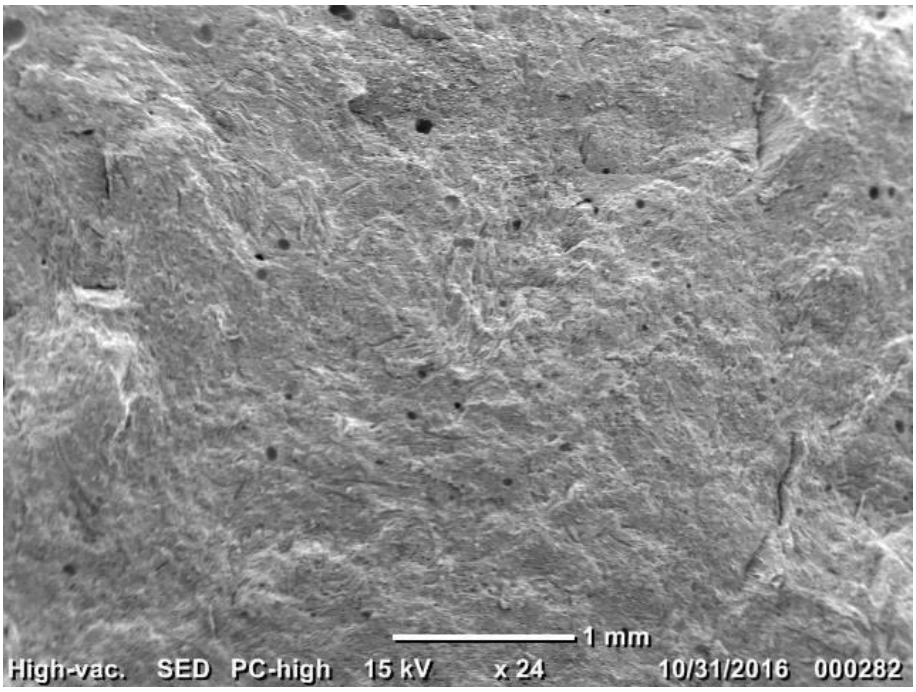

Fig. 131. SEM micrograph of 300°C heat treated sample at x24 magnification.

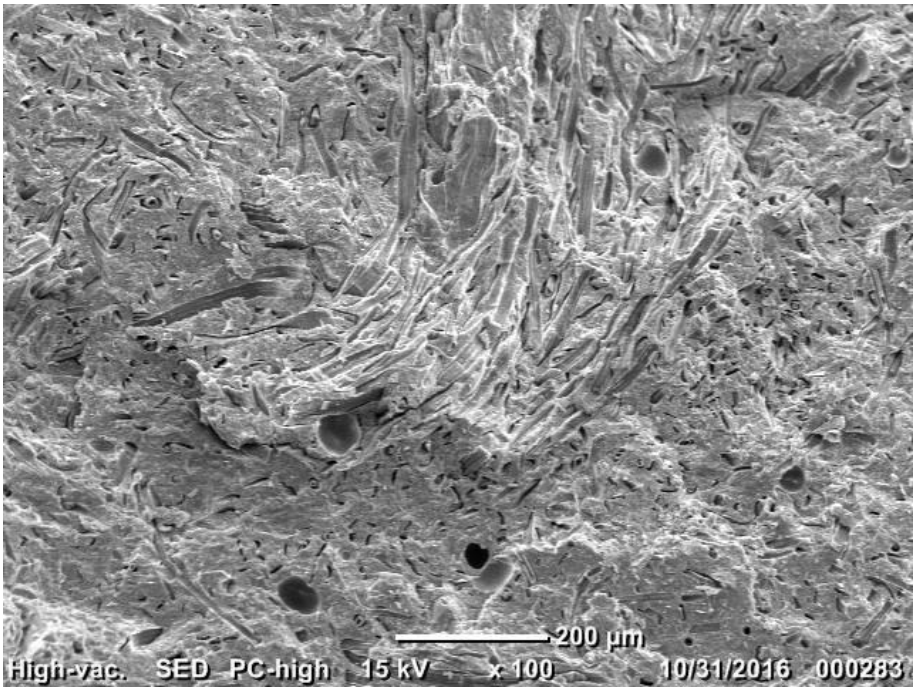

Fig. 132. SEM micrograph of 300°C heat treated sample at x100 magnification.

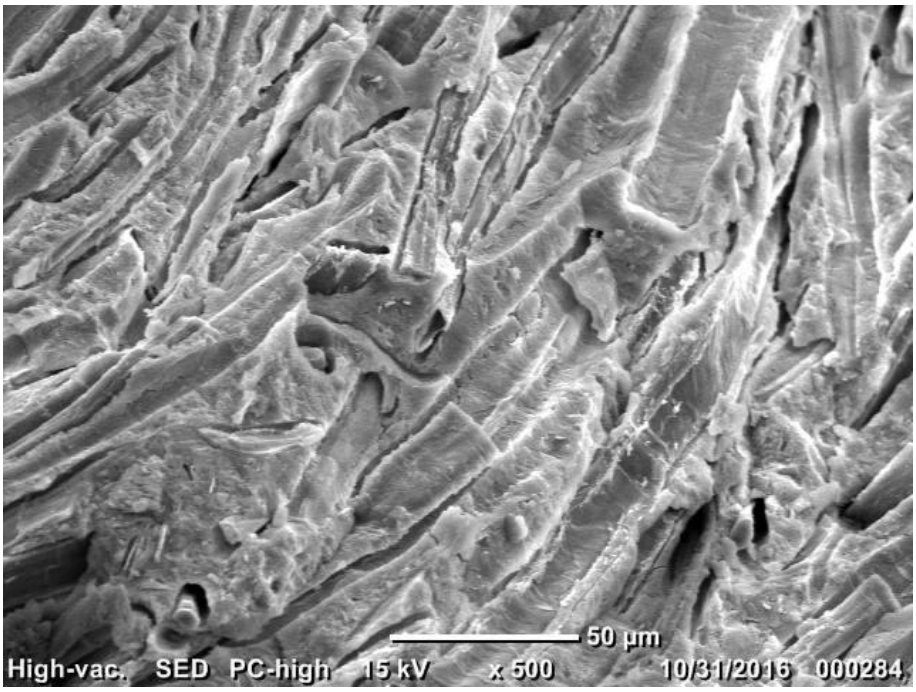

Fig. 133. SEM micrograph of 300°C heat treated sample at x500 magnification.

Fig. 134. SEM micrograph of 300°C heat treated sample at x1000 magnification.

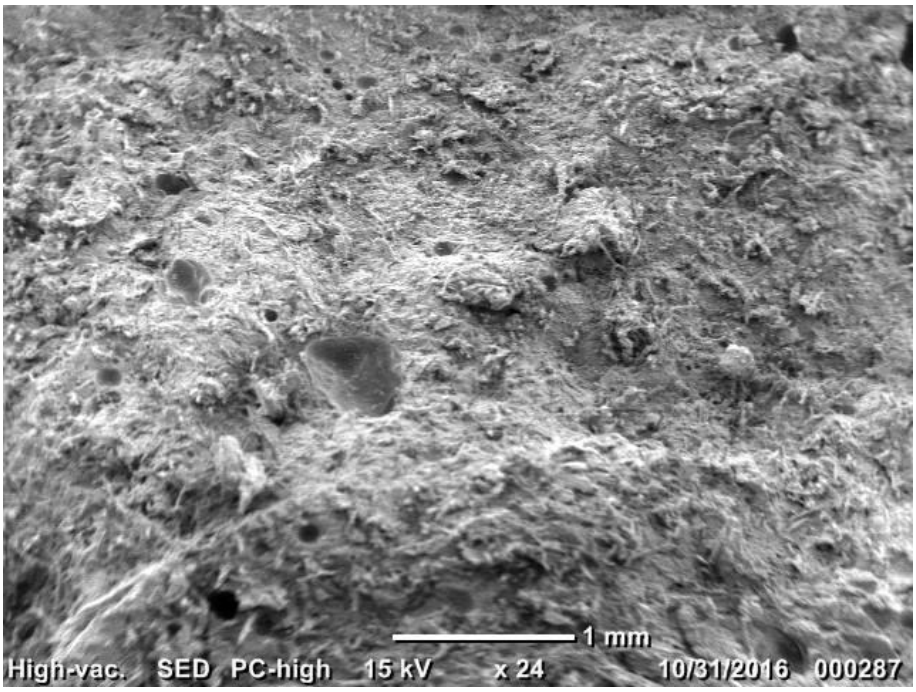

Fig. 135. SEM micrograph of freeze cycle durability sample at x24 magnification.

Fig. 136. SEM micrograph of freeze cycle durability sample at x100 magnification.

Fig. 137. SEM micrograph of freeze cycle durability sample at x500 magnification.

Fig. 138. SEM micrograph of freeze cycle durability sample at x1000 magnification.

Fig. 139. SEM micrograph of H_2SO_4 durability sample at x24 magnification.

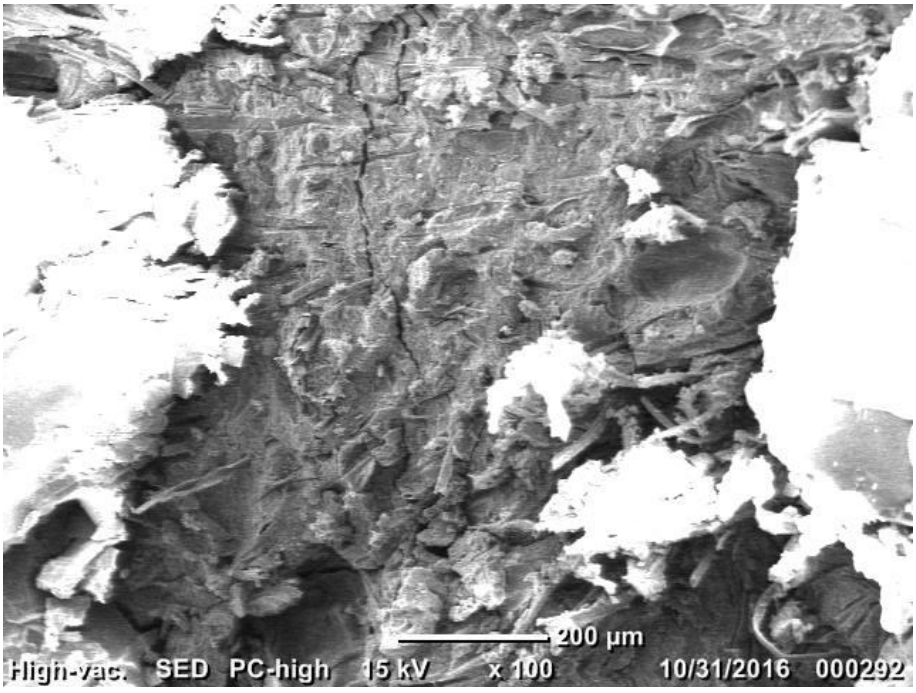

Fig. 140. SEM micrograph of H_2SO_4 durability sample at x100 magnification.

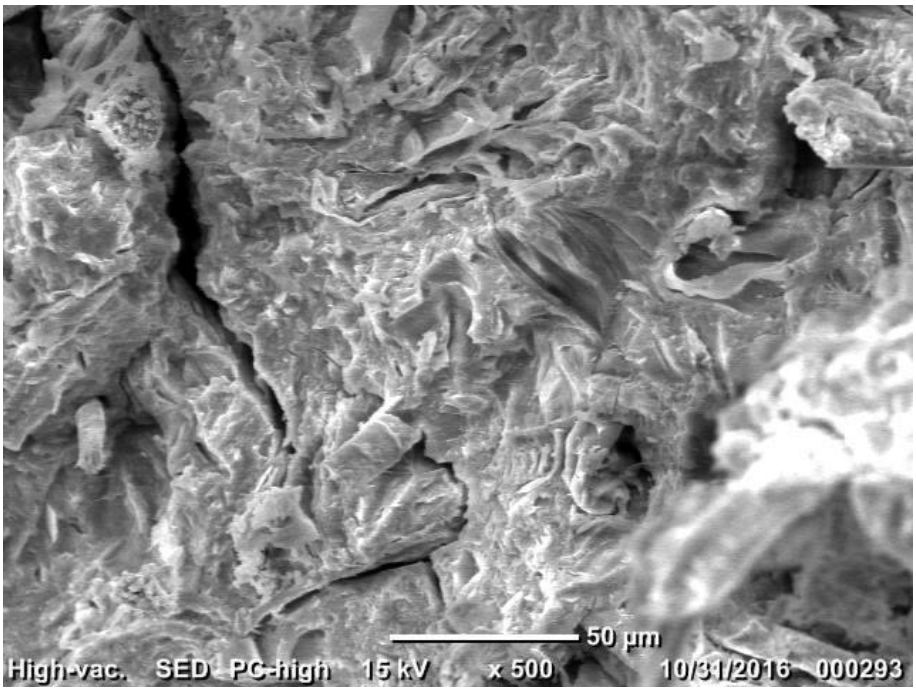

Fig. 141. SEM micrograph of H_2SO_4 durability sample at x500 magnification.

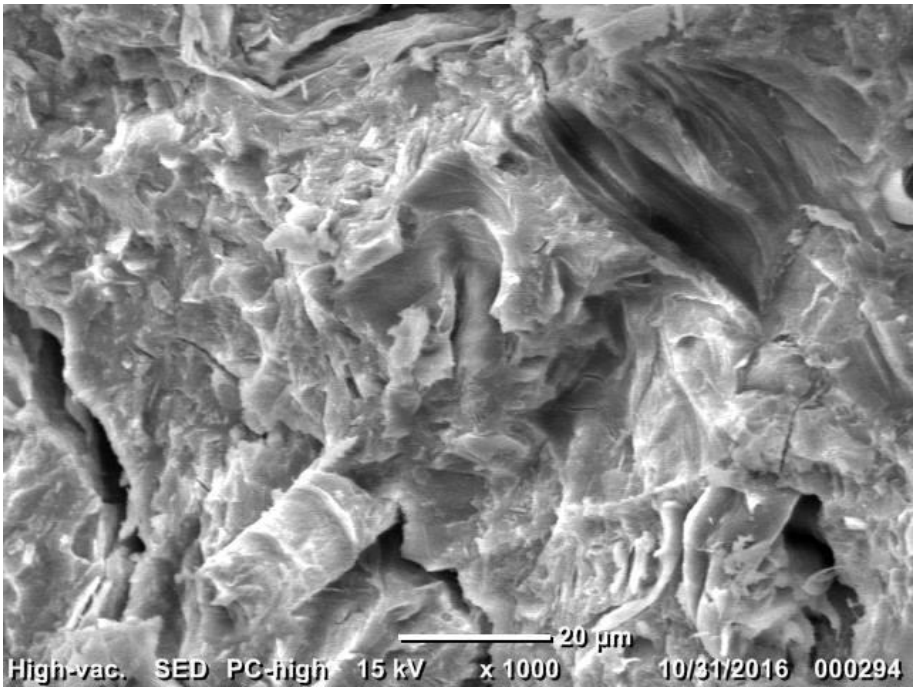

Fig. 142. SEM micrograph of H_2SO_4 durability sample at x1000 magnification.

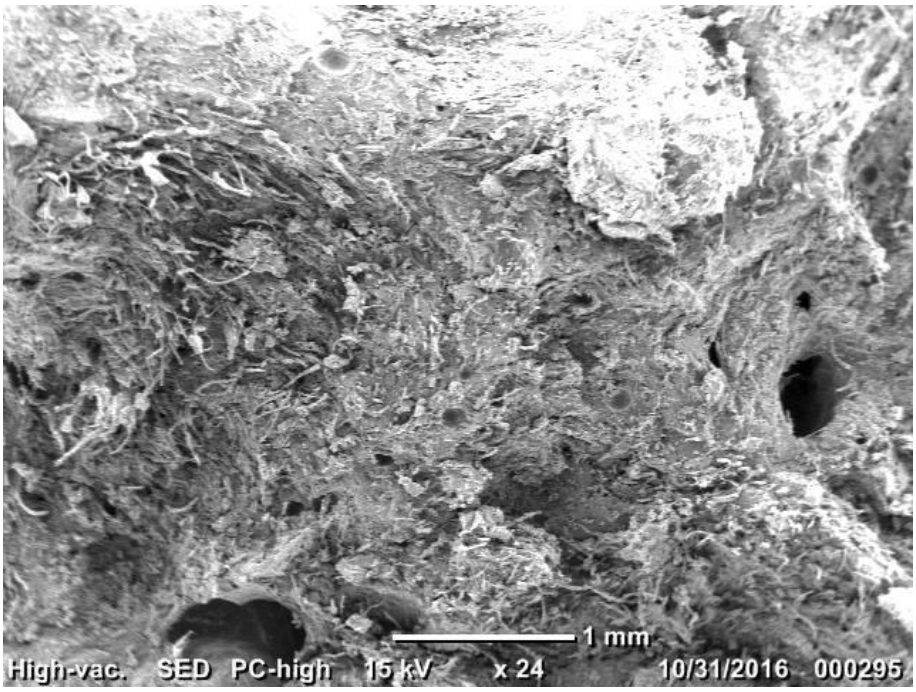

Fig. 143. SEM micrograph of NaOH durability sample at x24 magnification.

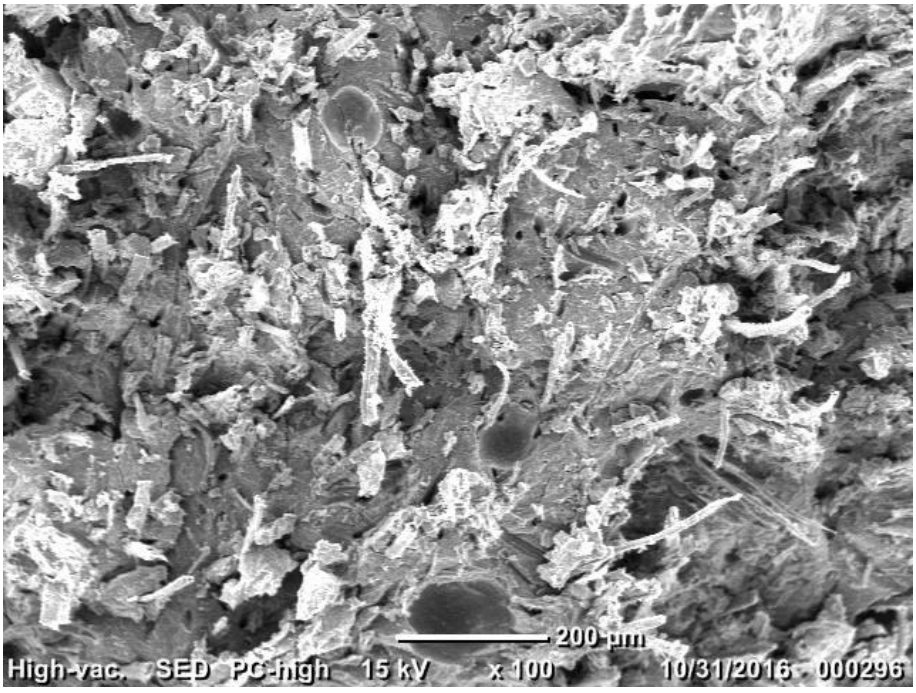

Fig. 144. SEM micrograph of NaOH durability sample at x100 magnification.

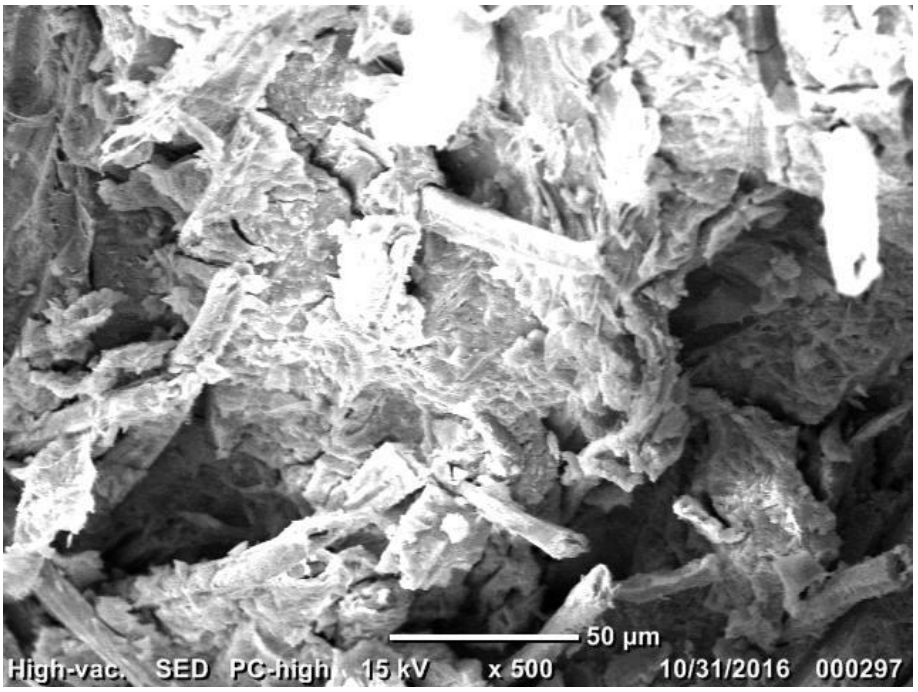

Fig. 145. SEM micrograph of NaOH durability sample at x500 magnification.

Fig. 146. SEM micrograph of NaOH durability sample at x1000 magnification.

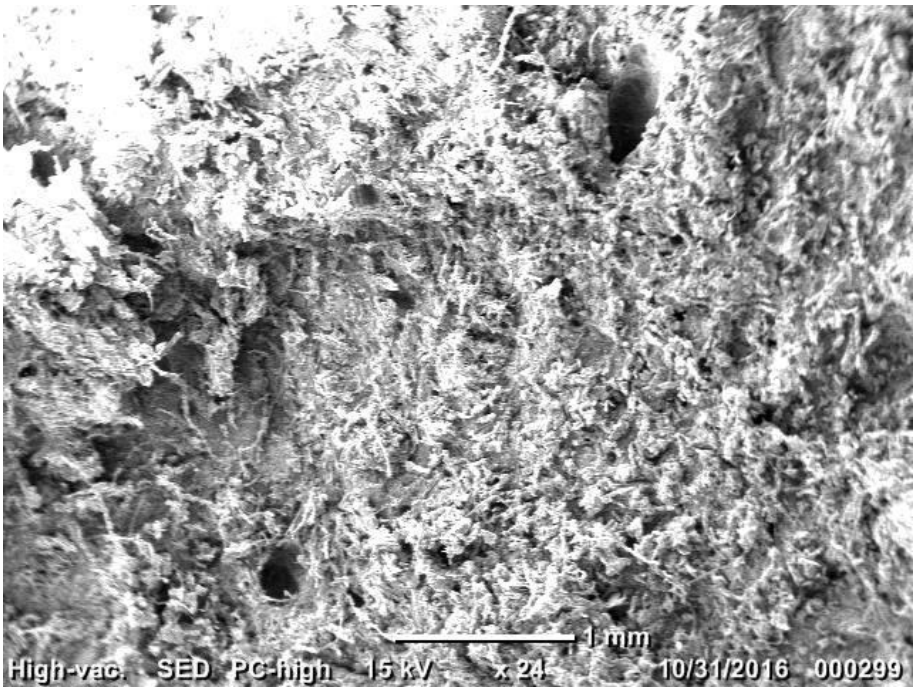

Fig. 147. SEM micrograph of salt water durability sample at x24 magnification.

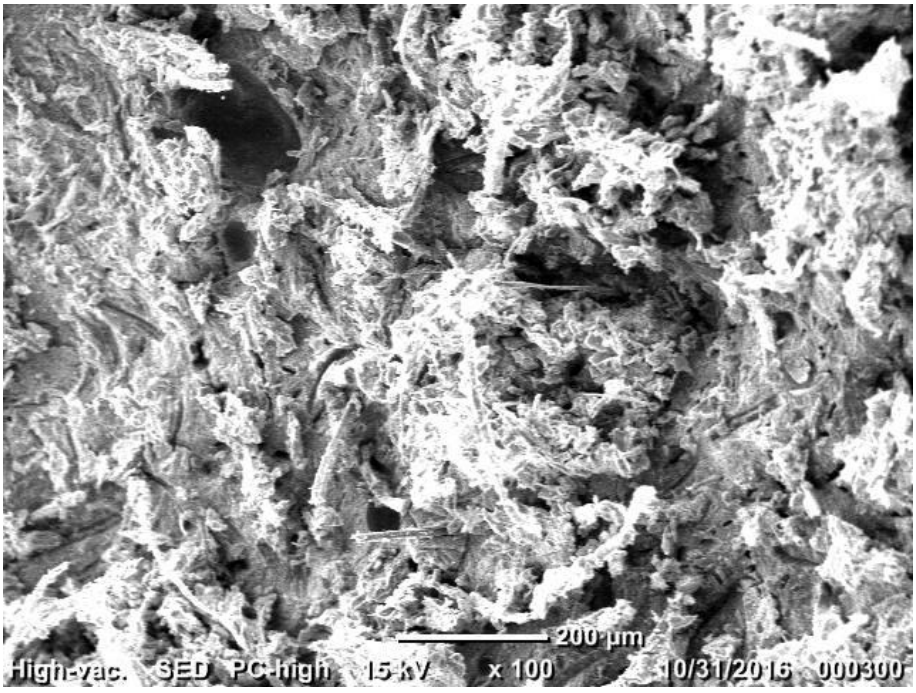

Fig. 148. SEM micrograph of salt water durability sample at x100 magnification.

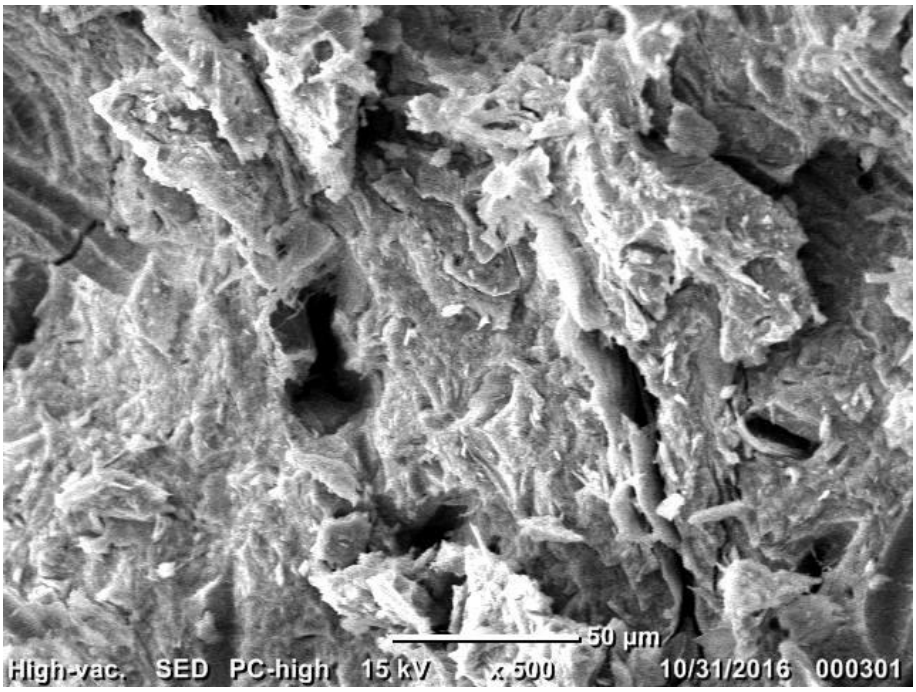

Fig. 149. SEM micrograph of salt water durability sample at x500 magnification.

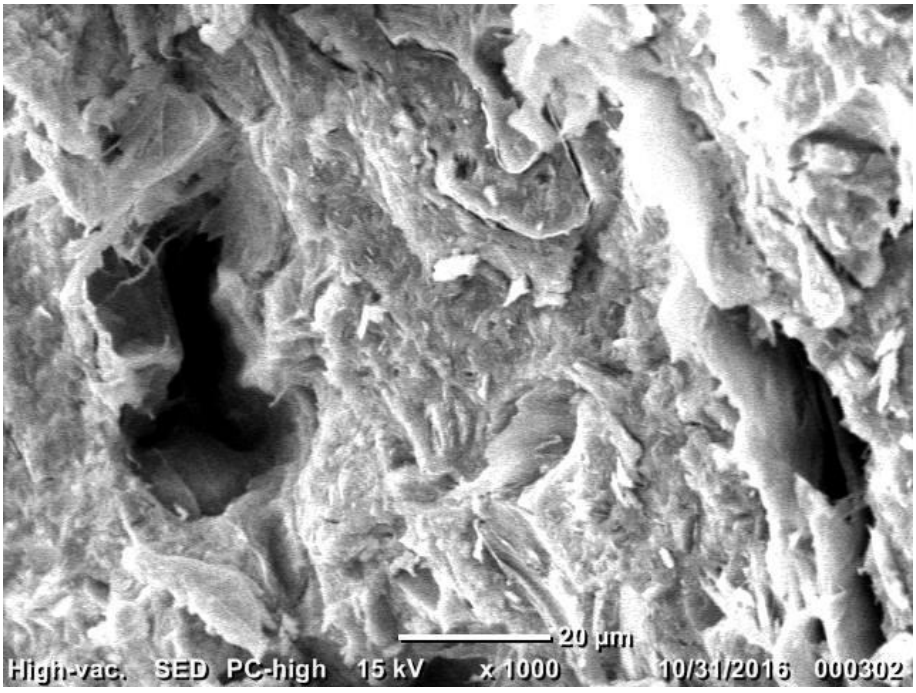

Fig. 150. SEM micrograph of salt water durability sample at x1000 magnification.

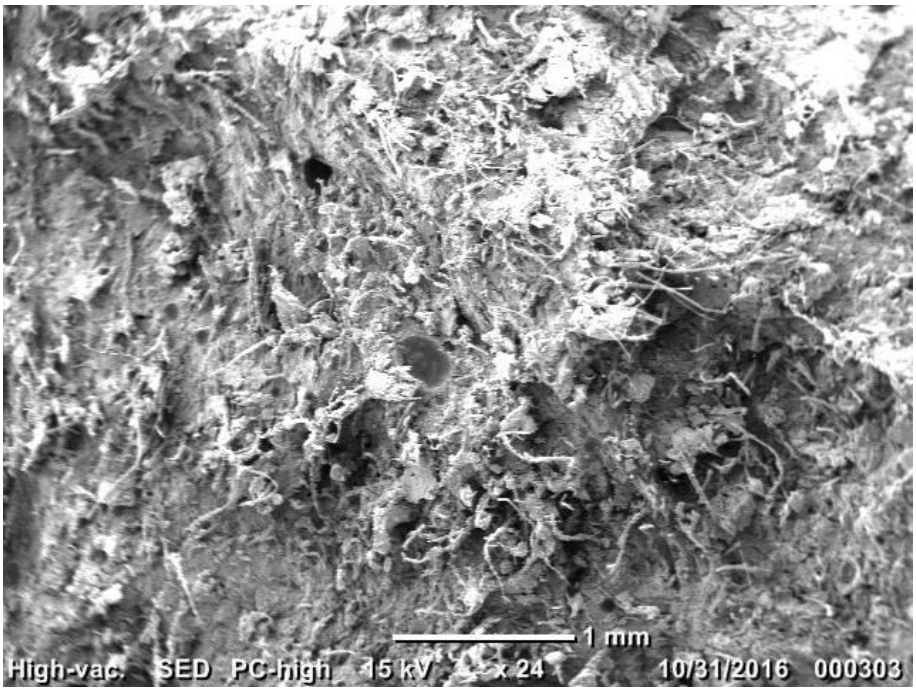

Fig. 151. SEM micrograph of water durability sample at x24 magnification.

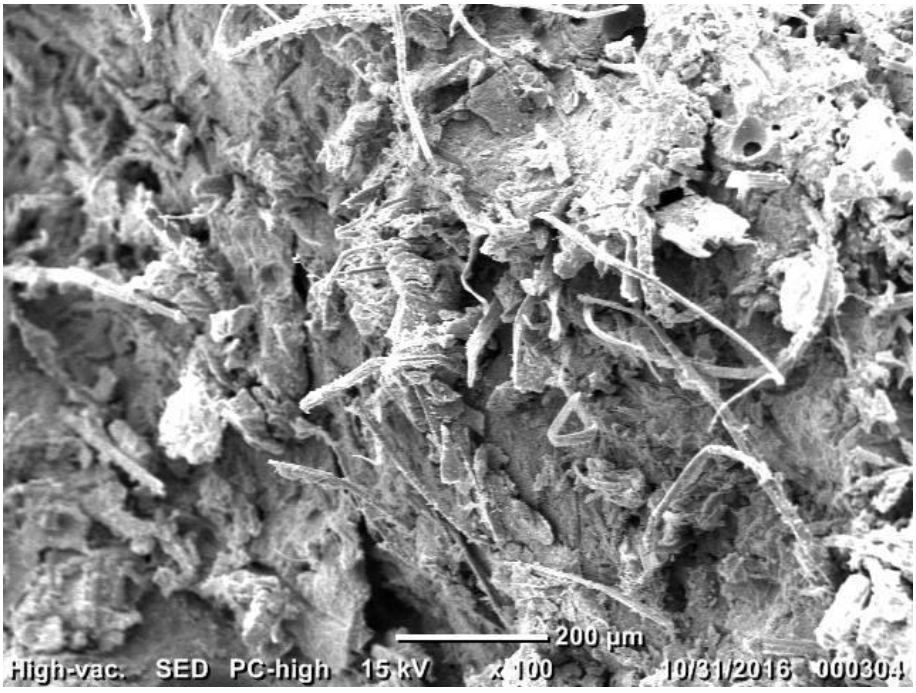

Fig. 152. SEM micrograph of water durability sample at x100 magnification.

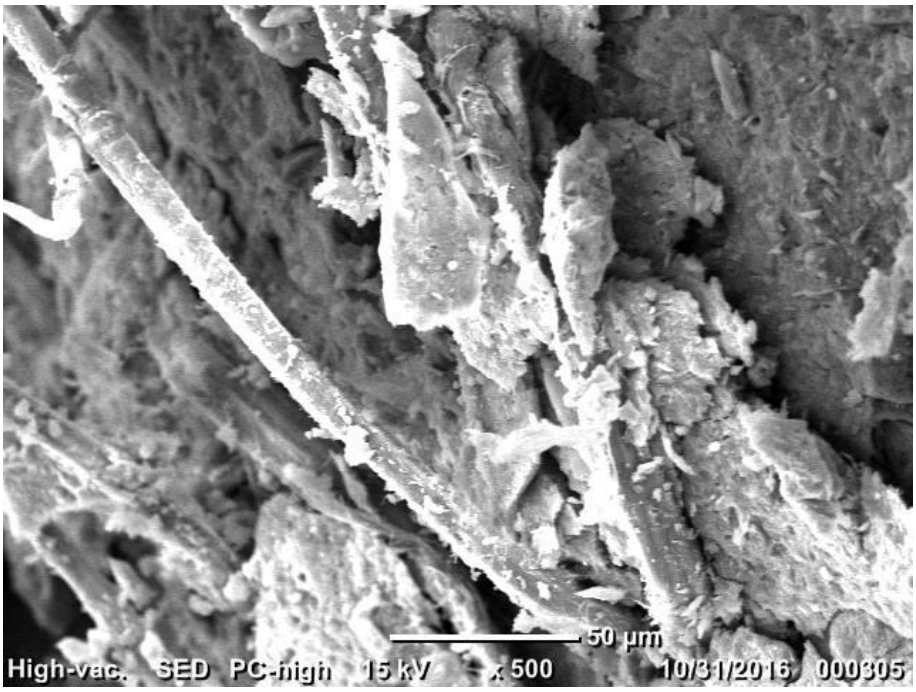

Fig. 153. SEM micrograph of water durability sample at x500 magnification.

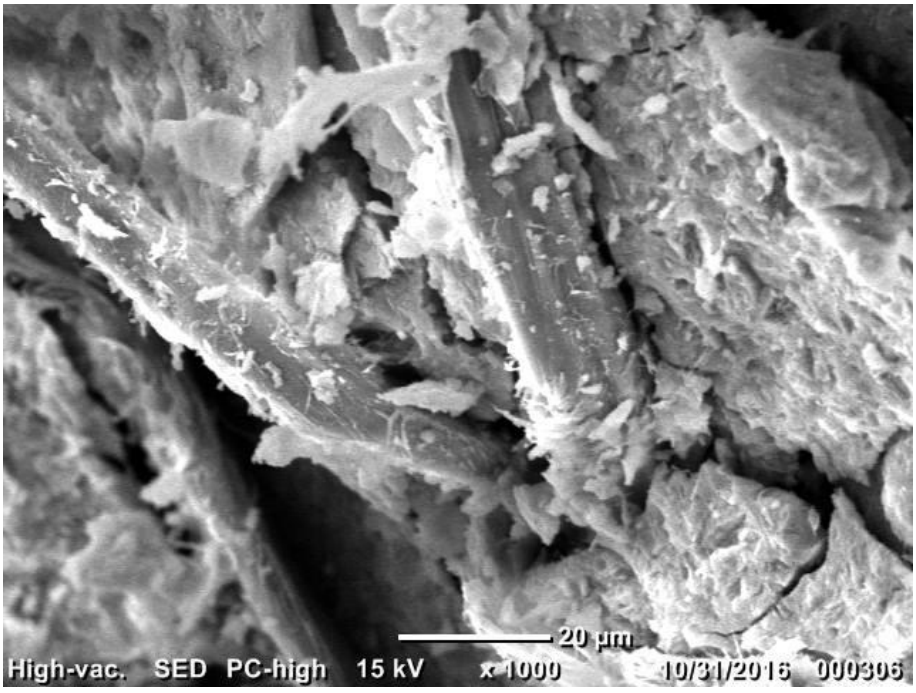

Fig. 154. SEM micrograph of water durability sample at x1000 magnification.